NATIONAL AERONAUTICS AND SPACE ADMINISTRATION

Technical Memorandum 33-570

A Combined Radar-Radiometer With Variable Polarization

David P. Martin

JET PROPULSION LABORATORY
CALIFORNIA INSTITUTE OF TECHNOLOGY
PASADENA, CALIFORNIA

October 15, 1972

NATIONAL AERONAUTICS AND SPACE ADMINISTRATION

Technical Memorandum 33-570

A Combined Radar-Radiometer With Variable Polarization

David P. Martin

JET PROPULSION LABORATORY
CALIFORNIA INSTITUTE OF TECHNOLOGY
PASADENA, CALIFORNIA

October 15, 1972

PREFACE

The work described in this report was performed by the Space Sciences Division of the Jet Propulsion Laboratory.

CONTENTS

CONTENTS (contd)

FIGURES (contd)

ABSTRACT

This report describes an instrument that provides both radar and radiometer data at the same time. The antenna and receiver are time shared for the two sensor functions. The antenna polarization can be electronically scanned at rates up to 5000 changes/s for both the transmit and receive signal paths. The purpose of the equipment is to investigate target signatures for remote sensing applications. The function of the equipment is described and the results for observations of asphalt, grass, and gravel surfaces are presented.

I. INTRODUCTION

A. Objectives

Both radar and radiometer instruments are employed for remote sensing applications at microwave frequencies. The interpretation of these sensor outputs for users in agriculture, hydrology, and forestry is currently being pursued in many research centers. This report describes an instrument that provides both radar and radiometer data at the same time. This is expected to aid in the comparison and interpretation of the active and passive sensor data (Ref. 1). There are other advantages of the equipment design and operation. Many components are shared by the combined instrument. The single antenna will assure that both the radar and radiometer are observing the same terrain or target under the same environmental conditions.

The signal parameters of amplitude, phase, polarization angle, and antenna beam incidence angle are the variables of the radar-radiometer through which the targets are to be characterized. The X-band radar stable oscillator permits coherent detection and observation of phase variations from targets with coherent echoes. With this capability it may be possible to determine the degree of partial coherency as a means of target discrimination even for complex natural targets. The radar could produce images by the coherent synthetic aperture technique if the appropriate recording device and antenna are mounted on an aircraft. However, the initial function of the instrument is to investigate the signature of appropriate targets from the aerial platform shown in Fig. 1.

Another unique feature of this radar-radiometer in addition to the time sharing of the radar and radiometer functions is the variable polarization capability. The linear polarization states can be scanned at rates up to 5000 changes/s for both the transmit and receive signal paths. How the

scanning is accomplished in 11-1/4° increments is presented in the antenna description. This dynamic polarization sensing capability is expected to provide an improved characterization of complex targets such as windblown vegetation. Each polarization state of the antenna has a corresponding data filter for obtaining the average radar amplitude and radiometric temperature per polarization state.

B. Related Investigations

The Committee on Remote Sensing for Agricultural Purposes was formed by the National Research Council in 1962. The Committee investigated not only aerial photography but also active (radar) and passive microwave techniques. Their report on remote sensing (Ref. 2) provides a summary of the state-of-the-art to 1970. Two quotations from that report are particularly applicable. From page 85,

> Radar return from vegetation is more complicated than radar return from surfaces, and return from surfaces is not yet fully understood. Nevertheless, empirical determination of differences in return from vegetation as a function of wavelength, polarization, incident angle, and moisture indicates the sensitivity of radar to many significant plant differences. More research is needed to catalog this sensitivity adequately.

From page 108,

> Some objects exhibit a time dependent (temporal) change in their effective temperatures. These changes can be seasonal or diurnal and can result from fluctuations in the actual object temperature, changes in sky temperature, or changes in the reflection and emittance properties of the object.

The Ohio State University Electrical Engineering Department has been investigating the design of radars and radiometers for determining terrain properties (Ref. 1). Their backscattering measurements with a continuous wave radar are a well known reference (Ref. 3). A more recent report (Ref. 4) describes the design and construction of the equipment, which

includes CW doppler radar systems and radiometer systems. The linear polarization can be changed by unbolting and mechanically rotating the antenna horn. The results reported therein are consistent with the preliminary observations of the radar-radiometer.

The University of Kansas Remote Sensing Laboratory is also investigating properties of various targets. A progress report for 1971 reports on the scattering properties of agricultural targets in the 4 to 8 GHz region (Ref. 5). The radar is operated CW-FM. It is continuously tunable from 4.2 to 7.8 GHz and can be switched between horizontal and vertical polarizations. This research is looking for spectral differences for crop condition identification. Although the techniques are different, the investigation has an objective similar to the radar-radiometer application objective.

The concept of combining a radar and a radiometer for improved target discrimination is being evaluated by the military (Ref. 6). A CW-FM radar at a 3.2-mm wavelength is combined with a Dicke-switched radiometer. The equipment shares a single receiving antenna, mixer, and RF power source. Preliminary results locate various cultural targets on a space defined by the radiometric temperature differences and the radar return power.

Another application of radar and radiometer sensors is to explore planetary surfaces. Research on the nature of the signals from various surfaces is required to prepare for the design of sensors with improved capabilities. Examples of the application of radar and radiometers to planetary exploration are indicated in Refs. 7 and 8. The polarization signatures obtained by the radar-radiometer offer a means of identifying planetary surface conditions.

C. Polarization Effects

The polarizing effect of reflection of light from a plane surface has been observed by everyone who has rotated a polarized pair of sunglasses to see the light intensity vary with the angle of rotation. Radio communication antennas and radar antennas are oriented to take advantage of the signal discrimination due to the antenna polarization. The laws governing polarization effects of electromagnetic waves interacting with matter have been derived by many investigators and are readily available in references. The change in polarization is called depolarization in a recent book devoted to that

subject (Ref. 9). As will be found in the later sections of this report, the polarization effects observed with the radar-radiometer are qualitatively consistent with the theory. The problem of analytically deriving the depolarization by a rough surface is not a part of this report.

II. FUNCTIONAL DESCRIPTION

The combined radar-radiometer design features are summarized in the functional diagram, Fig. 2. The performance parameters are summarized in Table 1. The following sections will describe the function of the experimental equipment.

A. Modes of Operation

There are five modes of radar-radiometer operation that provide operator control of the time sharing between the sensor functions. The modes are:

(1) The radar transmits one pulse and receives target information during part of each radiometric switching cycle. This mode is applicable for studying nearby objects with dynamic polarization changes since the polarization can be selected to change at the pulse repetition frequency (PRF).

(2) The instrument operates as a radar for 500 transmitter pulses, then as a radiometer for an equivalent time. The PRF can be selected between 312 and 5000 pulses/s.

(3) A mode similar to the second except that the time is 8000 PRF pulse intervals.

(4) Radar-only mode; the Dicke ferrite switch stays in the antenna position and the PRF increases by a factor of two.

(5) Radiometer-only mode; the radar pulses are inhibited.

The data has been taken in Mode 1 to evaluate this rapid time-share feature. The other modes have been used to verify correct operation of the equipment.

B. Variable Polarization Antenna

Polarization depends on the relative magnitude and direction of the electric vector at any instant of time. The electric vector can be resolved into two orthogonal components, $\vec{E} = E^{-}\vec{x} + E^{+}e^{i\phi}\vec{y}$, for a plane wave propagating in the z direction. The complex polarization factor is defined by

$$p = \left| \frac{E^{+}}{E^{-}} \right| e^{i\phi}$$

For reflection from a surface, the plane of incidence is defined by the direction of propagation and the normal to the surface. E^{-} is perpendicular to the plane of incidence (horizontal component), E^{+} is parallel to the plane of incidence (vertical component) and ϕ is the phase difference between E^{+} and E^{-} in spatial coordinates. Elliptic, circular, and linear polarizations are uniquely described by this complex polarization factor. Linear polarization is represented by the real axis of the complex P plane, right elliptical is the positive half-plane, and left elliptical is the negative half-plane. The radar-radiometer measures the relative amplitude or modulus of the electric vector in its sine and cosine detectors. The polarization angle is determined by scanning the states of the antenna polarizer, which is analogous to rotating an optical polarizer. The radar transmitted signal polarization also can be rotated with an independent polarizer. In general, there will be more than one reflecting source so the resultant echo is a superposition of many vector components. By means of the coherent radar detectors, the resultant amplitude is measured with the phase referenced to the transmitted phase. For example, if only a simple, plane, linearly polarized wave were received, the amplitude would vary as the sine function with an arbitrary phase depending on the distance to the target. However, for complex targets, waves of different amplitude, phase, and polarization will be superimposed. The resultant polarization is sensed by scanning through the antenna polarization states. There is an ambiguity of 180° since the angle of polarization is controlled and not the vector direction. In summary, the radar echo electric field amplitudes are measured for known antenna polarization states. The phase is compared to a constant frequency reference and thus the mean electrical phase of the scattered wave can be determined.

The radiometer measures the thermal radiation emitted and scattered from the target surface. Although thermal emission is usually not polarized, the reflected radiation is polarized by the different reflection coefficients for the vertical and horizontal components. Thus, when observing near the Brewster angle, the radiometric temperature will vary with the polarization scan.

The polarization control is achieved by adding equal amplitude right and left circularly polarized waves in the feed horn, resulting in a linear polarized wave. The phase shift in one of the paths can be digitally selected by actuating latching ferrite shifters of 22.5, 45, 90, or 180 electrical degrees, thus varying the angular orientation of the resultant linearly polarized wave. Because the ferrite phase shifters are nonreciprocal, separate signal paths are provided for the transmit and receive functions. The antenna polarization network is shown schematically in Fig. 3 and in the photograph, Fig. 4. The change of state can be selected at the PRF or once in 8000 radar pulse intervals.

The ferrite phase shifters provide greater than 20-dB isolation between orthogonal polarization states with the phase shift maintained within 4° over an ambient temperature range of 0 to 55°C. The gain in the two transmission paths is equalized within ±2 dB. These factors limit the dynamic range over which the amount of depolarization can be determined.

An antenna positioner and control unit provides a means of selecting the antenna beam angle of incidence. The antenna can be pointed to any elevation angle with the positioner. The azimuth angle pointing is controlled by the aerial platform on the field vehicle. The aerial platform can be extended 10 m above the surface and rotated 360° in azimuth.

The antenna is a parabola 1.2 m in diameter with a Cassegrain feed. It has low sidelobes to minimize spurious polarization components and to simplify the interpretation of the radiometer data. The antenna patterns obtained for the vertical and horizontal planes are shown in Figs. 5 and 6.

C. Timing Control

The coherent radar pulses and frequencies are synchronized with the 5-MHz stable local oscillator (STALO). The timing control functional diagram is shown in Fig. 7. The pulse repetition frequency is selected by

programming a counter with a 16-position switch. The synchronous delay and pulse generators provide a precise start and stop time for each pulse. In Mode 1, the radar receiver is connected for 2 μs in each radiometer switching cycle. Transmitted pulse width can be selected to be a nominal 50 ns or 100 ns. The radar and radiometer functions have equal on and off times in Modes 2 and 3. At 1-kHz PRF this time is 0.5 s in Mode 2 and 8 s in Mode 3. The timing diagram for 1-kHz PRF is shown in Fig. 8. The various delays were adjusted to account for inherent device delays in the ferrite switches and DC modulator. The sample and hold pulse shows the range of time delay at which a 50-ns sample of the radar echo amplitude is taken. The functional diagram, Fig. 3, shows where the timing pulses are applied in the equipment.

D. Radar Transmitter

The 5-MHz STALO is frequency multiplied by 243 to produce the 1215-MHz coherent local oscillator signal. The 1215 MHz is multiplied by 6 to give the 7290-MHz local oscillator frequency and by 7 to produce the 8505-MHz radar center frequency. Two diode switches in series modulate the CW signal to produce the 1-mW output pulse. This is sufficient power for nearby targets. For more distant ones, a TWT amplifier provides 57-dB gain for the transmitted pulse.

E. Receiver

The receiver is shared by the radar and radiometer. The radiometer is the Dicke type with a ferrite switch at the input (Fig. 3). A low noise traveling wave amplifier (TWTA) is mounted on the antenna to obtain a low noise figure for the system. The TWTA and the waveguide switching for the radiometer are shown in Fig. 9. The signal is converted to the intermediate frequency 1215 MHz for amplification and switching to either the radar or radiometer detectors. The radar has two coherent detectors that are phased to give sine and cosine bipolar signals. Figure 10 shows the radar coherent-detector-amplifier package. The radiometer signal is mixed in a balanced mixer-amplifier that translates the 1215 ±160-MHz band to a 1- to 130-MHz band. The radar center-frequency is filtered out of the radiometer by this technique. A video detector recovers the Dicke-switched signal, which is amplified and synchronously detected at the pulse repetition frequency.

F. Signal Processors

The radar bipolar video signal is observed on an oscilloscope and the time delay of the 50-ns-wide sampling gate adjusted to sample the echo. The time-delay range is shown on Fig. 8. This echo amplitude is read into a 16-channel gated filter. The average echo of each polarization state is read out sequentially and recorded during a polarization scan. Similarly, the radiometer voltage is filtered with another 16-channel processor. Figure 11 is a functional diagram of both of the 16-channel processors. The radiometer voltage is read out sequentially and recorded at the same time as the radar voltage.

III. CALIBRATION

The antenna polarization network was designed and verified in the laboratory of the vendor to have less than 3° phase error for each of the polarization states. Ideally the feed, the parabola, and the radar system should not contribute additional phase error that would appear as polarization error.

A calibration of the antenna polarization was performed with the instrument mounted on the aerial platform. Transmit polarization calibration was performed by inserting a precision phase shifter (Hewlett-Packard Model X 885A) in the transmit coaxial cable leading to the antenna. The signal returned by a Luneberg reflector (Emerson Cumming Model 2B-118) was observed at the radar video output with an oscilloscope. The amplitude was changed from a positive to a negative peak by rotating the phase shifter. The most sensitive and easiest to determine point occurs as the amplitude goes through zero. The measured phase shifts are plotted with the laboratory data on Figs. 12 and 13. The receive polarization was also checked with a standard gain horn (Scientific Atlanta Model SCH 8.2) illuminating the antenna with the phase shifter in the line to the horn. The data obtained with the horn vertically polarized is a closer fit to the laboratory data than is the horizontal data. This is probably due to multi-path since the fit is better around the cross-polarized state. The relative power as a function of polarization state is plotted in Fig. 14. The transmit polarization data was obtained with the standard gain horn and spectrum analyzer as a receiver. The receive

data was obtained with the radar transmitter radiating through the standard gain horn.

The radar cross-section calibration is obtained with two sizes of corner reflector and a Luneberg lens reflector. The corner reflectors are 30 and 10 cm on an edge and provide cross-sectional areas of -12.7 and -22.1 $dB(m)^2$, respectively. The Luneberg lens reflector cross section is +24.3 $dB(m)^2$. The reflectors are smaller than the principal lobe of the antenna pattern so the antenna gain is constant to a good approximation. The radar cross section is

$$\sigma = \frac{P_r}{P_t} \frac{(4\pi)^3 R^4}{\lambda^2 G^2} (\text{meters})^2$$

where P_r is received power, P_t is transmitted power, R is range, λ is wavelength, and G is antenna gain. The received power with the reflectors at 10-m range and 1-mW radiated power will be -50.8, -41.4, and -4.4 dBm, respectively, with each reflector successively placed in the beam. The normal cross-sectional area of the antenna beam at 10 m is

$$\pi R^2 (\Delta\theta)^2 = 0.385 \ (\text{m})^2 \text{ or } -4.1 \ dB(m)^2$$

The radar cross section is commonly normalized by the area illuminated when studying the backscatter characteristic of terrain or similar large targets.

$$\sigma_0 = \frac{\sigma \cos \theta}{\pi R^2 (\Delta\theta)^2}$$

where θ is the angle of incidence. The terrain scattering parameter (γ) of Ref. 3 is related to the radar cross section $\sigma_0 = \gamma \cos \theta$.

Thus the three reference reflectors provide calibration for the radar backscatter that may be expressed in terms of σ_0 or γ.

The radiometer is calibrated with hot and cold loads that are attached for the calibration at the reference load port. The hot load is electrically heated and thermostatically controlled. The cold load is a special waveguide termination immersed in liquid nitrogen. Dry nitrogen gas flows

within the waveguide to prevent frost from condensing on the load element. There is a dc-offset-voltage difference for each PRF due to switching transients. The calibration data for the 312-, 1000-, and 5000-Hz operating frequencies are shown on Fig. 15. A precision variable attenuator was inserted with the calibration load to obtain various effective temperatures and to check the linearity. Figure 16 is a diagram of the radiometer calibration configuration with the attenuation factors and temperatures identified. The attenuation factor (A_i) is the ratio of the power out to the power in for each device, and T_i is the kinetic temperature in Kelvin.

Attenuation of -20 dB coupler $A_2 = 0.99$

Attenuation of variable attenuation $A_3 = 1.00$ to 0.001

Temperature $T_2 = T_3 = T_r = 298$ K

$T_1 = 323$ K

$T_L = 77$ K or 320 K

After establishing the apparent temperature (T_{appl}) with the hot and cold loads, the radiometer is switched to the antenna. The antenna is pointed at the clear sky, which has a temperature of 5 K at 8.5 GHz. Assume the back-lobes are looking at 300 K ambient, then $T_{ant} \simeq 17$ K and the attenuation of the polarizer $A_1 = 0.76$ or 1.2 dB loss. The apparent temperature with the antenna and polarizer is

$$T_{app2} = A_2\left[A_1 T_{ant} + (1 - A_1)T_1\right]T_2$$

The voltage response determined with the hot and cold loads is

$$T_{appl} = 201 \text{ K} + 109.5 \text{ K/V(V)}$$

The apparent temperature with the antenna connected is equated to the voltage response to obtain the antenna temperature calibration, which is shown in Fig. 17.

$$T_{ant} = 144 \text{ K/V(V)} + 167 \text{ K}$$

When rapid scanning the polarization there is a voltage offset for each polarization that is found by comparison with the voltage offsets in the reference load condition.

IV. DATA REDUCTION AND RESULTS

To evaluate the operation of the equipment, observations have been made of three different surfaces: asphalt, grass, and gravel. The asphalt surface is the parking lot shown in Fig. 18. The truck was parked next to a building and the radar-radiometer was pointed toward an unobstructed area. The grass surface is part of a baseball playground. The grass is growing in tufts that point in all directions as shown in Fig. 19. Bare ground is visible in a few areas. The gravel surface is shown in Fig. 1 and is the naturally mixed gravel in a dry wash. The incidence angle is the number of degrees from the vertical to the center of the antenna beam. For each incidence angle, the radar-radiometer is looking at a different part of the same general surface.

The radar-radiometer was operated in the pulse-to-pulse time sharing mode at 1-kHz pulse repetition frequency with 100-ns pulse width. The polarization was electronically scanned at the slow rate. That is, data for each polarization state was recorded for 8 s before switching to the next polarization state. The radar transmitter polarizer was scanned in the same polarization state (direct) or at a 90° angle to the received polarization (cross) for the asphalt and grass. The gravel was scanned over the received polarization states with the transmitter polarization held at vertical or zero degrees. Both the radar and the radiometer outputs were recorded simultaneously on a Sanborn 297.

The average voltage for each polarization was read from the recording and used for the computer data input. The radar cosine detector amplitude was plotted as a function of polarization angle for each material and angle of incidence. The radiometric antenna temperature was similarly plotted. These graphs are in the Appendix. To show the characteristic pattern for each surface, the normalized radar power as a function of polarization is plotted in polar diagrams (Figs. 20 and 21). Vertical polarization with the electric vector parallel to the plane of incidence is at zero degrees.

The normalized radar echo power is obtained by taking the sum of the squares of the sine and cosine detector outputs and dividing by the maximum value. Because only one 16-channel filter is available, the relative power is approximated by shifting the echo 90 electrical degrees or 4 polarization states to obtain an equivalent sine detector output. The echo power at each incidence angle is normalized to the maximum value to emphasize the polarization pattern variations. These polarization signatures are compared in Figs. 20 and 21. Note that the patterns are different for the different materials. The difference with incidence angle is not so great especially between 20° and 30° for all these materials. The differences at 10° and 70° may be partly due to reflections from the truck or other objects that could not be prevented from intercepting the antenna sidelobes. Because no cross-polarized scan was observed for the gravel, the direct and cross data are compared for grass. The purpose of Fig. 20 and 21 is to demonstrate that different materials have different polarization signatures. There are problems of establishing the uniqueness and variance of the patterns that can be investigated with more measurements. Development of the electromagnetic scattering theory is not included in this report. In general, the theoretical solution is not needed for successful application of the technique to remote sensing problems.

It may be noted, however, that the same electromagnetic boundary value problem description is applicable to both the radar and the radiometer. The sum of reflectivity and emissivity is equal to one if the transmittance is zero and if the surface is in thermal equilibrium with its surroundings. For the case of a plane wave incident on a plane surface, the emissivity and reflectivity are known functions of the angle of incidence, the polarization, and the material constants. The brightness temperature sensed by the radiometer is the sum of the temperature radiated by the surface and reflected from the sky.

$$T_{\text{brightness}}(\theta) = \epsilon T_{\text{equilibrium}}(\theta) + \rho T_{\text{sky}}(\theta)$$

where ϵ = emissivity and ρ = reflectivity.

The antenna behaves as a viewing aperture for the thermal radiation that impinges the antenna from all directions. The antenna temperature is the sum of all the radiation as weighted by the antenna pattern $F(\theta, \phi)$.

$$T_{ant} = \frac{\iint T_{brightness}(\theta) F(\theta, \phi) \sin\theta \, d\theta \, d\phi}{\iint F(\theta, \phi) \sin\theta \, d\theta \, d\phi}$$

For antennas with a high beam efficiency, most of the power is in the main beam and to a first approximation the measured antenna temperature equals the brightness temperature.

The measured antenna temperatures are presented in the Appendix. All of the temperatures for asphalt are summarized on Fig. 22. As expected for a smooth reflecting surface, the vertical polarized temperature is greater than the horizontal polarized temperature. The antenna temperature is plotted as a function of the incidence angle with the vertical (E^+) and horizontal (E^-) polarization as parameters in Fig. 23. The temperature of the grass does not change much with incidence angle whereas the asphalt clearly separates into vertical and horizontal components as expected. There is an anomolous rise in E^- at the higher incidence angles, which is probably due to reflections from a building. The temperature of the building could be substituted for the sky temperature in deriving the radiometric brightness and emissivity above 50° incidence angle.

The degree of polarization for the radar and radiometer observation of the asphalt surface is plotted as a function of incidence angle in Fig. 24. The degree of polarization (P) is a measure of the vectorial properties of electromagnetic waves. A coherence matrix can be defined (Ref. 10) to describe the measured wave properties.

$$\vec{J} = \begin{bmatrix} J_{xx} & J_{xy} \\ J_{yx} & J_{yy} \end{bmatrix} = \begin{bmatrix} \langle E_x E_x^* \rangle & \langle E_x E_y^* \rangle \\ \langle E_y E_x^* \rangle & \langle E_y E_y^* \rangle \end{bmatrix}$$

The intensity (I) or power is a function of the polarization angle (α) in degrees and the retardation (ϵ) in radians, which is the phase delay of E_y with respect to E_x.

$$I(\alpha, \epsilon) = J_{xx} \cos^2 \alpha + J_{yy} \sin^2 \alpha + J_{xy} e^{-i\epsilon} \cos\alpha \sin\alpha + J_{yx} e^{i\epsilon} \sin\alpha \cos\alpha$$

For the radar, the transmit polarizer provides the retardation since the cross-polarized field component is shifted $\pi/2$ radians from the direct polarized field. Thus,

J_{xx} = I(0,0) = power measured vertically; α = 0 and direct ϵ = 0

J_{yy} = I(90,0) = power measured horizontally; α = 90 and direct ϵ = 0

$$J_{xy} = \frac{1}{2}\left[I(45,0) - I(135,0)\right] + \frac{1}{2}i\left[I\left(45, \frac{\pi}{2}\right) - I\left(135, \frac{\pi}{2}\right)\right]$$

$$J_{yx} = \frac{1}{2}\left[I(45,0) - I(135,0)\right] - \frac{1}{2}i\left[I\left(45, \frac{\pi}{2}\right) - I\left(135, \frac{\pi}{2}\right)\right]$$

The intensity varies from a maximum to a minimum as the polarization is varied. The ratio of the polarized intensity to the total intensity can be shown to be:

$$P = \frac{I_{max} - I_{min}}{I_{max} + I_{min}} = \sqrt{1 - \frac{4\left[J_{xx}J_{yy} - J_{xy}J_{yx}\right]}{\left[J_{xx} + J_{yy}\right]^2}}$$

When P = 1 the wave is completely polarized. When P = 0, the wave is completely unpolarized. For the case of thermal radiation, the sources are expected to be unpolarized except that part due to reflection.

$$P = \left|\frac{J_{xx} - J_{yy}}{J_{xx} + J_{yy}}\right| = \frac{T_{max} - T_{min}}{T_{max} + T_{min}}$$

There is an alternative description of the state of polarization by the Stokes parameters, which are related to the elements of the coherency matrix as follows:

$$S_0 = J_{xx} + J_{yy}$$

$$S_1 = J_{xx} - J_{yy}$$

$$S_2 = J_{xy} + J_{yx}$$

$$S_3 = i(J_{yx} - J_{xy})$$

The Stokes parameters are of historical interest for relating the microwave measurements to optical investigations of polarization.

In summary, the preliminary observations have shown distinctive polarization signatures for different surfaces. The method of data reduction was described. The polarization effects for both the radar and the radiometer behave as expected for a smooth, reflecting surface. The problems of establishing the variance and uniqueness of the polarization signatures and of eliminating spurious reflections and antenna sidelobe effects were pointed out. The degree of polarization was defined by the coherency matrix description and the results for the degree of polarization as a function of incidence angle were plotted.

V. CONCLUSIONS

A general description of an instrument that rapidly time shares the functions of a radar and a radiometer has been presented. The time sharing of the antenna and receiver components has ensured that the target and geometry are the same for the radar and the radiometer measurements. The unique dynamic polarization capability adds a new dimension to remote sensing for improved discrimination of surface conditions. The instrument is mounted on an aerial platform on a truck and is ready to go to areas selected for remote sensing study. Calibration techniques have been developed and preliminary measurements made. Additional work is recommended to investigate various targets to show how the features of the instrument will contribute to remote sensing.

REFERENCES

1. Peake, W. H., R. L. Riegler, and C. H. Schultz, The Mutual Interpretation of Active and Passive Microwave Sensor Outputs, Antenna Lab Report 1903-3, Ohio State University, Columbus, Ohio, July 15, 1966.

2. Committee on Remote Sensing for Agricultural Purposes, Remote Sensing, National Academy of Sciences, Washington, D. C., 1970.

3. Cosgriff, R. L., W. H. Peake, and R. C. Taylor, Terrain Scattering Properties for Sensor System Designs, Ohio State University, Columbus, Ohio, May 1960.

4. Oliver, T. L., A Mobile Facility for Measuring the Backscattering and Brightness Temperature of Terrain at Microwave Frequencies, Report 1903-6, Ohio State University, Columbus, Ohio, October, 1968.

5. Eighth Semi-Annual Report, Project Themis: A Center for Remote Sensing, University of Kansas, Center for Research, Inc., Lawrence, Kansas, 1971.

6. Foiani, D. L., and R. H. Pearce, "Combined Radar and Radiometer at Millimeter Wavelengths," Symposium of Submillimeter Waves, *Polytechnic Institute of Brooklyn, Brooklyn, N. Y., April, 1970.*

7. Rea, D. G., N. Hetherington, and R. Mifflin, "Calculation of the Effect of Roughness on Microwave Emissivity with Application to the Moon and Venus," J. of Geophys. Res. Vol. 73, No. 22, pp. 7009-7017, November 1968.

8. Brown, W. E., Jr., "Radar Studies of the Earth," Proc. IEEE, Vol. 57, No. 4, pp. 612-620, April 1969.

9. Beckman, P., The Depolarization of Electromagnetic Waves, Golem Press, Boulder, Colorado, 1968.

10. Born, M., and E. Wolf, Principles of Optics, Pergamon Press, New York, 1970, p. 655.

Table 1. System parameters

Frequency	8.505 GHz
Wavelength	3.53 cm
Pulse width	50 or 100 ns
PRF (selectable)	5000/(m + 1), m = 0, 1 ... 15 pulses/s
Peak power	1 mW or 500 W
Antenna 3 dB beamwidth	3.8°
Polarization	Linear, variable orientation in 11-1/4° steps, 16 states total, both for transmit and receive
Rate of polarization scan	PRF or PRF/8000
Antenna beam efficiency	96%
Noise figure	8 dB
Predetection bandwidth	320 MHz
Radar processor filter	0.002 s
Radiometer time constant	0.3 s
Oscillator stability	10^{-11}
ΔT sensitivity	2 K

Fig. 1. Radar-radiometer on the aerial platform

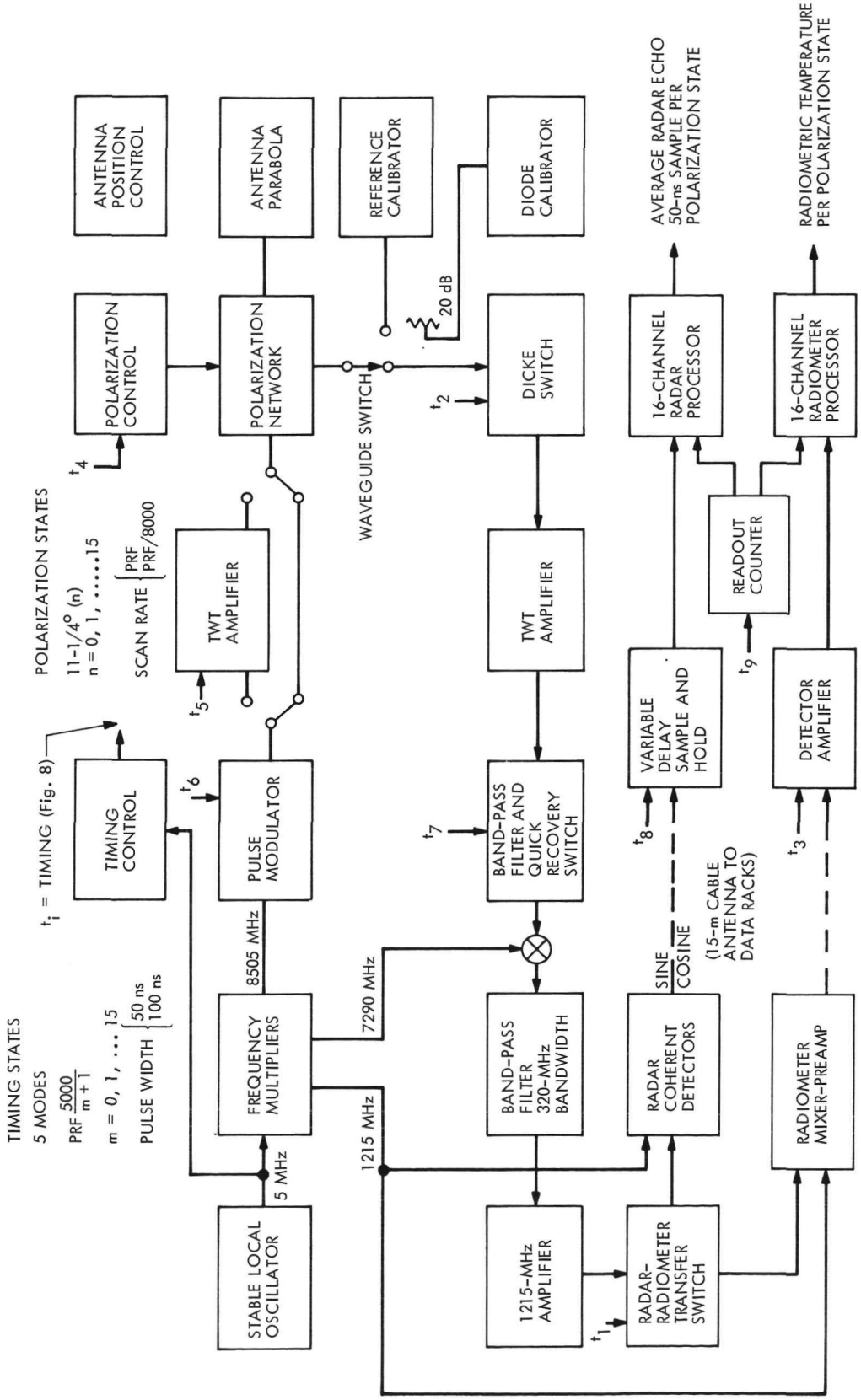

Fig. 2. Radar-radiometer functional diagram

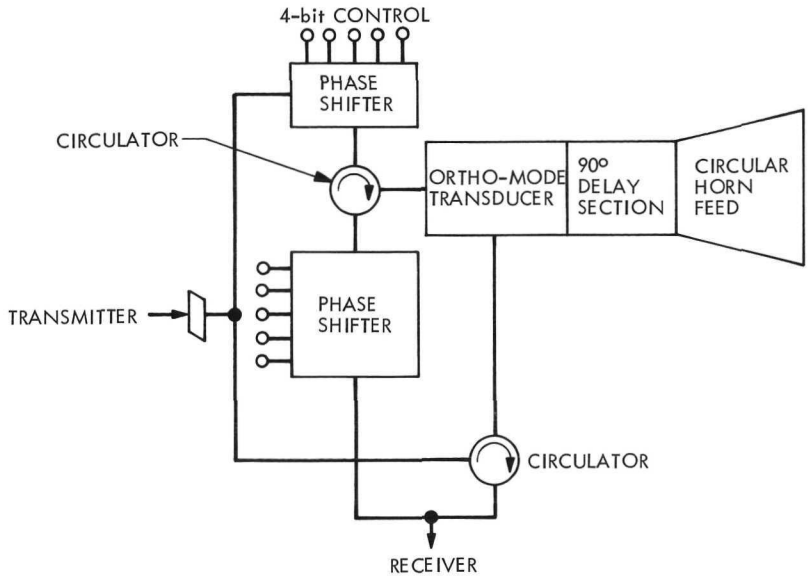

Fig. 3. Antenna polarization network, functional diagram

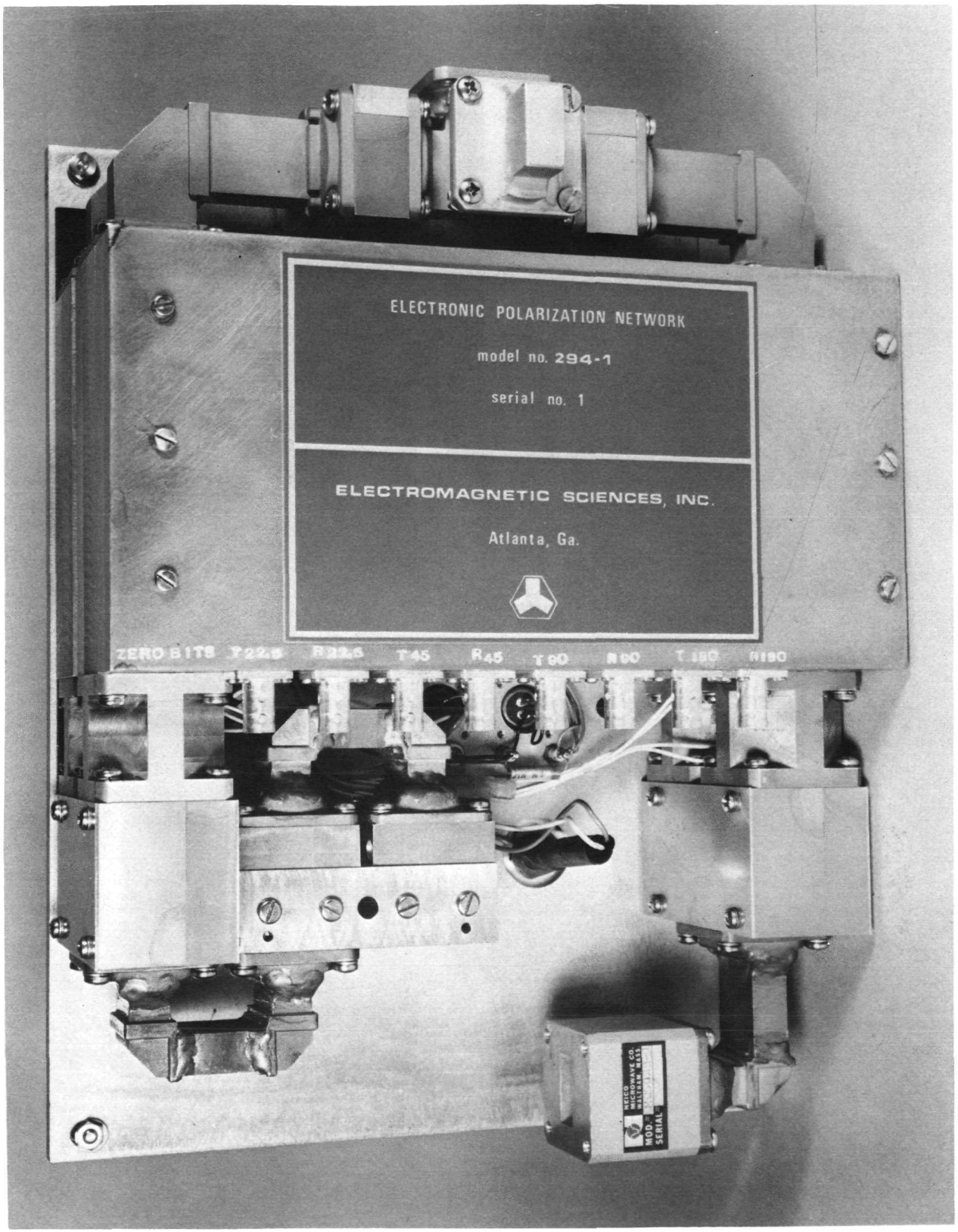

Fig. 4. Antenna polarization network, hardware

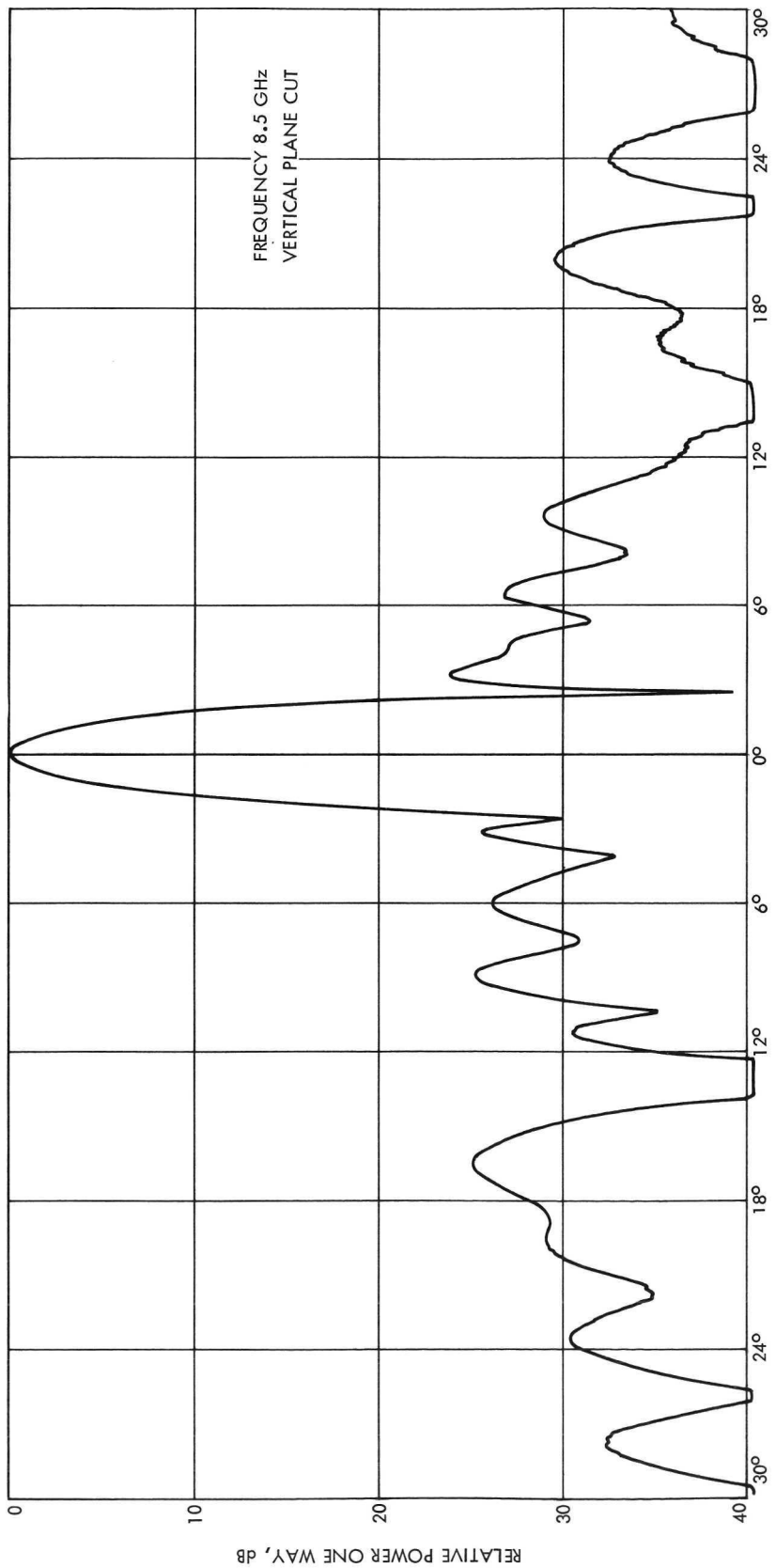

Fig. 5. Vertical plane antenna pattern

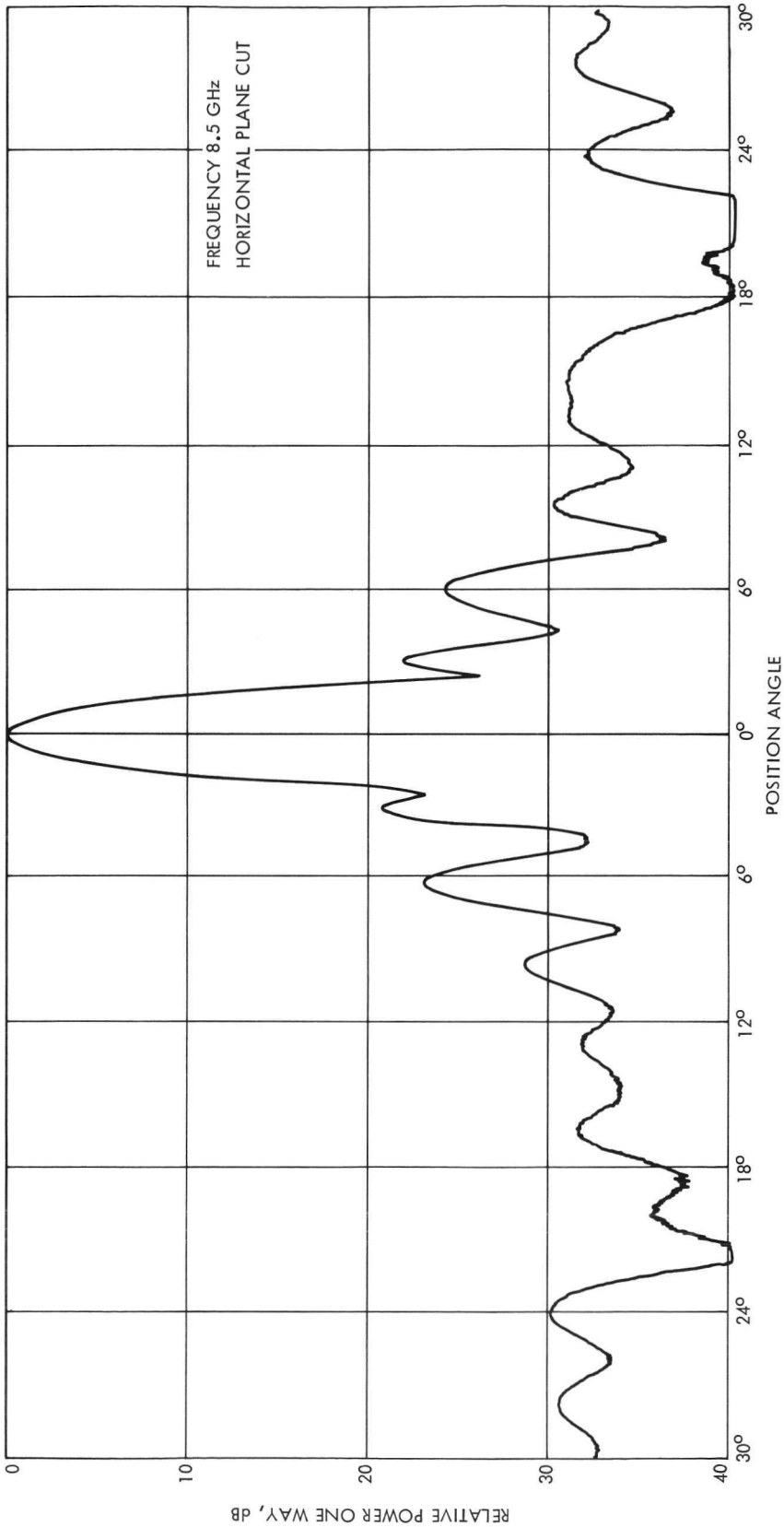

Fig. 6. Horizontal plane antenna pattern

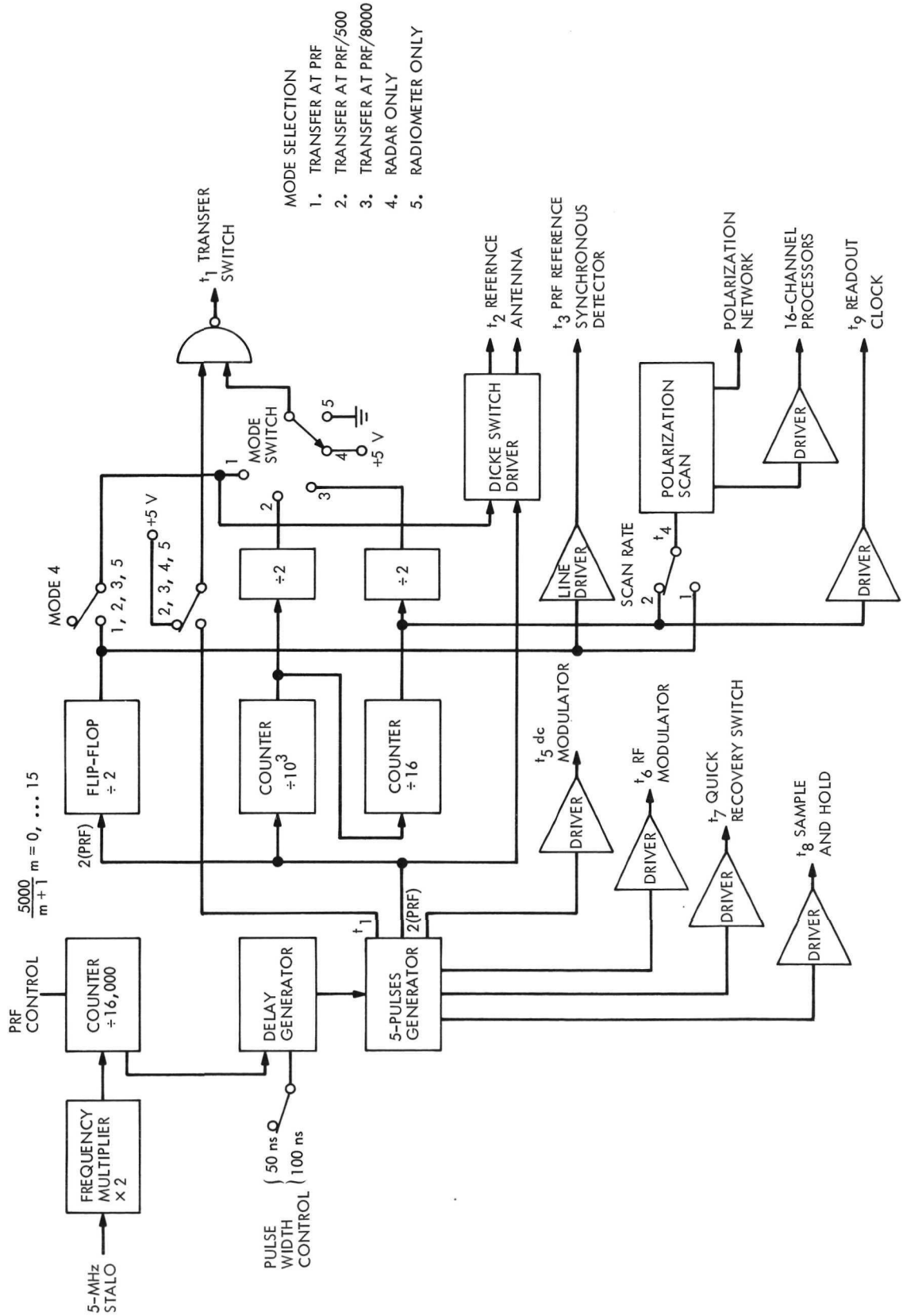

Fig. 7. Timing control functional diagram

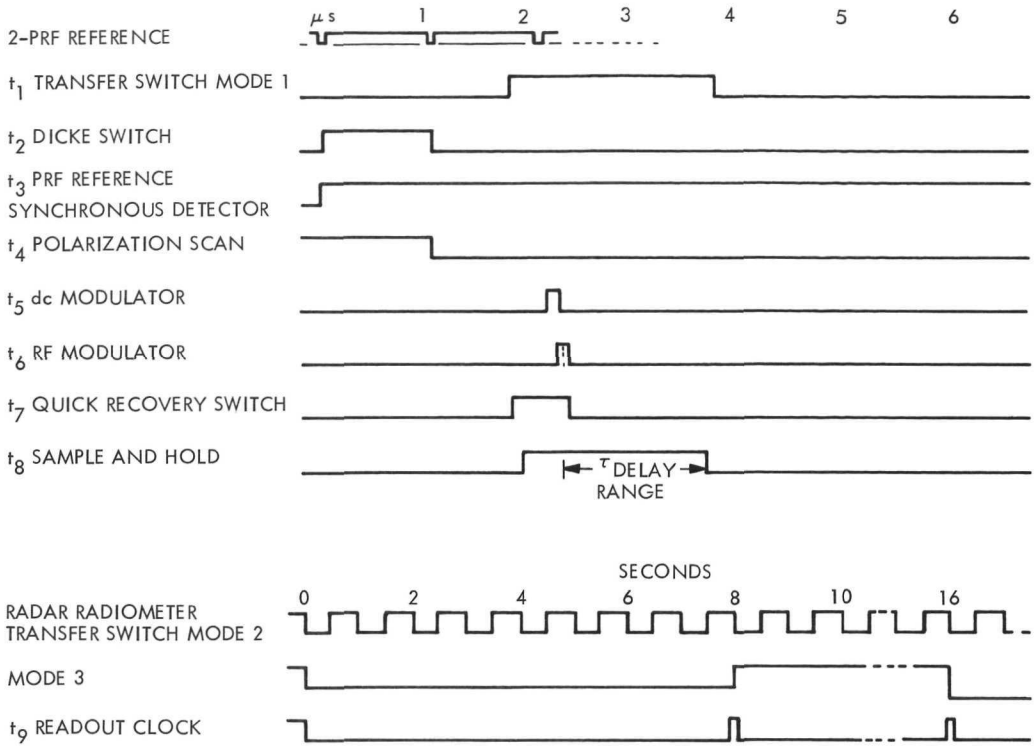

Fig. 8. Timing diagram for 1-kHz, PRF

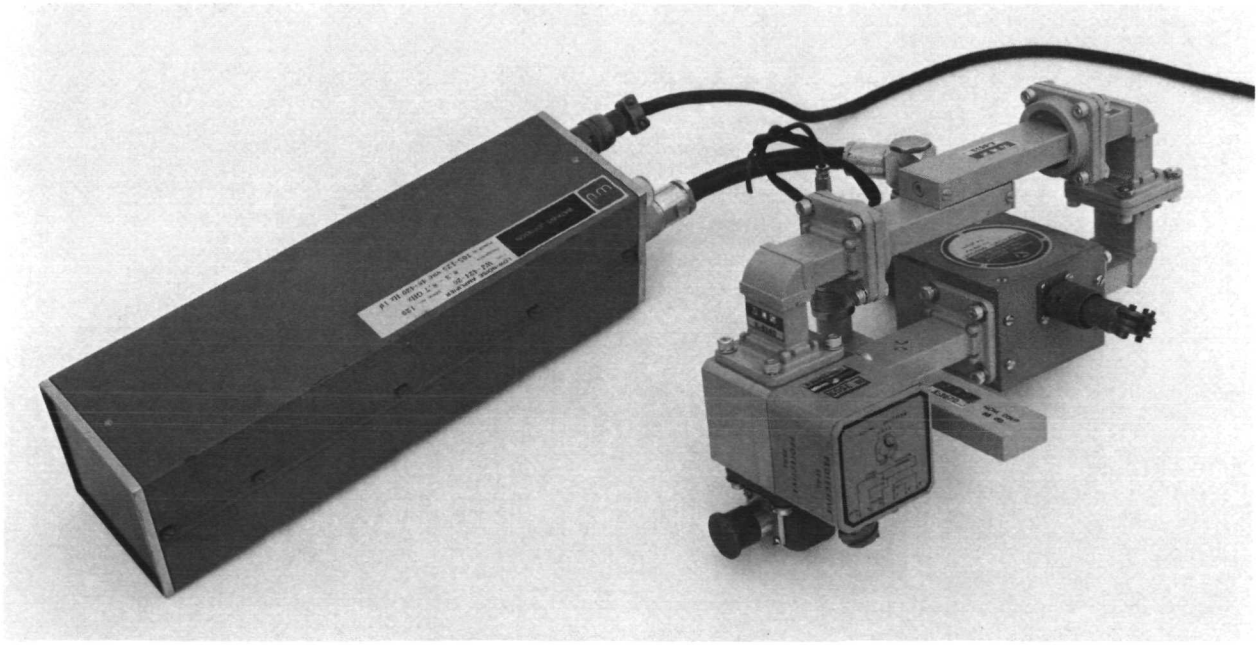

Fig. 9. TWTA and waveguide switch assembly

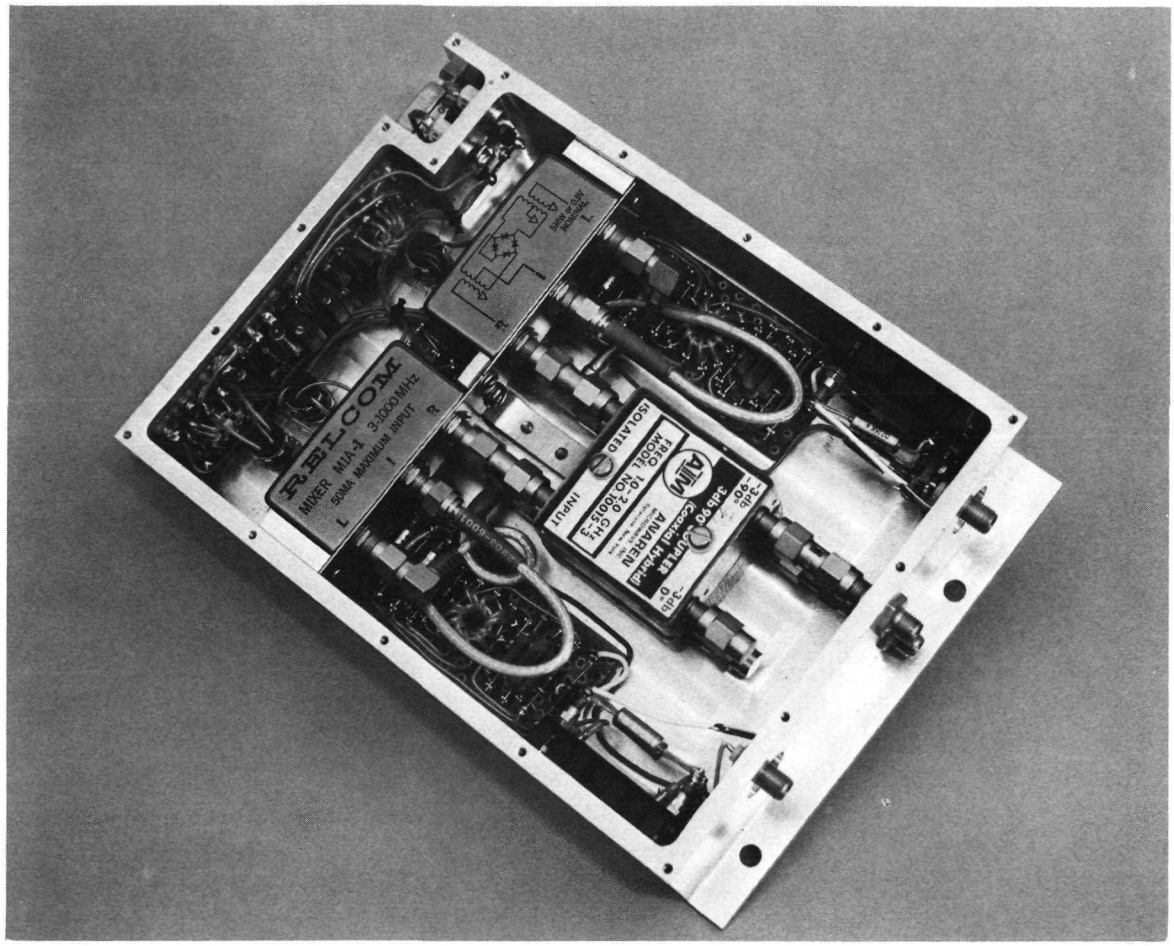

Fig. 10. Radar coherent detector-amplifier

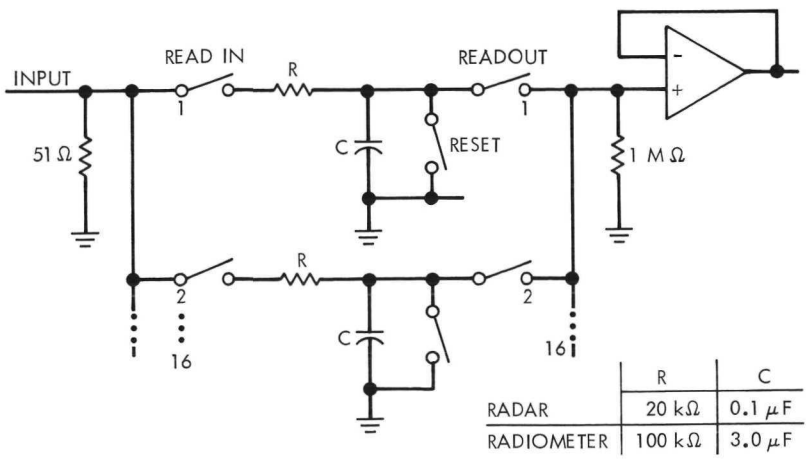

Fig. 11. 16-channel processor functional diagram

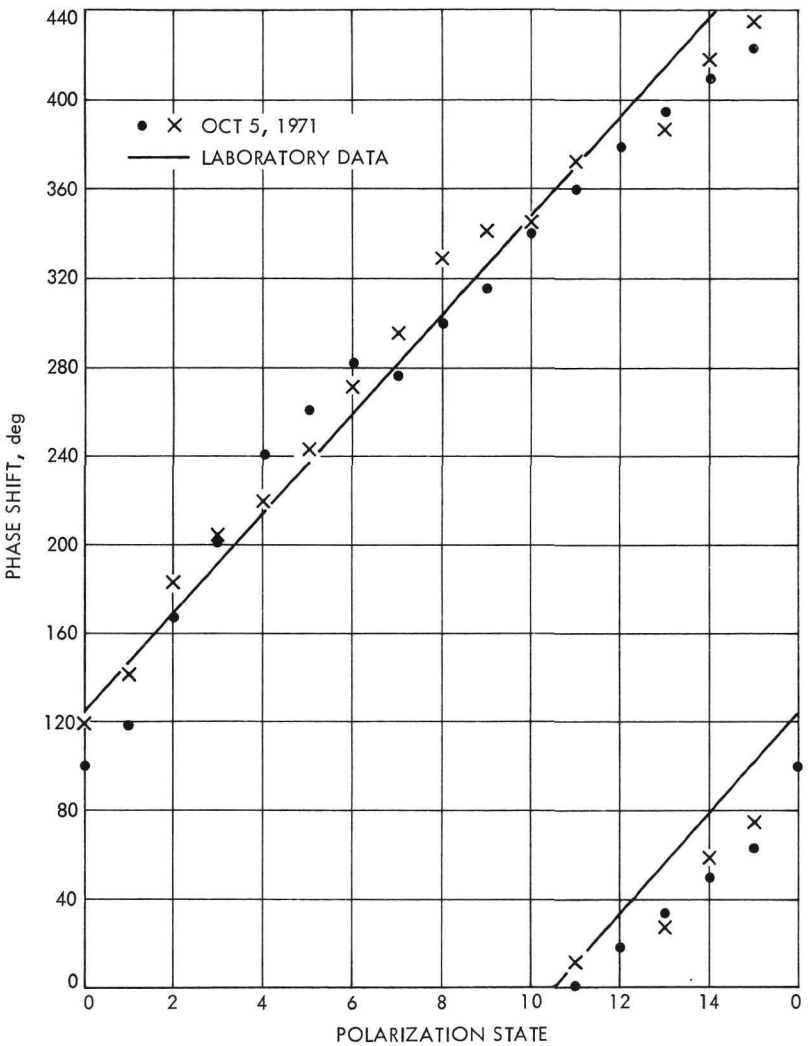

Fig. 12. Antenna calibration, transmit polarization

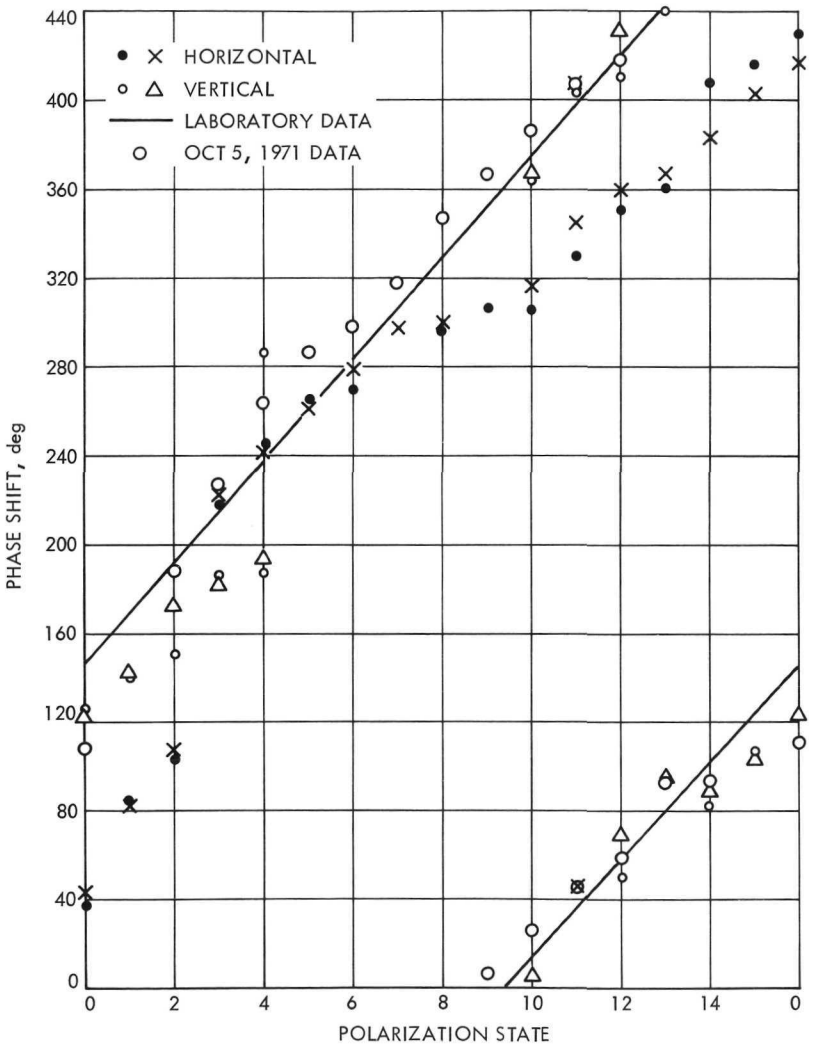

Fig. 13. Antenna calibration, receive polarization

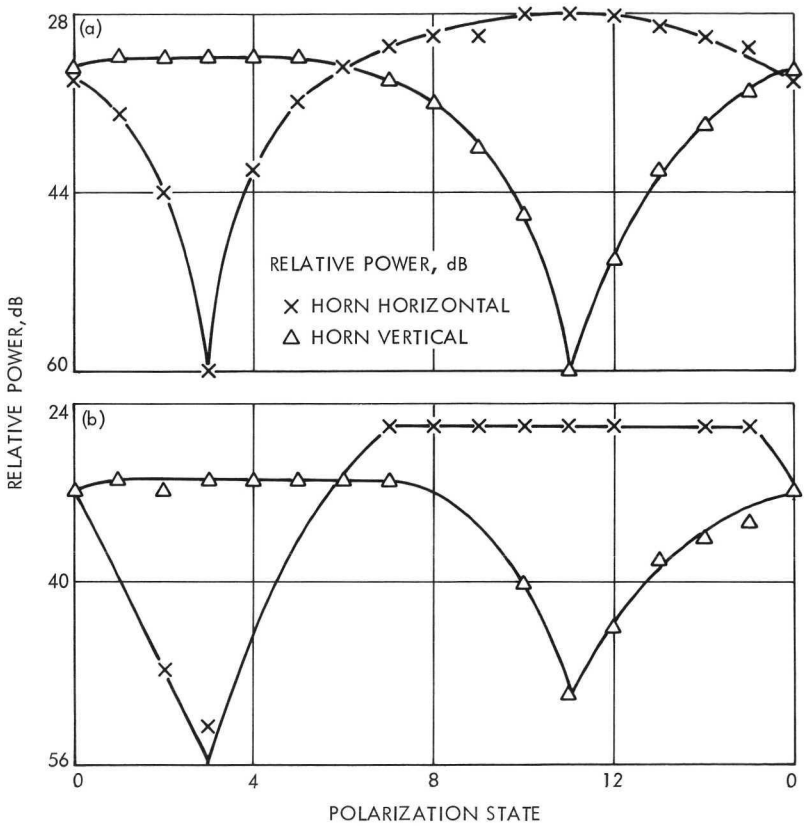

Fig. 14. Power response

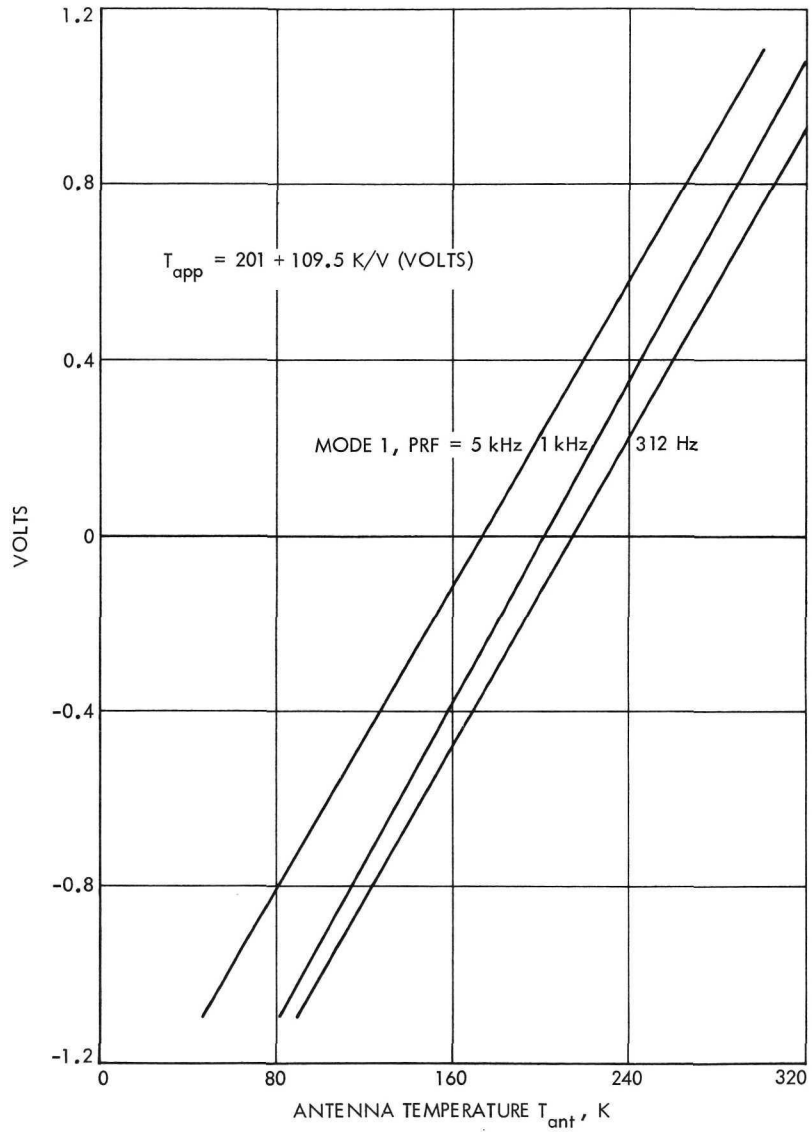

Fig. 15. Radiometer calibration

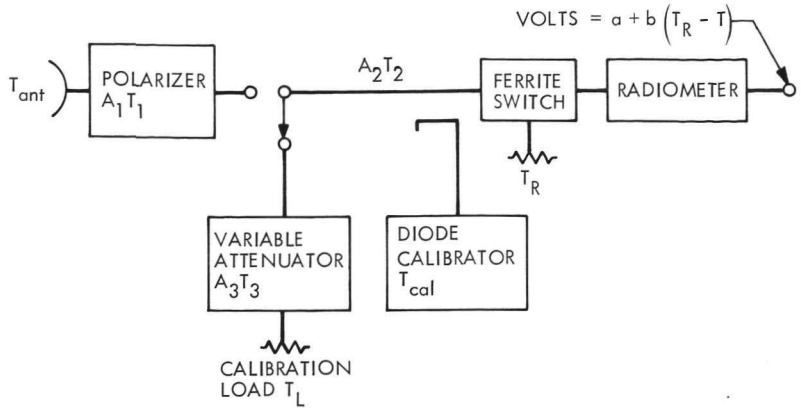

$$T_{app1} = A_2\left[A_3T_L + \left(1 - A_3\right)T_3\right] + \left(1 - A_2\right)T_2$$

$$T_{app2} = A_2\left[A_1T_{ant} + \left(1 - A_1\right)T_1\right] + \left(1 - A_2\right)T_2$$

Fig. 16. Radiometer calibration configuration

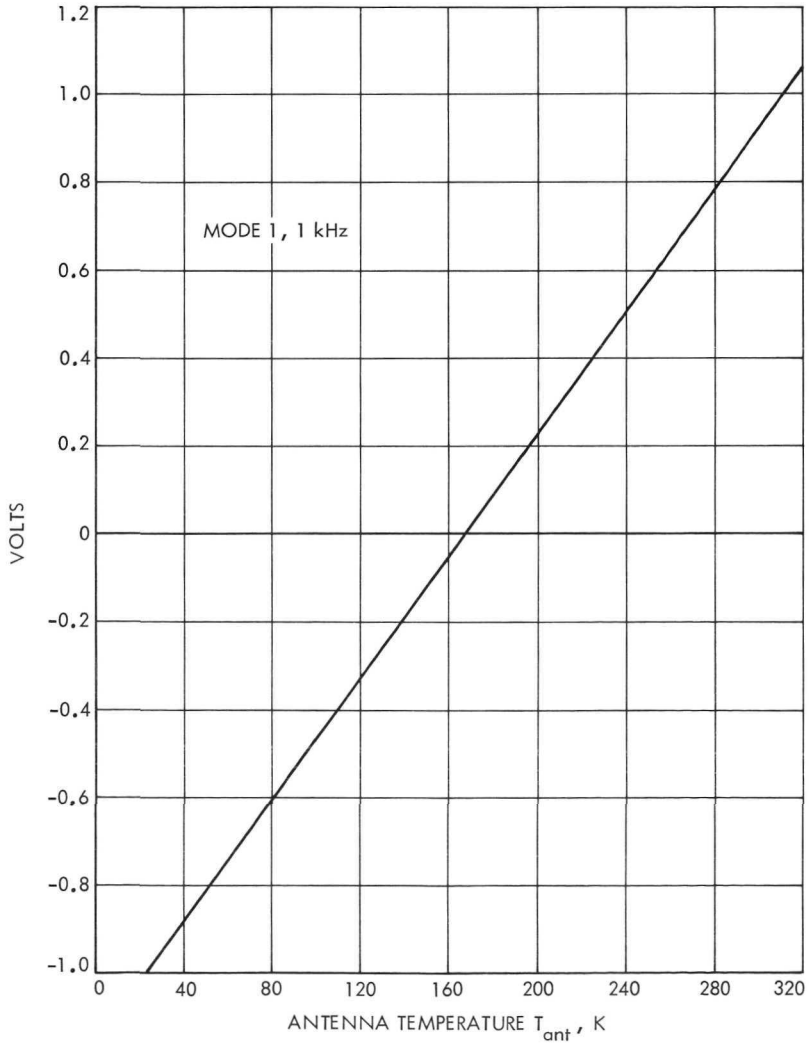

Fig. 17. Antenna temperature calibration

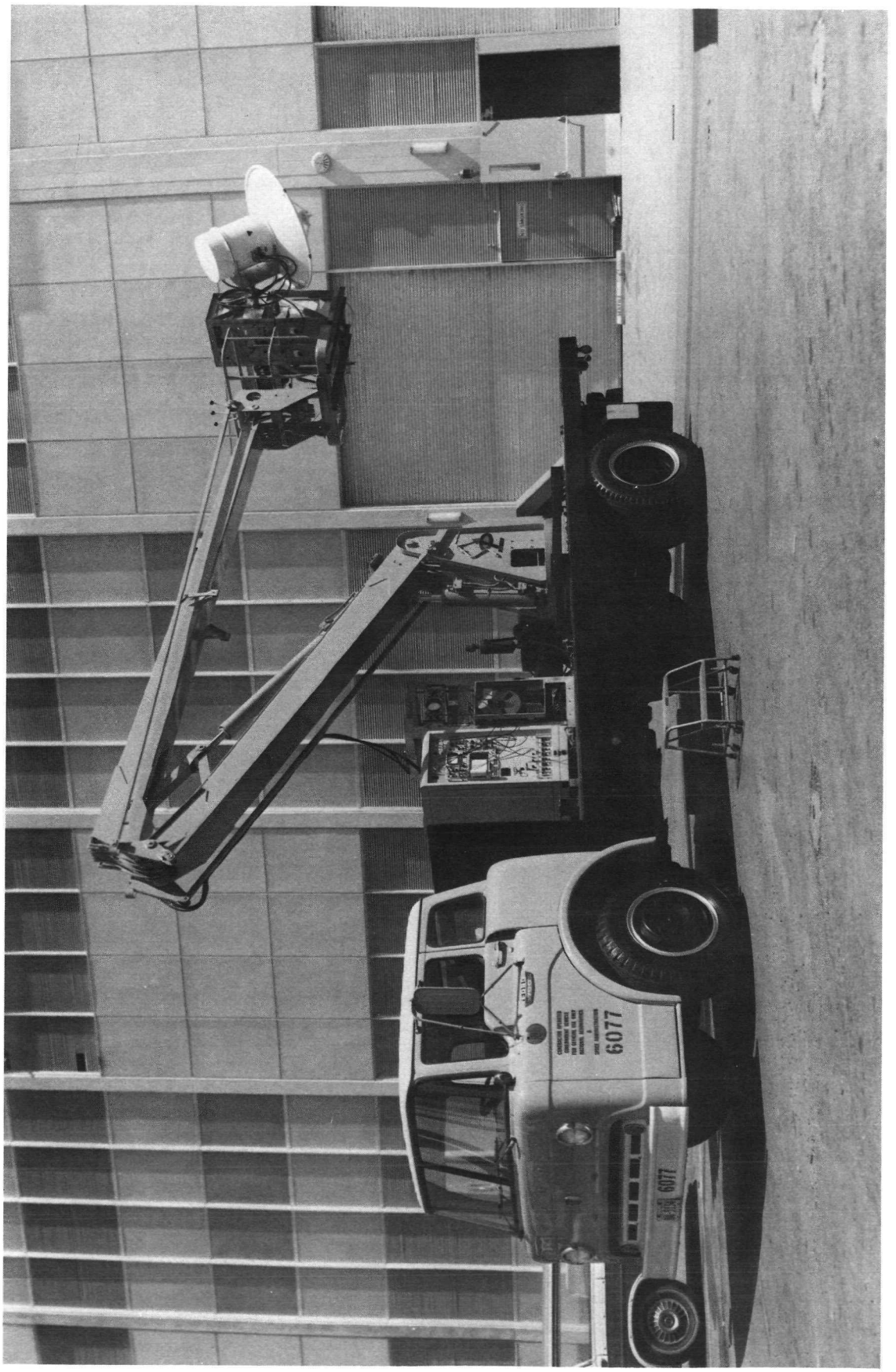

Fig. 18. Asphalt surface observed

Fig. 19. Grass surface observed

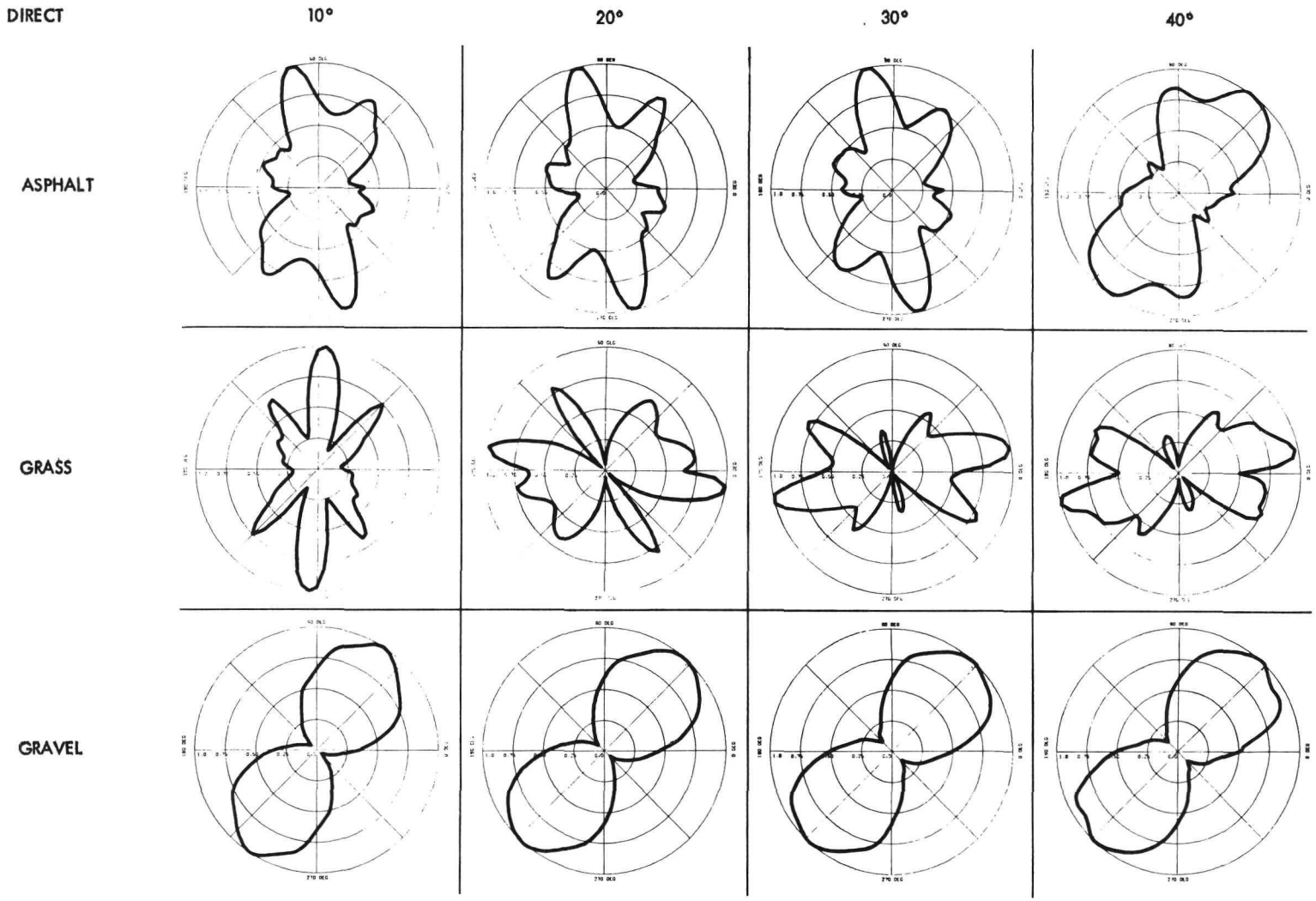

Fig. 20. Direct polarization signatures

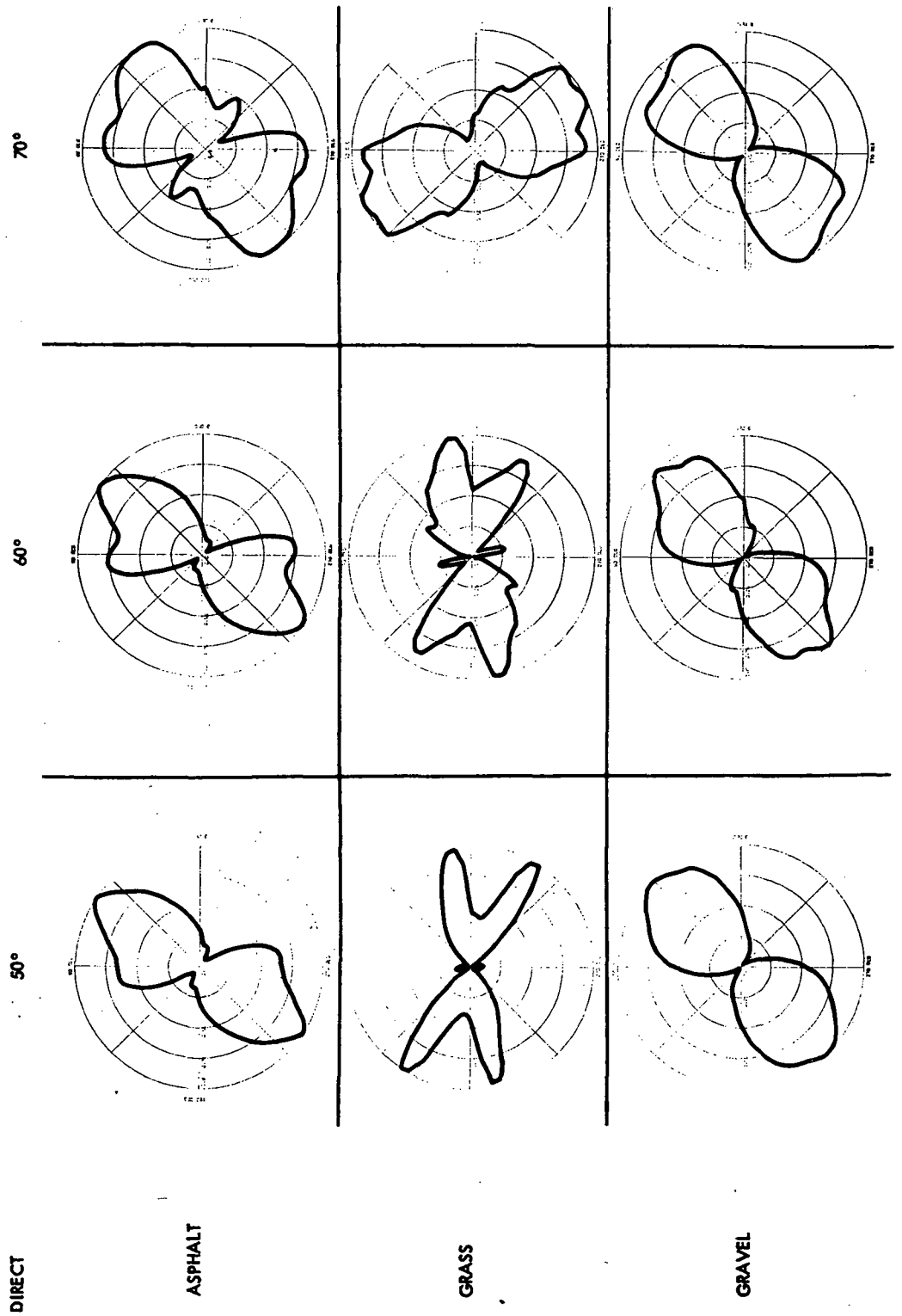

Fig. 20 (contd)

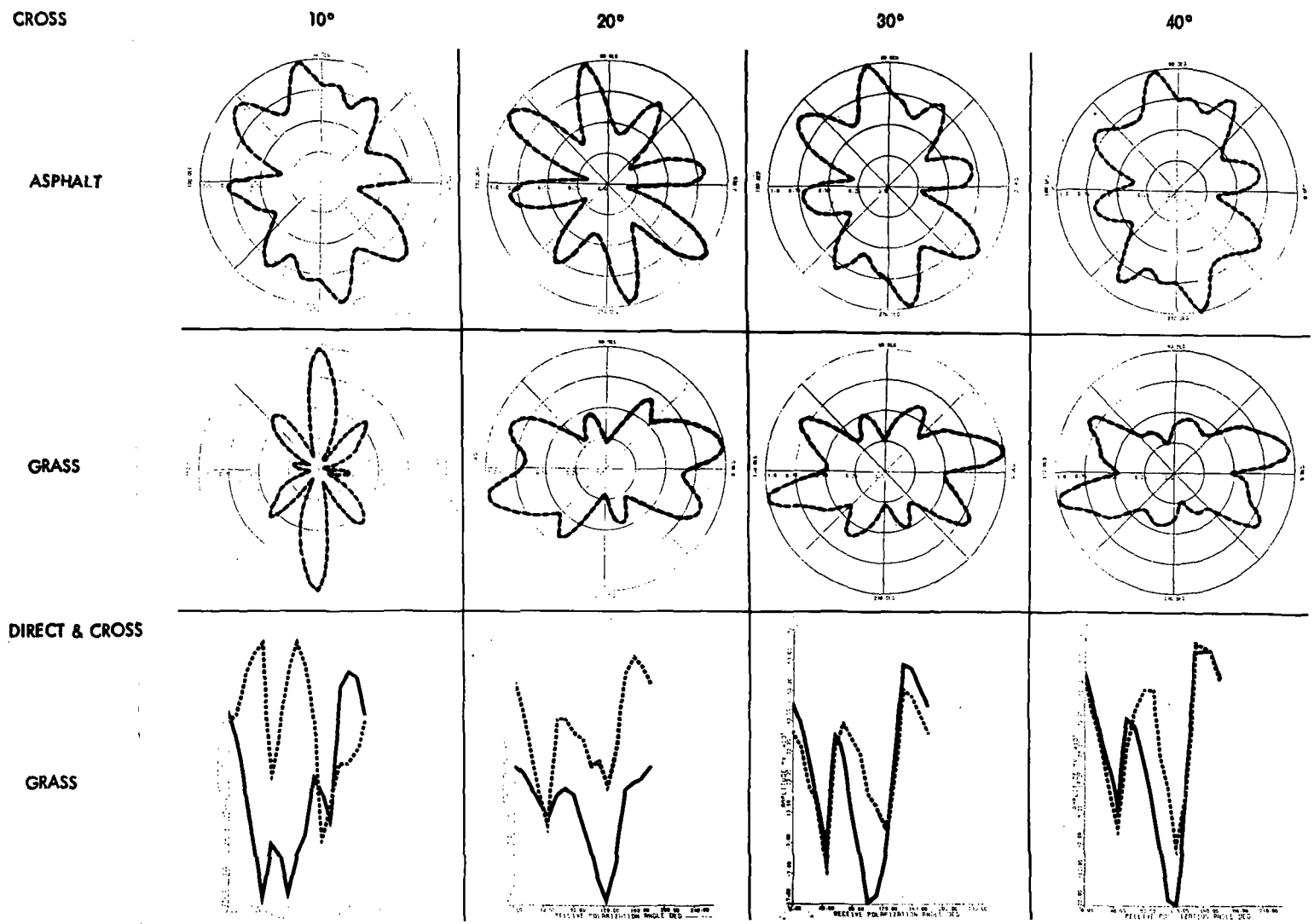

Fig. 21. Cross polarization signatures

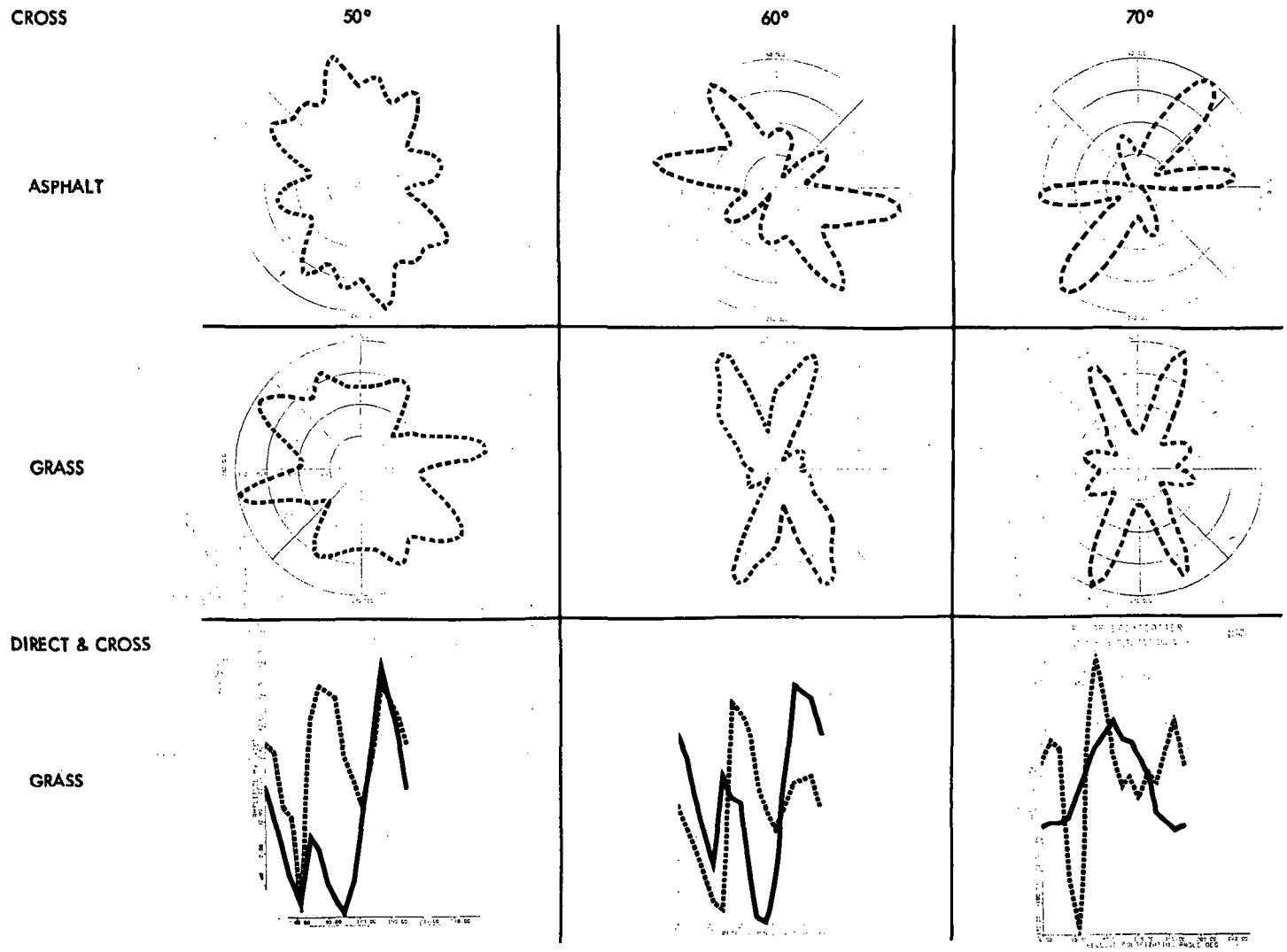

Fig. 21 (contd)

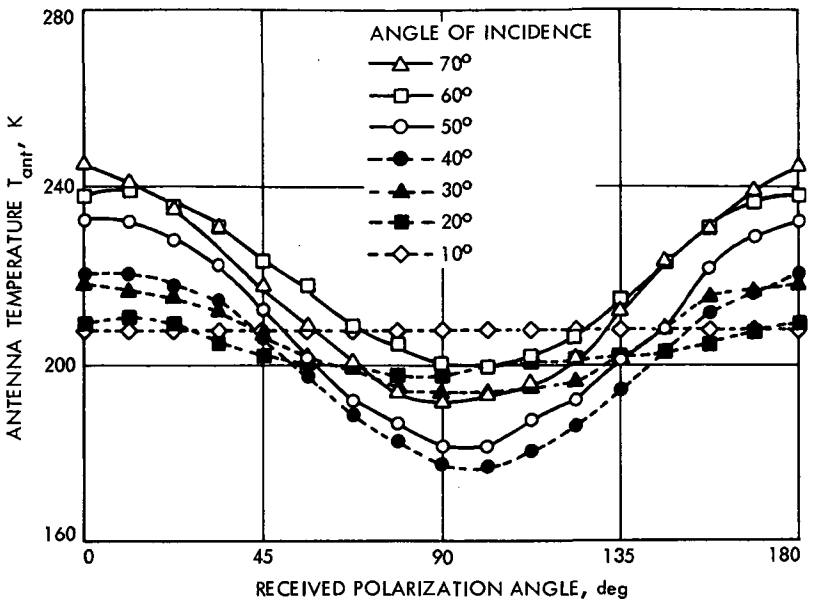

Fig. 22. Asphalt temperature vs polarization

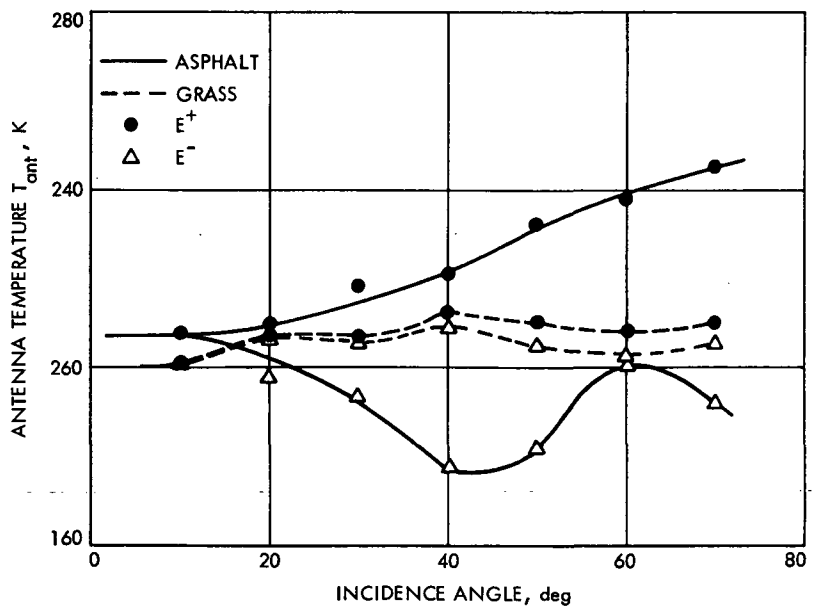

Fig. 23. Temperature of asphalt and grass vs incidence angle

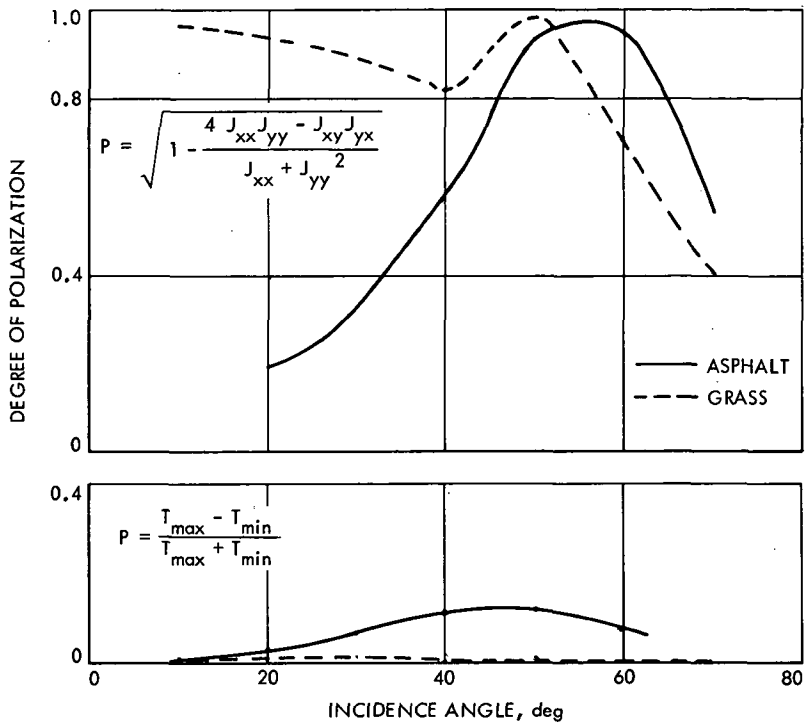

Fig. 24. Degree of polarization vs incidence angle

APPENDIX. COMPUTER PLOTS

The radar-radiometer made observations of asphalt, grass, and gravel on April 17 and March 15, 1972, and December 9, 1971, respectively. For all the surfaces, the equipment was operated in Mode 1, 1 kHz PRF, 100 ns pulse width, and slow polarization scan. For the gravel surface, the transmit polarization was vertical, i.e., parallel to the plane of incidence. For the other two surfaces, the transmit polarization was scanned in synchronism with the receive polarization and both direct and cross-polarized states were recorded sequentially. The computer was programmed to plot the radar data in units of the detected voltage as a function of polarization angle with no smoothing. The scales were selected to show the maximum amount of variation. The radiometer data were similarly plotted except the voltage units were changed to antenna temperature by the calibration of Fig. 17. For a summary of the antenna temperatures for asphalt, see Fig. 22.

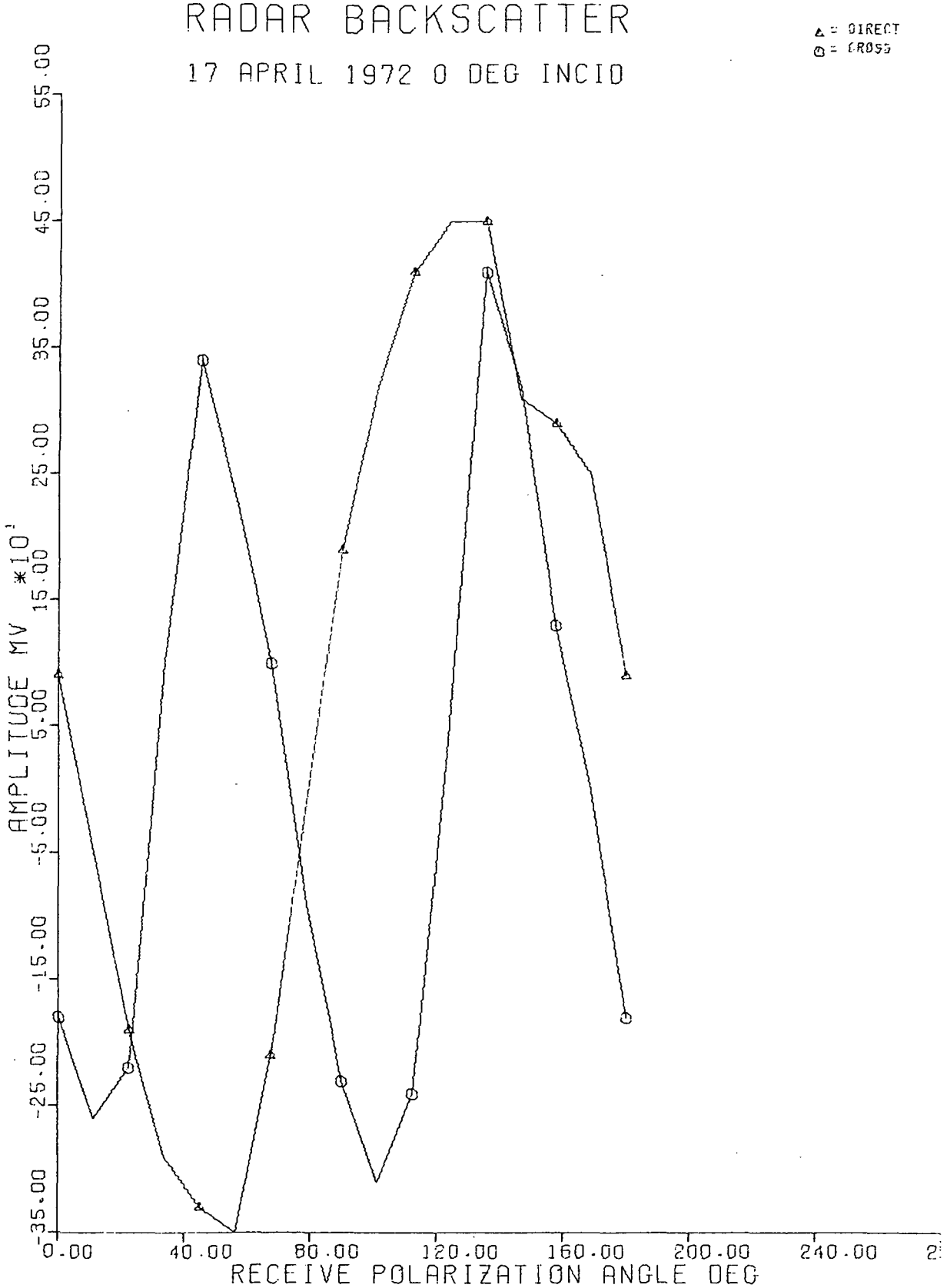
RADAR BACKSCATTER
17 APRIL 1972 0 DEG INCID
△ = DIRECT
○ = CROSS
AMPLITUDE MV *10¹
55.00
45.00
35.00
25.00
15.00
5.00
-5.00
-15.00
-25.00
-35.00
0.00
40.00
80.00
120.00
160.00
200.00
240.00
RECEIVE POLARIZATION ANGLE DEG

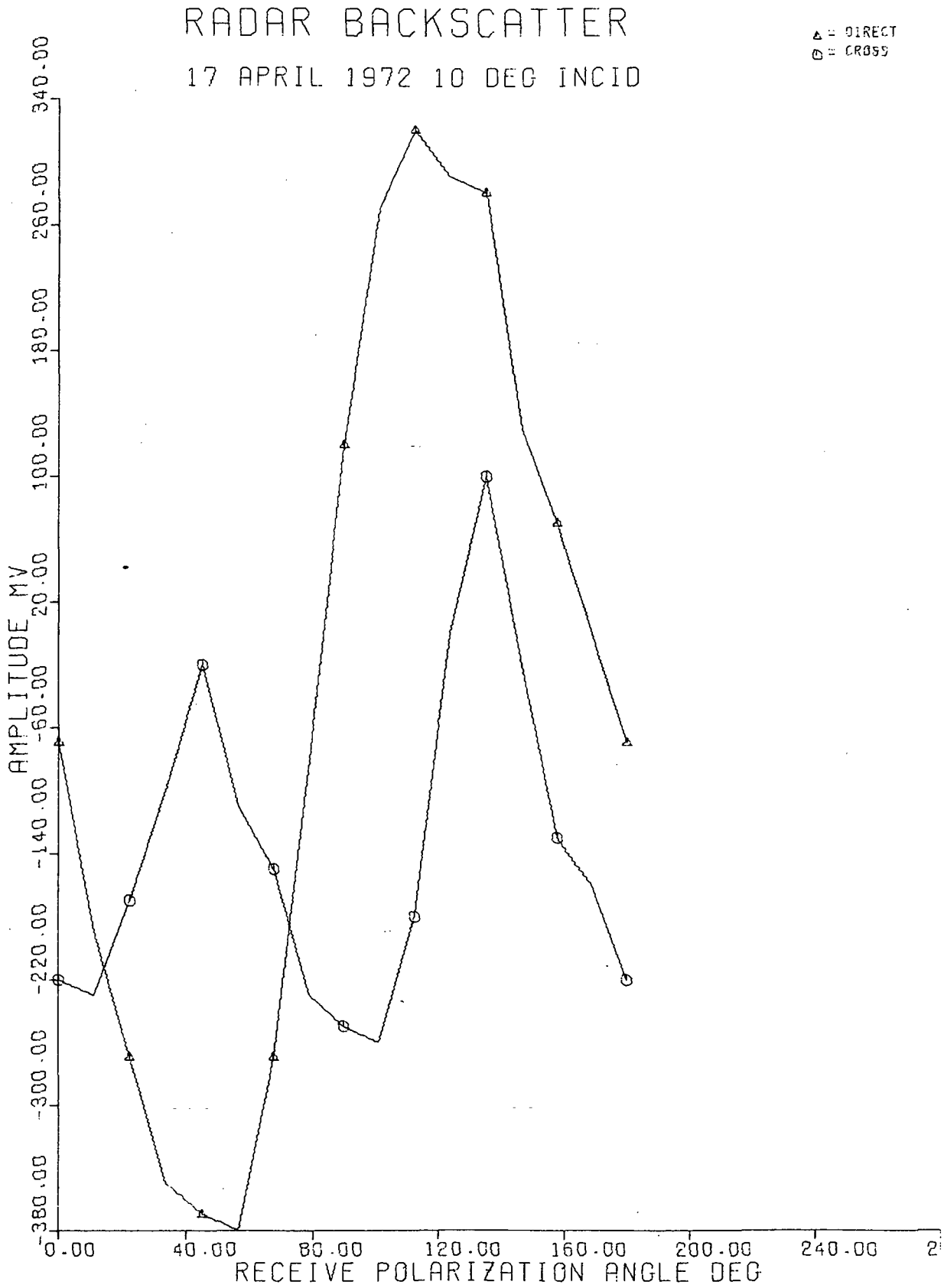
RADAR BACKSCATTER
17 APRIL 1972 10 DEG INCID
△ = DIRECT
○ = CROSS
AMPLITUDE MV
340.00
260.00
180.00
100.00
20.00
-60.00
-140.00
-220.00
-300.00
-380.00
0.00
40.00
80.00
120.00
160.00
200.00
240.00
RECEIVE POLARIZATION ANGLE DEG

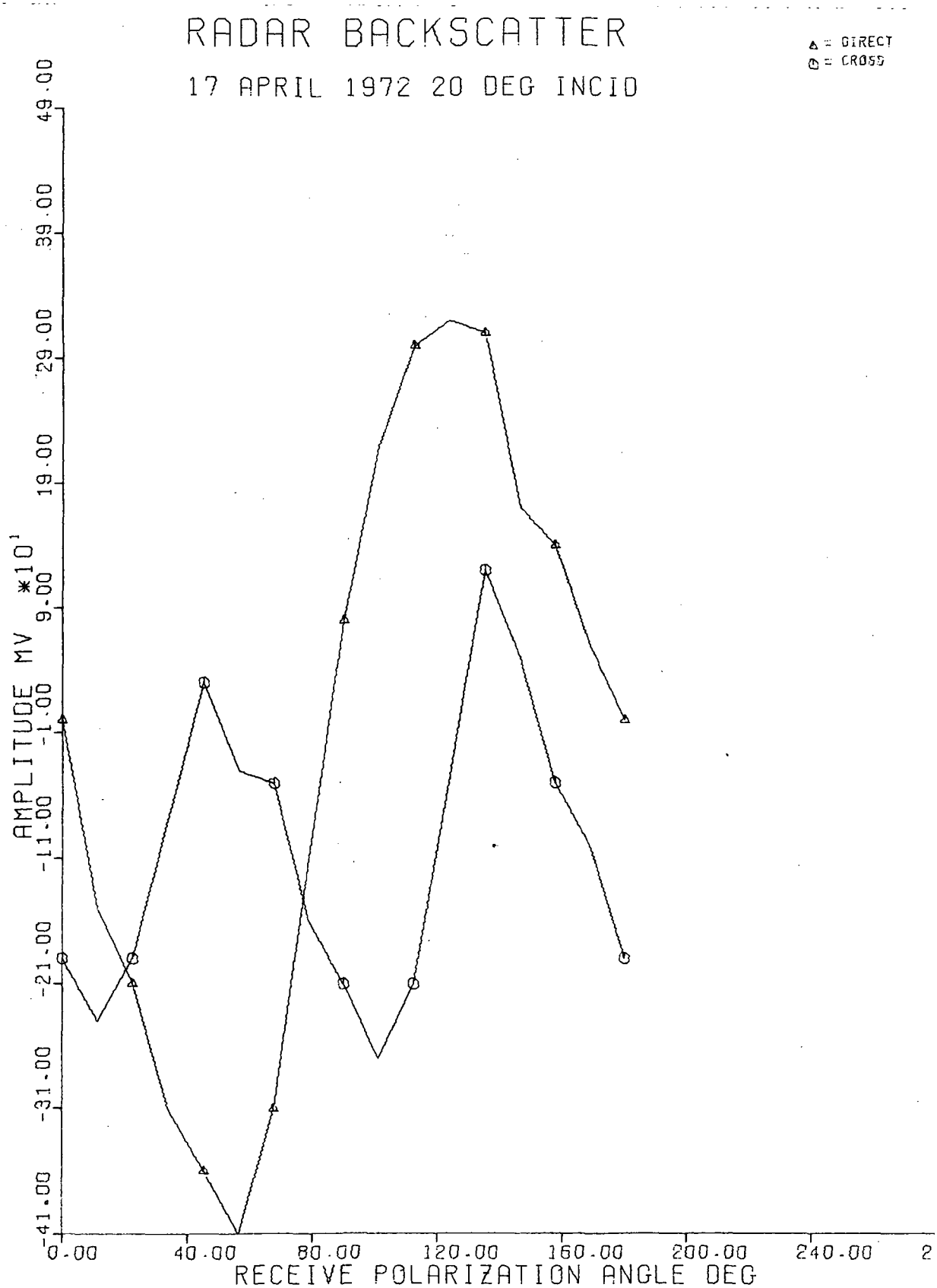
RADAR BACKSCATTER
17 APRIL 1972 20 DEG INCID
△ = DIRECT
○ = CROSS
AMPLITUDE MV *10¹
49.00
39.00
29.00
19.00
9.00
-1.00
-11.00
-21.00
-31.00
-41.00
0.00
40.00
80.00
120.00
160.00
200.00
240.00
RECEIVE POLARIZATION ANGLE DEG

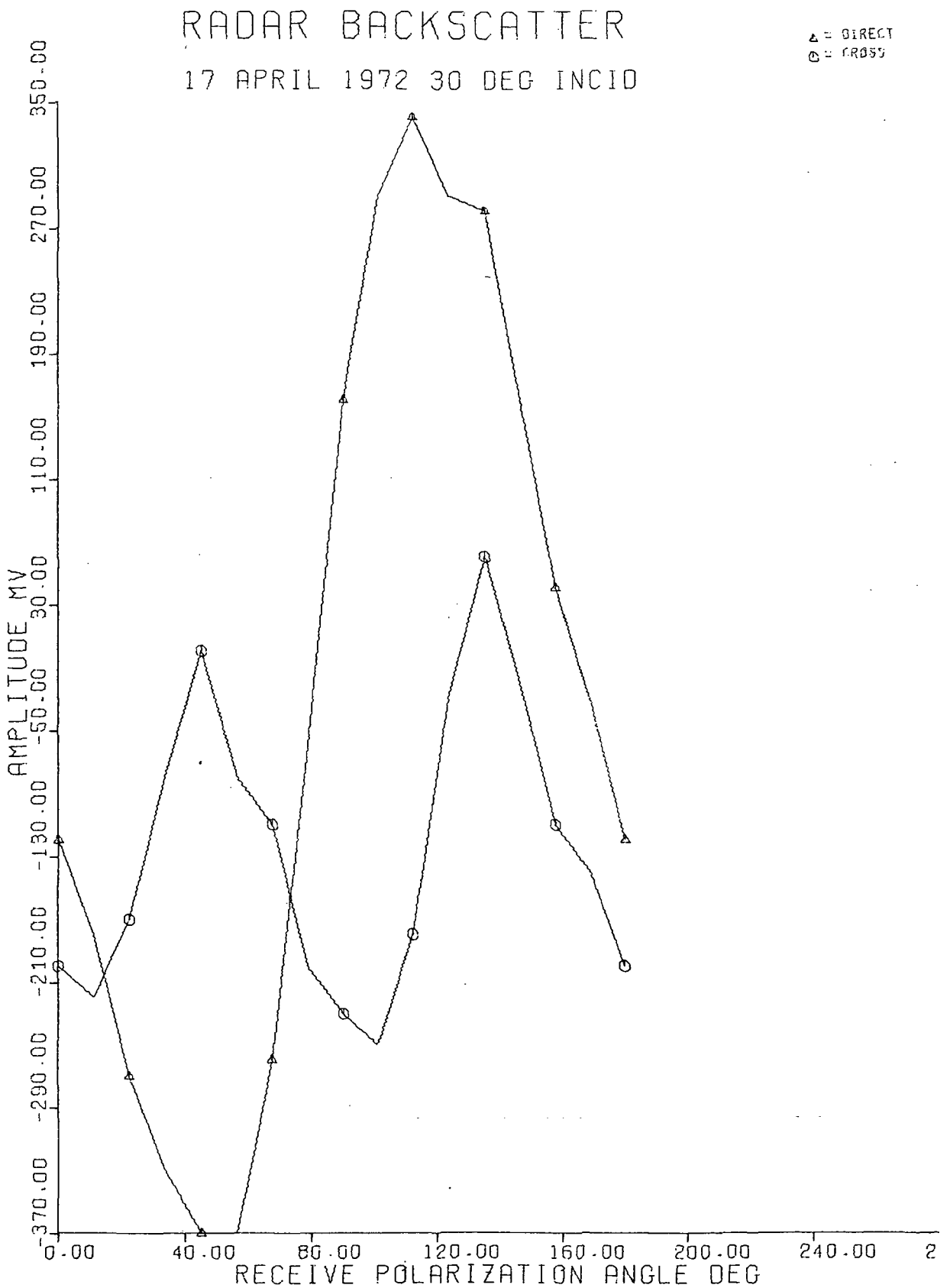
RADAR BACKSCATTER
17 APRIL 1972 30 DEG INCID
△ = DIRECT
○ = CROSS
AMPLITUDE MV
350.00
270.00
190.00
110.00
30.00
-50.00
-130.00
-210.00
-290.00
-370.00
0.00
40.00
80.00
120.00
160.00
200.00
240.00
RECEIVE POLARIZATION ANGLE DEG

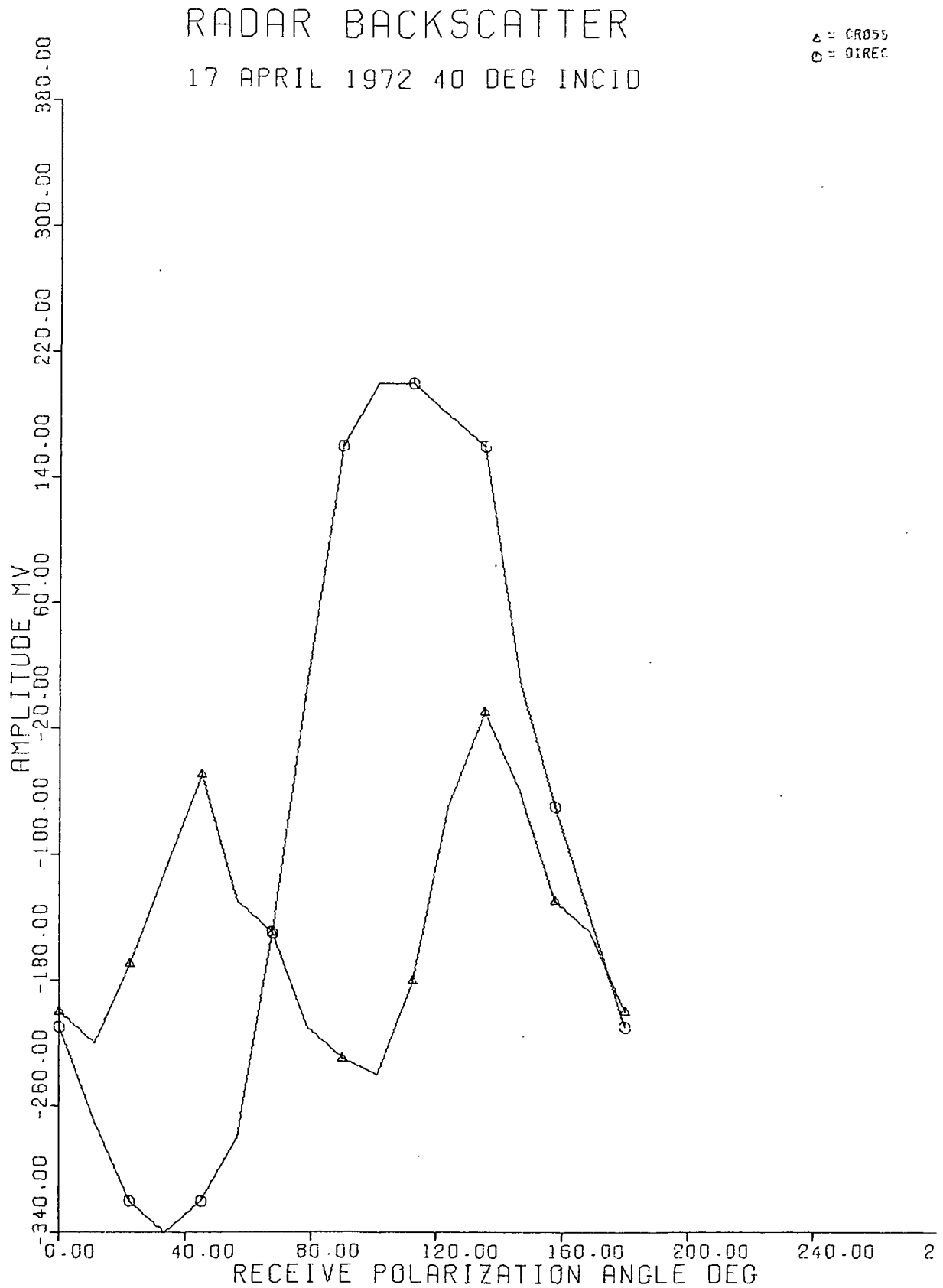
RADAR BACKSCATTER
17 APRIL 1972 40 DEG INCID
△ = CROSS
○ = DIREC
AMPLITUDE MV
380.00
300.00
220.00
140.00
60.00
-20.00
-100.00
-180.00
-260.00
-340.00
0.00
40.00
80.00
120.00
160.00
200.00
240.00
RECEIVE POLARIZATION ANGLE DEG

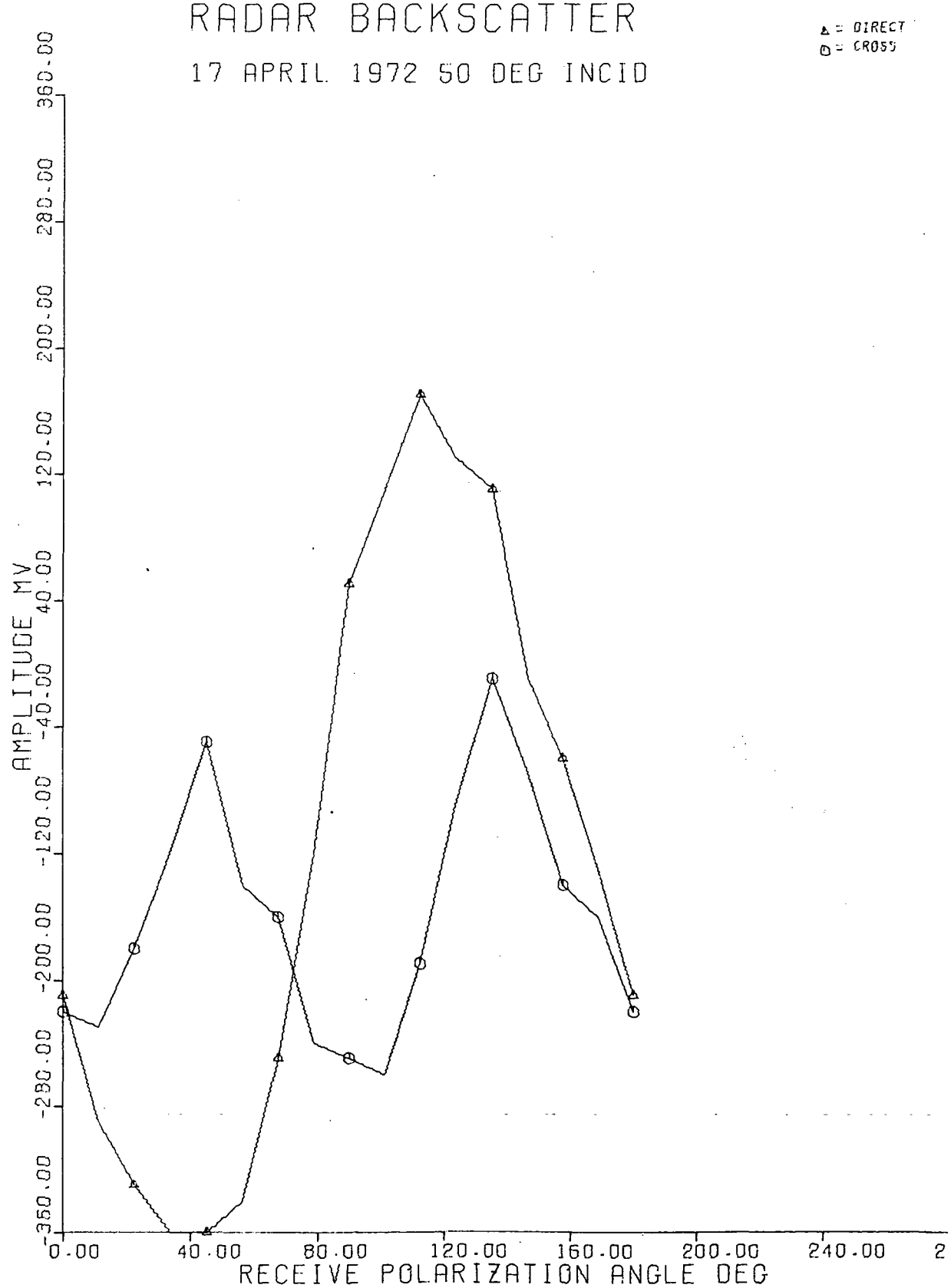
RADAR BACKSCATTER
17 APRIL 1972 50 DEG INCID
▲ = DIRECT
⊙ = CROSS
AMPLITUDE MV
360.00
280.00
200.00
120.00
40.00
-40.00
-120.00
-200.00
-280.00
-350.00
0.00
40.00
80.00
120.00
160.00
200.00
240.00
2
RECEIVE POLARIZATION ANGLE DEG

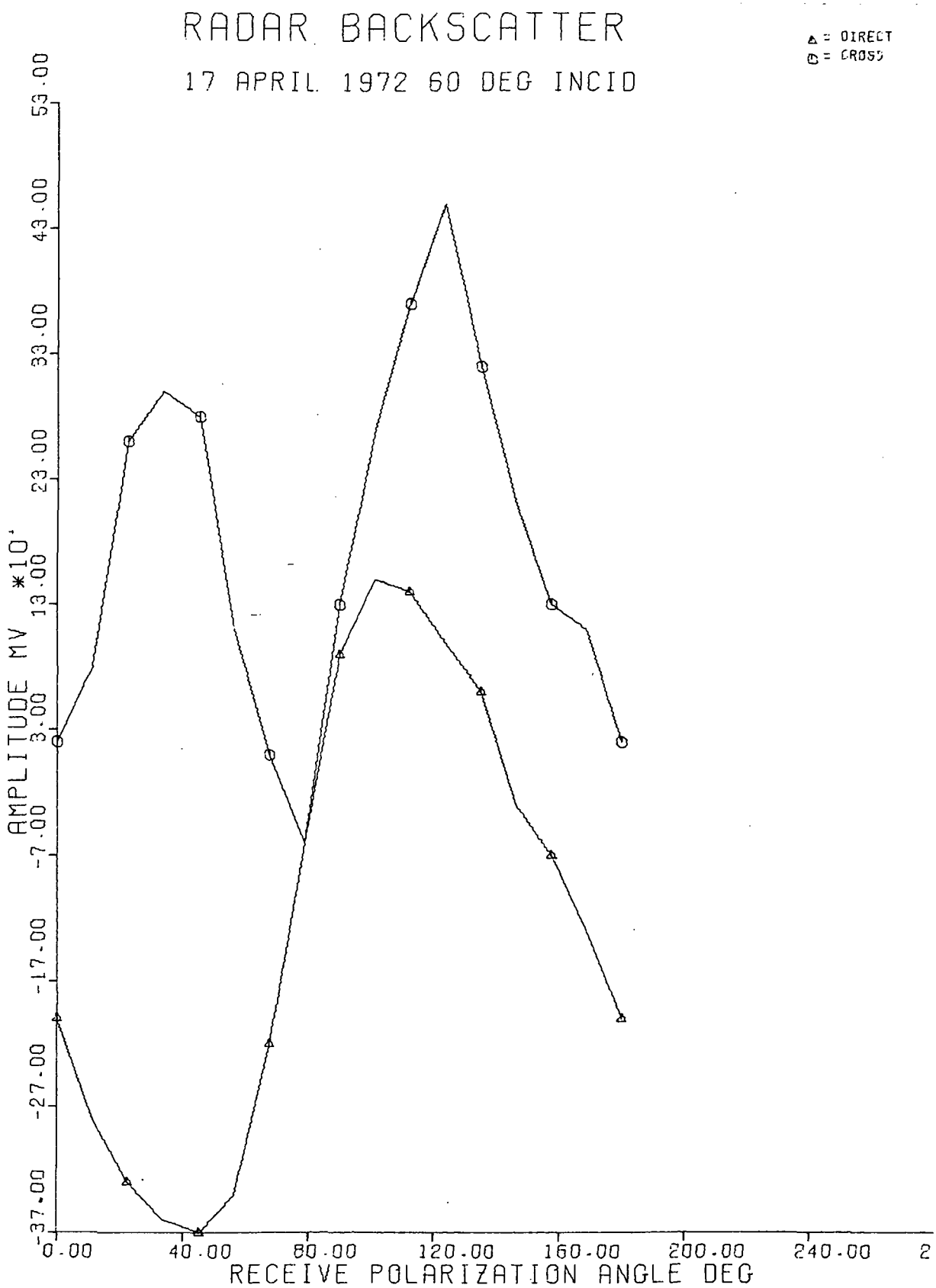
RADAR BACKSCATTER
17 APRIL 1972 60 DEG INCID
△ = DIRECT
○ = CROSS
AMPLITUDE MV *10'
53.00
43.00
33.00
23.00
13.00
3.00
-7.00
-17.00
-27.00
-37.00
0.00
40.00
80.00
120.00
160.00
200.00
240.00
RECEIVE POLARIZATION ANGLE DEG

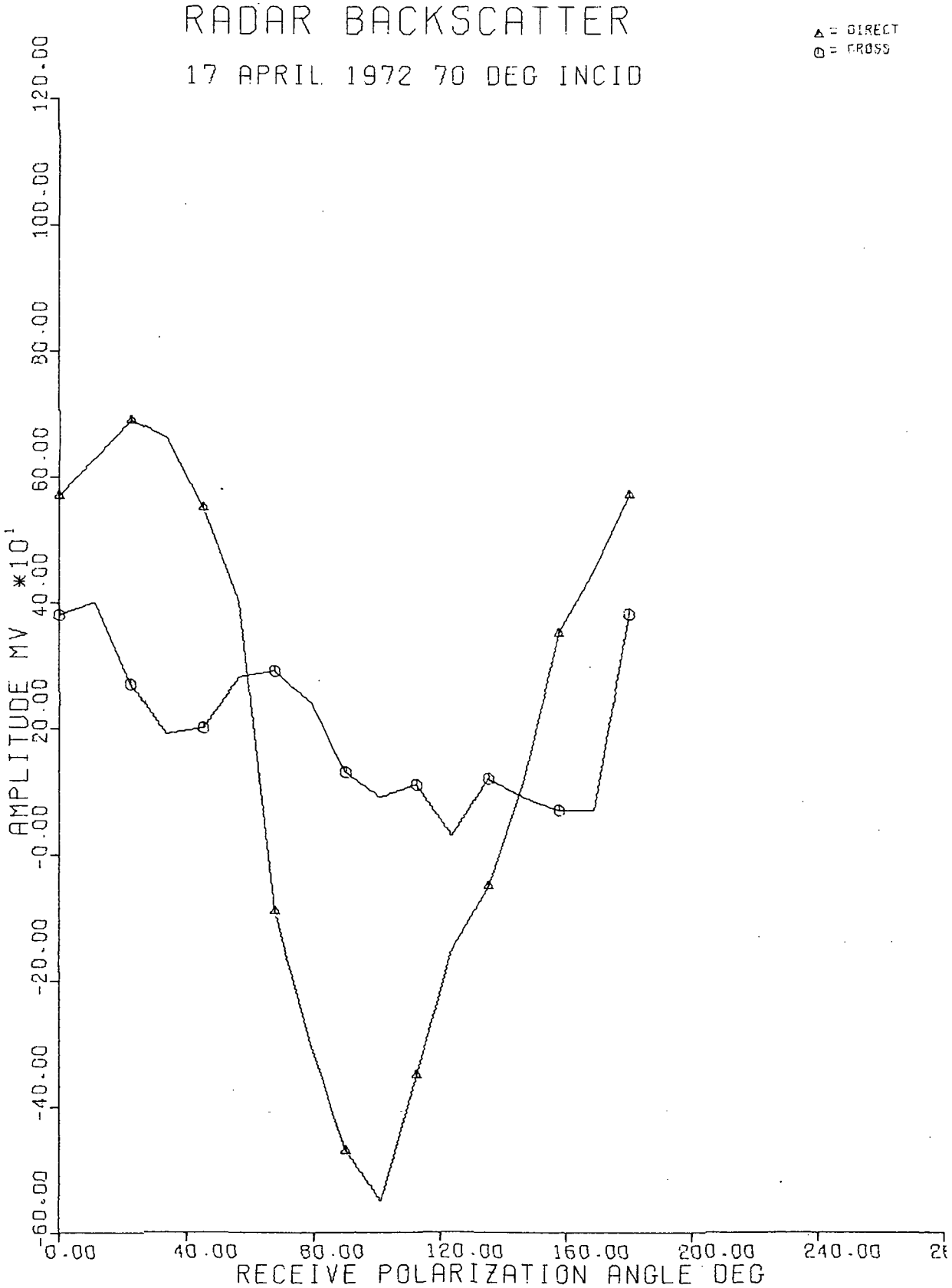
RADAR BACKSCATTER
17 APRIL 1972 70 DEG INCID
△ = DIRECT
⊙ = CROSS
AMPLITUDE MV *10¹
120.00
100.00
80.00
60.00
40.00
20.00
-0.00
-20.00
-40.00
-60.00
0.00
40.00
80.00
120.00
160.00
200.00
240.00
RECEIVE POLARIZATION ANGLE DEG

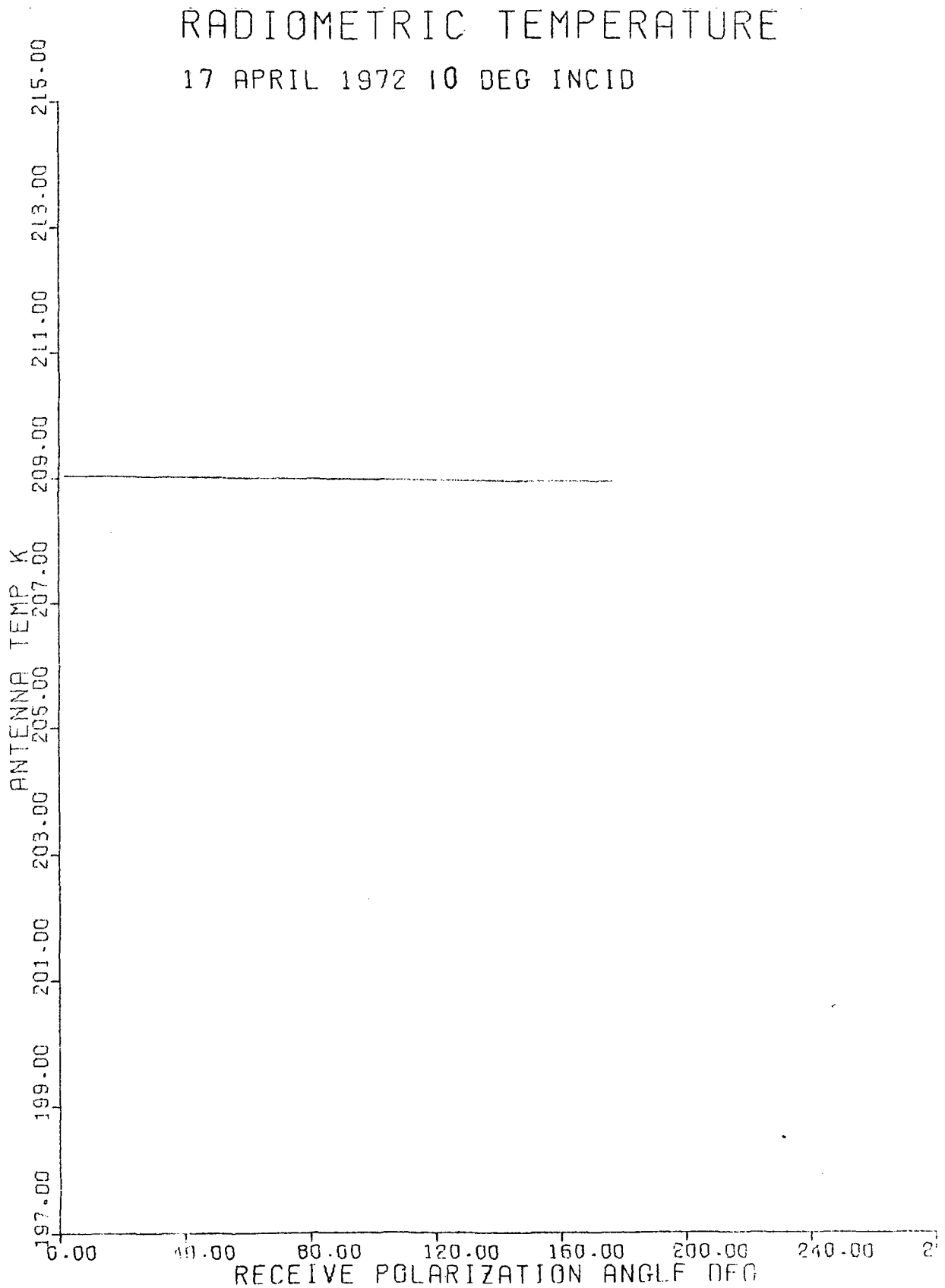
RADIOMETRIC TEMPERATURE
17 APRIL 1972 10 DEG INCID
ANTENNA TEMP K
215.00
213.00
211.00
209.00
207.00
205.00
203.00
201.00
199.00
197.00
0.00
40.00
80.00
120.00
160.00
200.00
240.00
RECEIVE POLARIZATION ANGLE DEG

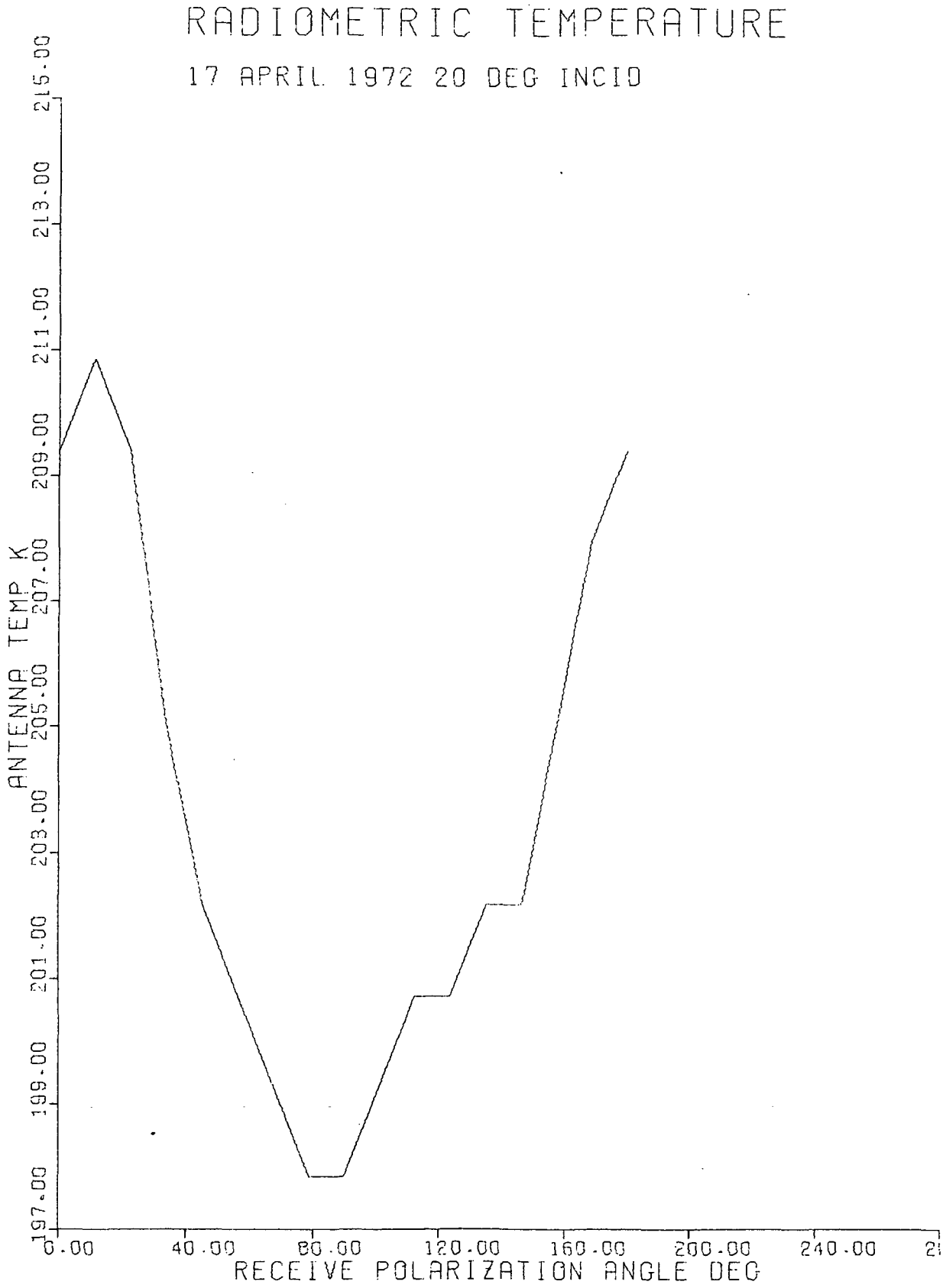
RADIOMETRIC TEMPERATURE
17 APRIL 1972 20 DEG INCID
ANTENNA TEMP K
197.00
199.00
201.00
203.00
205.00
207.00
209.00
211.00
213.00
215.00
0.00
40.00
80.00
120.00
160.00
200.00
240.00
RECEIVE POLARIZATION ANGLE DEG

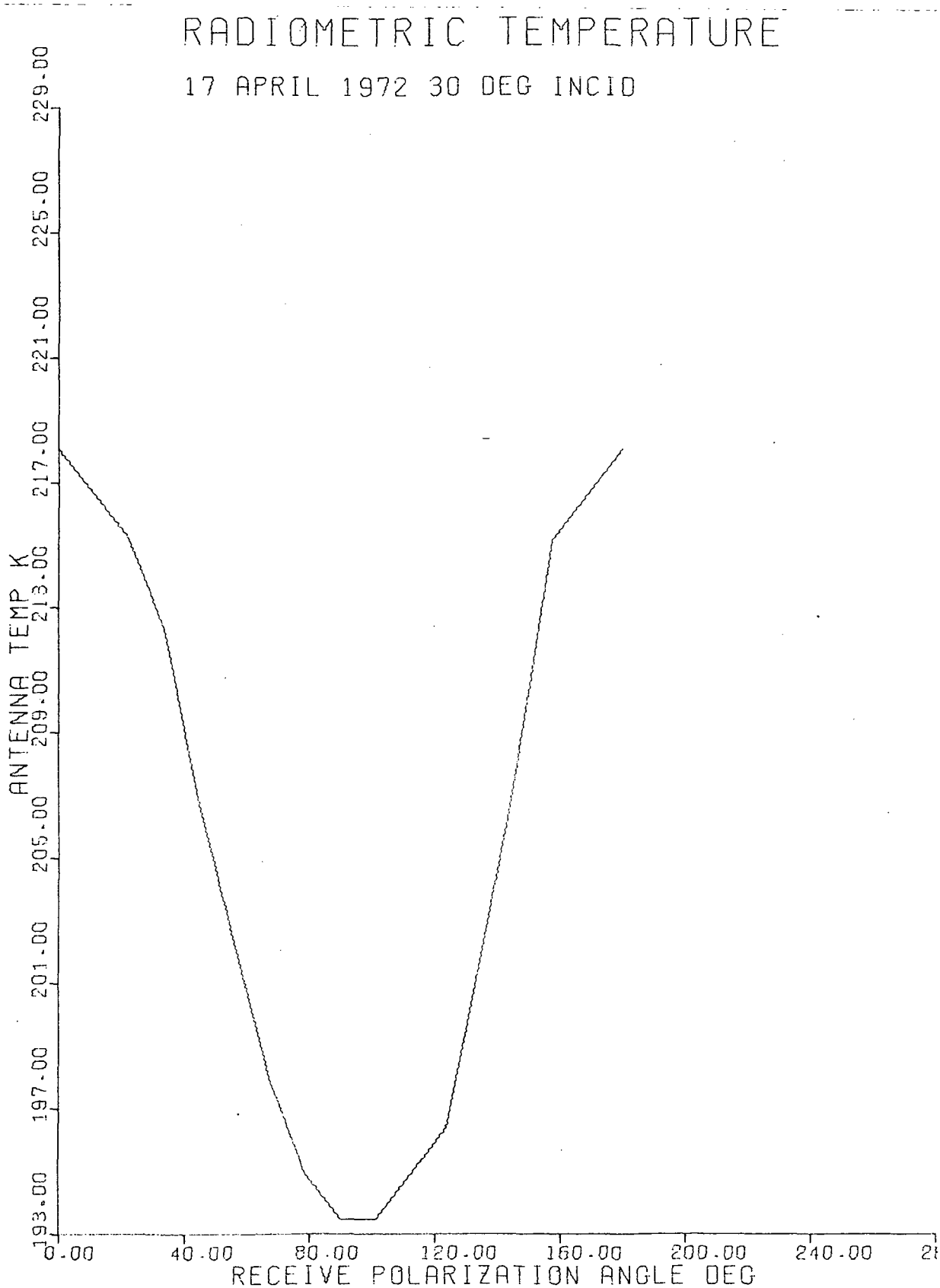
RADIOMETRIC TEMPERATURE
17 APRIL 1972 30 DEG INCID
ANTENNA TEMP K
229.00
225.00
221.00
217.00
213.00
209.00
205.00
201.00
197.00
193.00
0.00
40.00
80.00
120.00
160.00
200.00
240.00
RECEIVE POLARIZATION ANGLE DEG

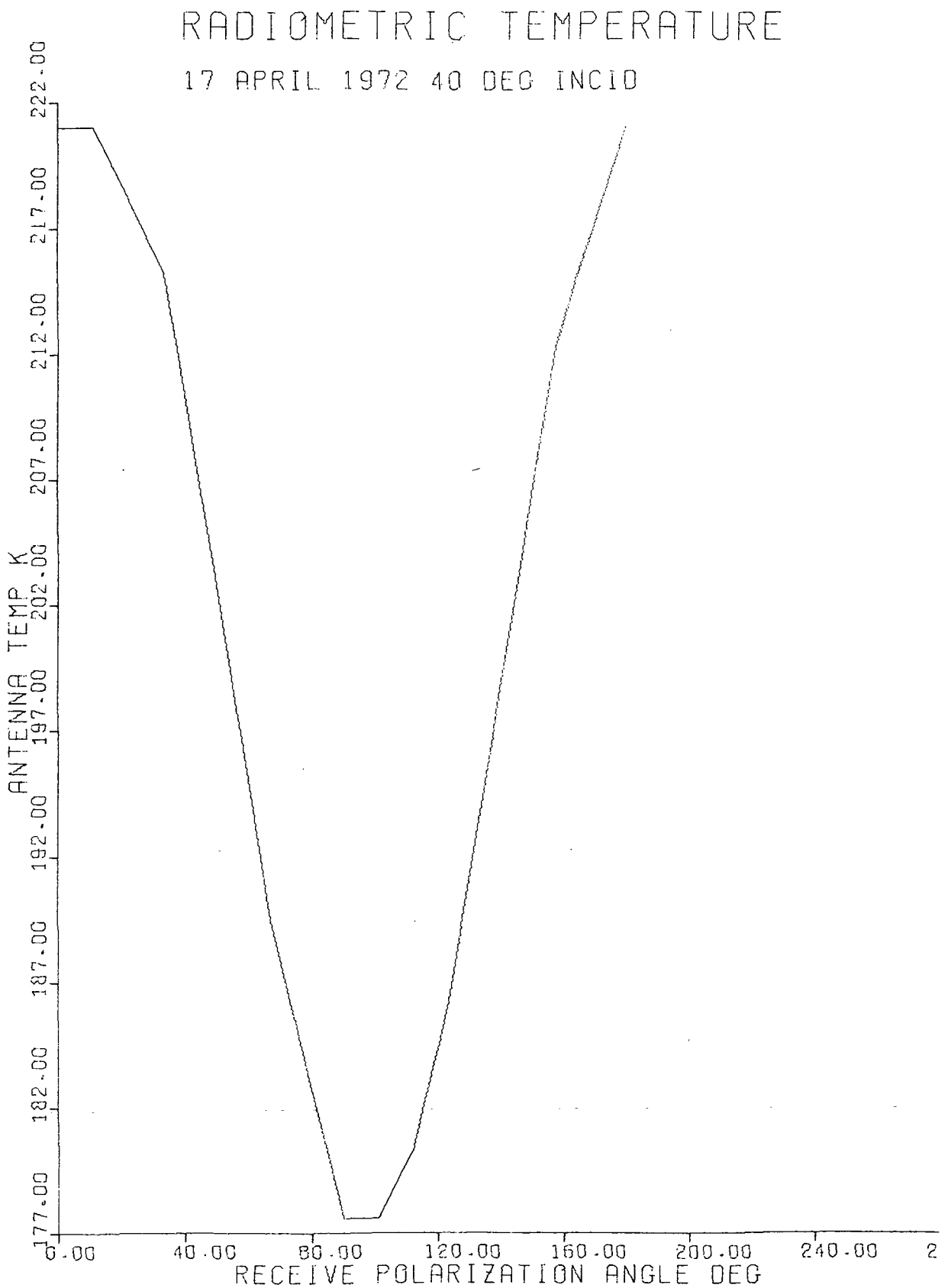
RADIOMETRIC TEMPERATURE
17 APRIL 1972 40 DEG INCID
ANTENNA TEMP K
177.00
182.00
187.00
192.00
197.00
202.00
207.00
212.00
217.00
222.00
0.00
40.00
80.00
120.00
160.00
200.00
240.00
RECEIVE POLARIZATION ANGLE DEG

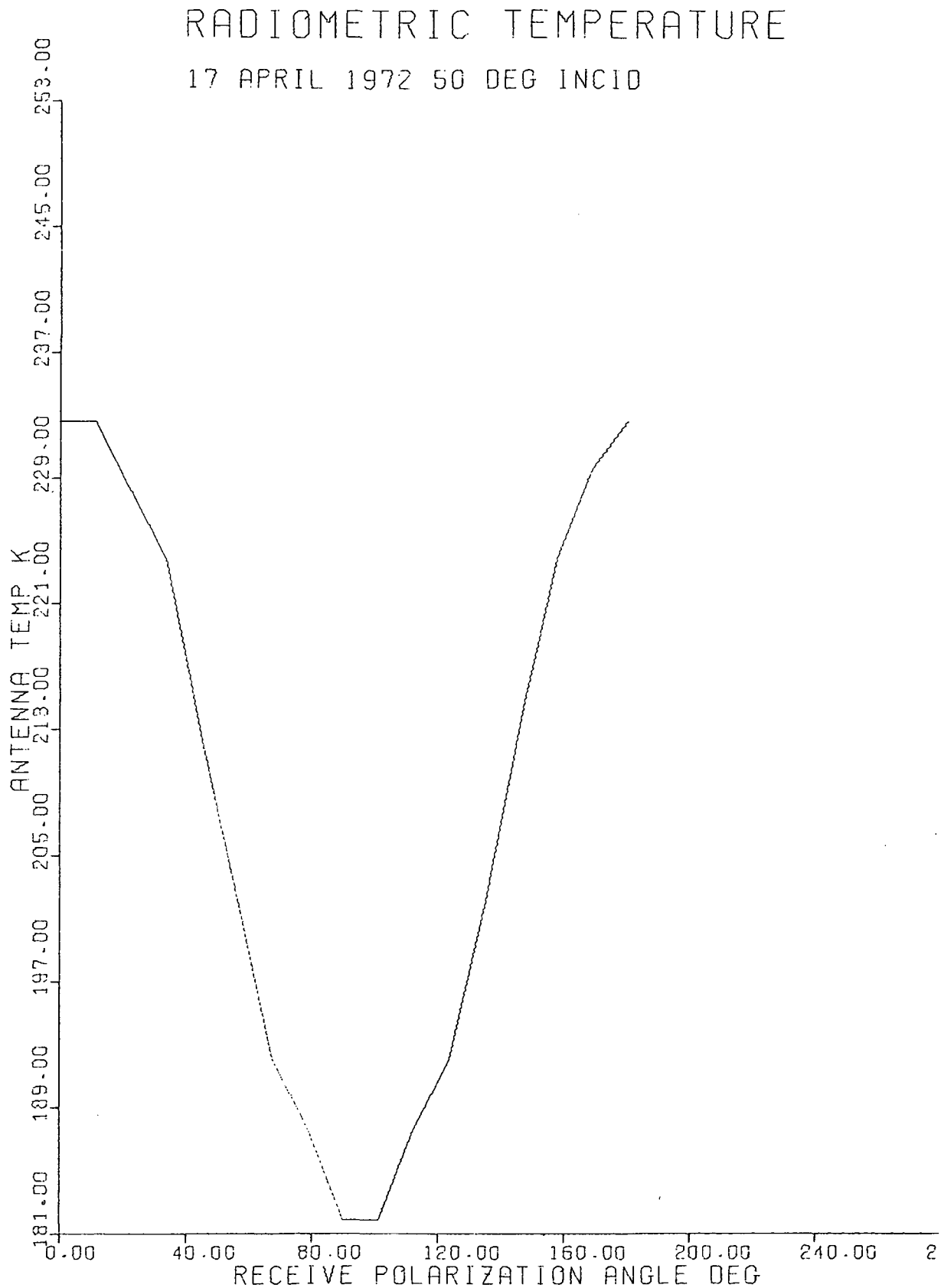
RADIOMETRIC TEMPERATURE
17 APRIL 1972 50 DEG INCID
ANTENNA TEMP K
253.00
245.00
237.00
229.00
221.00
213.00
205.00
197.00
189.00
181.00
0.00
40.00
80.00
120.00
160.00
200.00
240.00
RECEIVE POLARIZATION ANGLE DEG

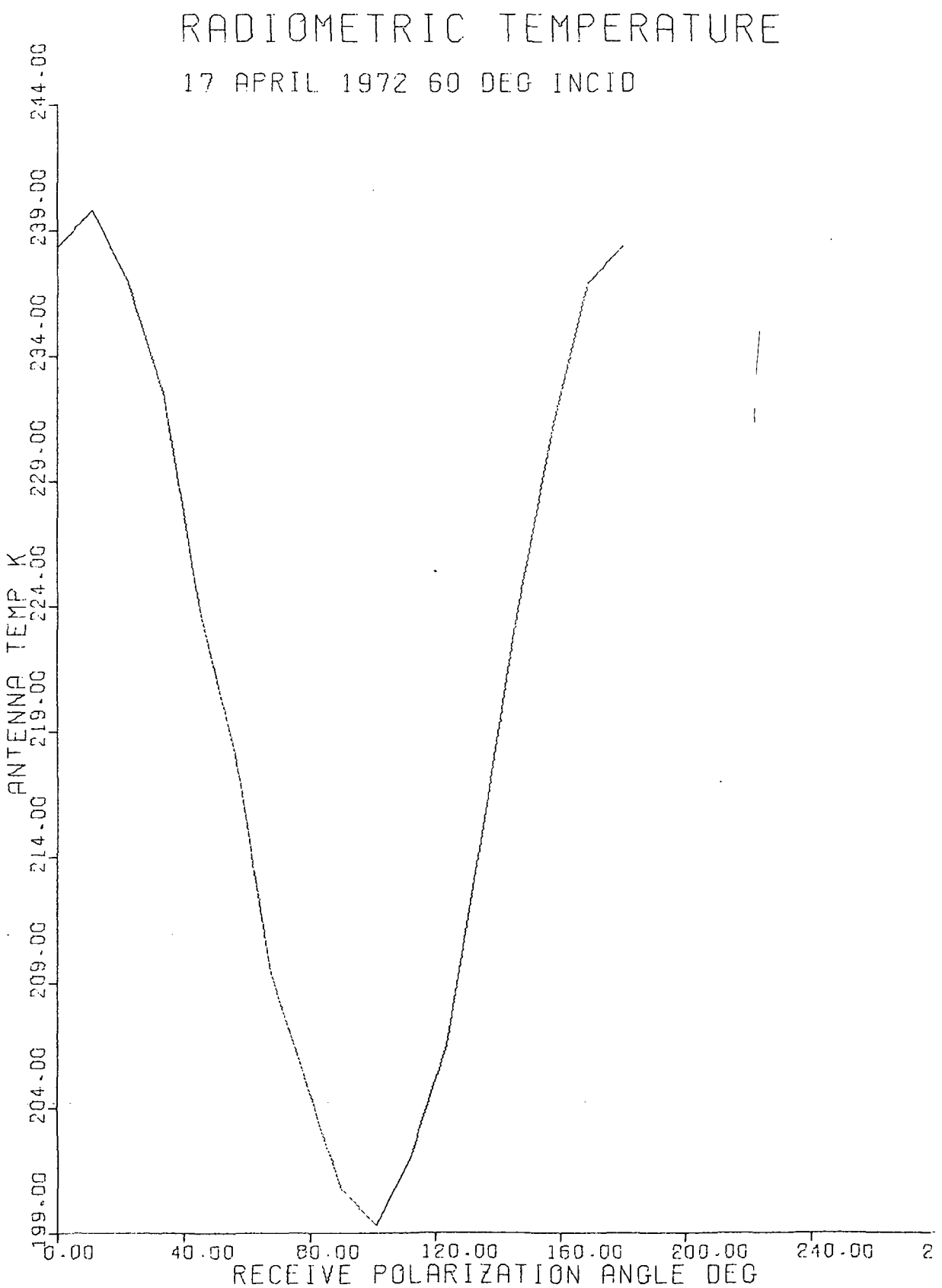
RADIOMETRIC TEMPERATURE
17 APRIL 1972 60 DEG INCID
ANTENNA TEMP K
199.00
204.00
209.00
214.00
219.00
224.00
229.00
234.00
239.00
244.00
0.00
40.00
80.00
120.00
160.00
200.00
240.00
RECEIVE POLARIZATION ANGLE DEG

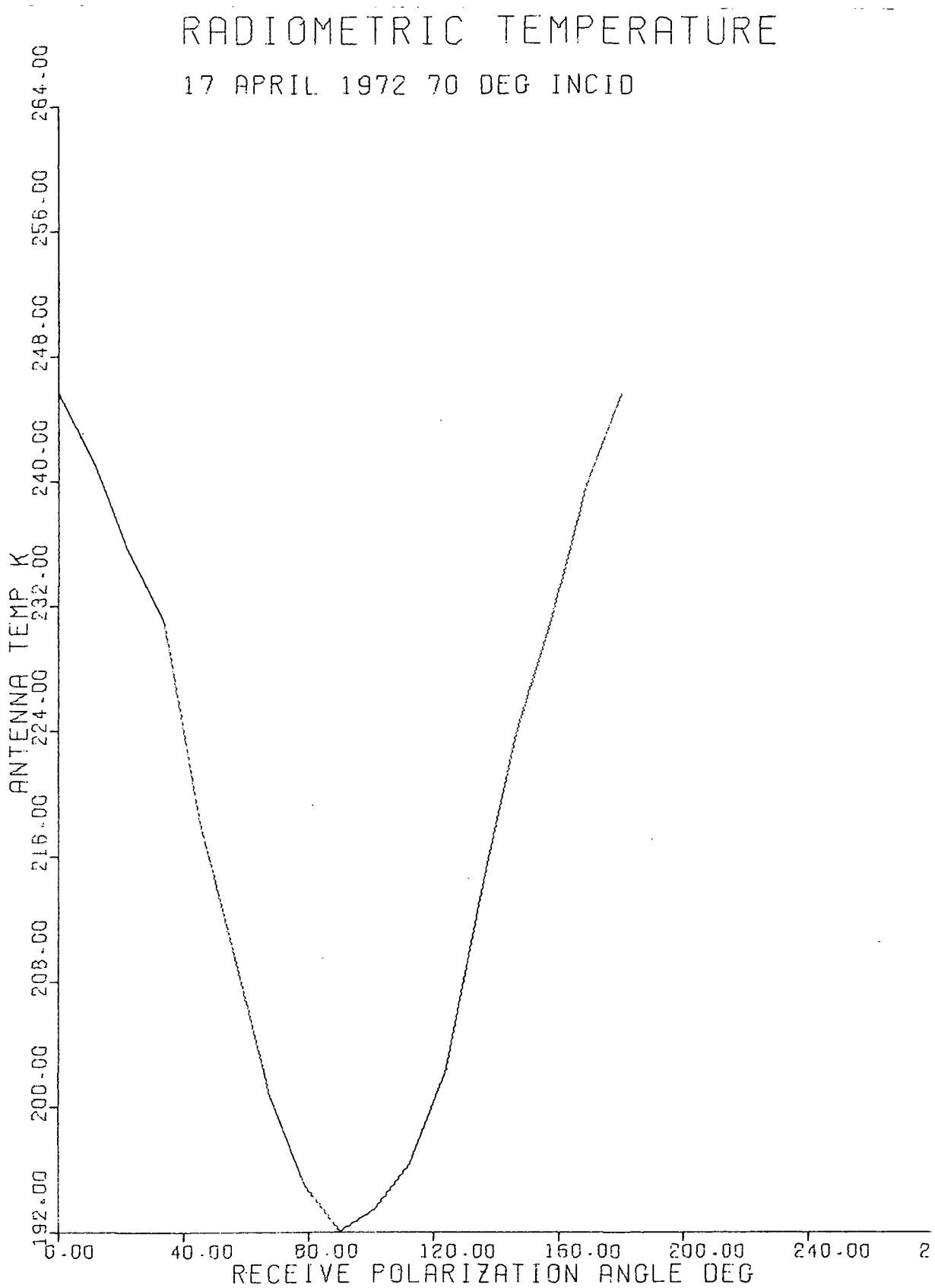
RADIOMETRIC TEMPERATURE
17 APRIL 1972 70 DEG INCID
ANTENNA TEMP K
192.00
200.00
208.00
216.00
224.00
232.00
240.00
248.00
256.00
264.00
0.00
40.00
80.00
120.00
160.00
200.00
240.00
RECEIVE POLARIZATION ANGLE DEG

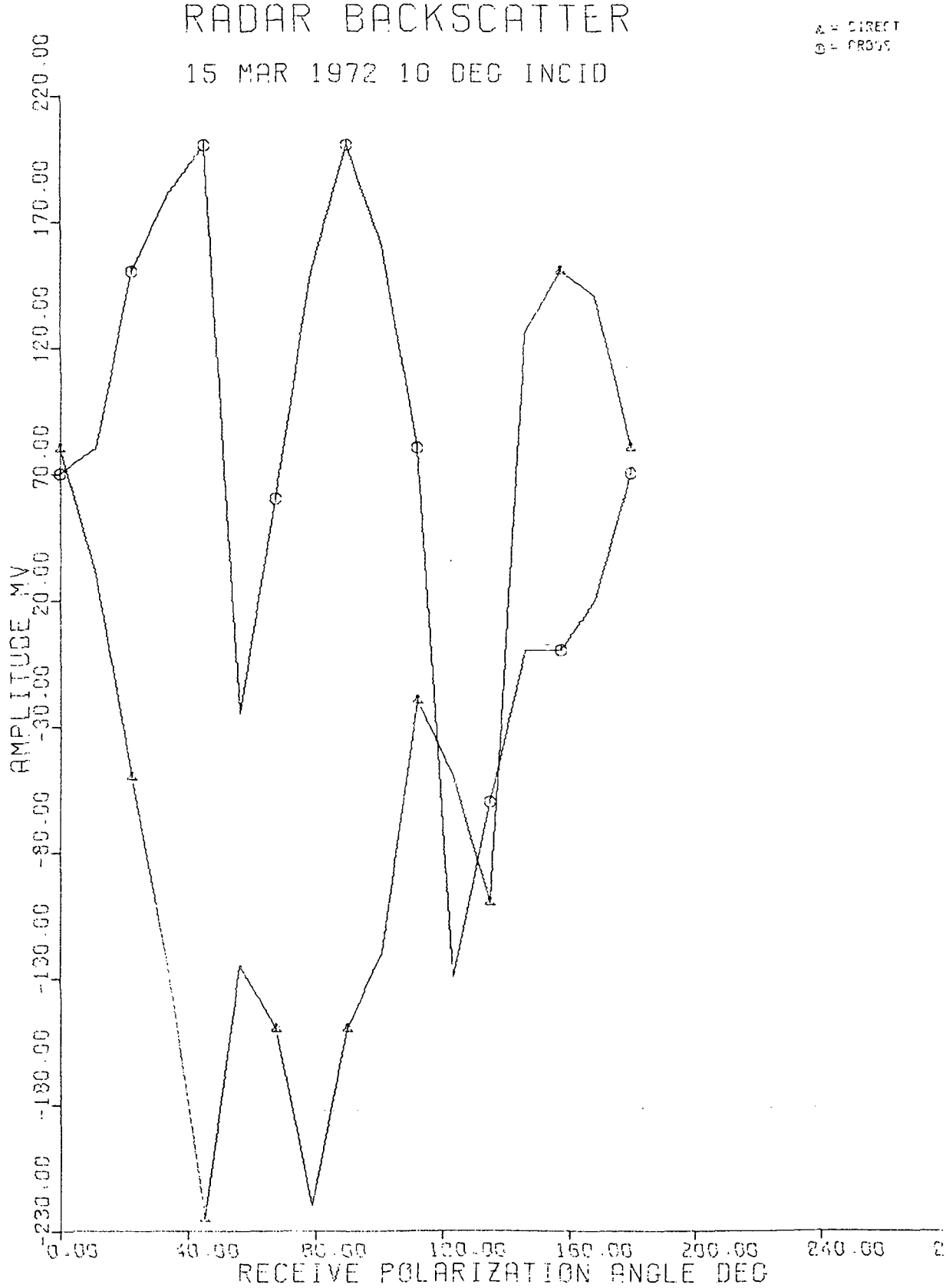
RADAR BACKSCATTER
15 MAR 1972 10 DEG INCID
Δ = DIRECT
⊙ = CROSS
AMPLITUDE MV
220.00
170.00
120.00
70.00
20.00
-30.00
-80.00
-130.00
-180.00
-230.00
0.00
40.00
80.00
120.00
160.00
200.00
240.00
RECEIVE POLARIZATION ANGLE DEG

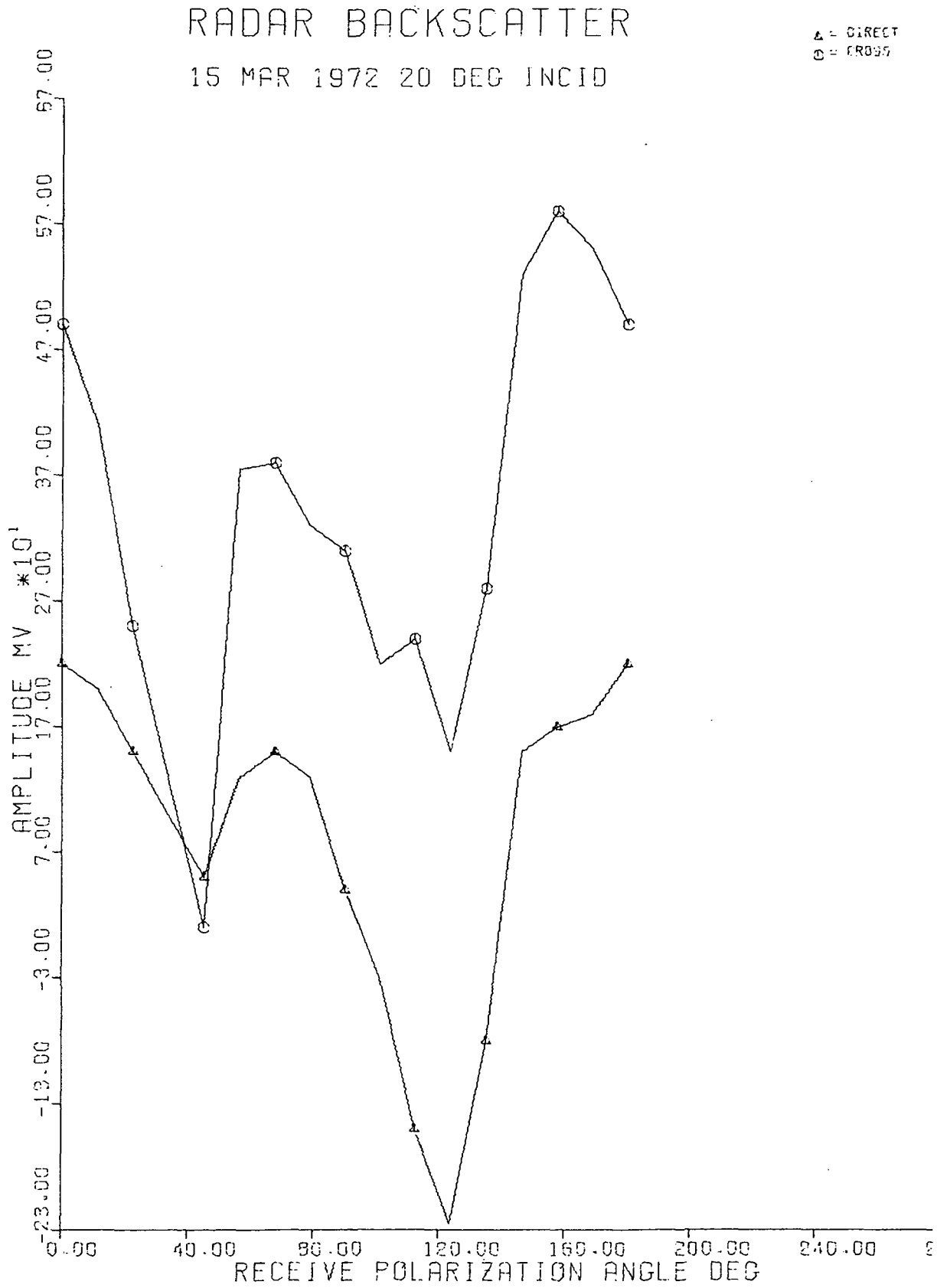
RADAR BACKSCATTER
15 MAR 1972 20 DEG INCID
Δ = DIRECT
⊕ = CROSS
AMPLITUDE MV *10¹
67.00
57.00
47.00
37.00
27.00
17.00
7.00
-3.00
-13.00
-23.00
0.00
40.00
80.00
120.00
160.00
200.00
240.00
RECEIVE POLARIZATION ANGLE DEG

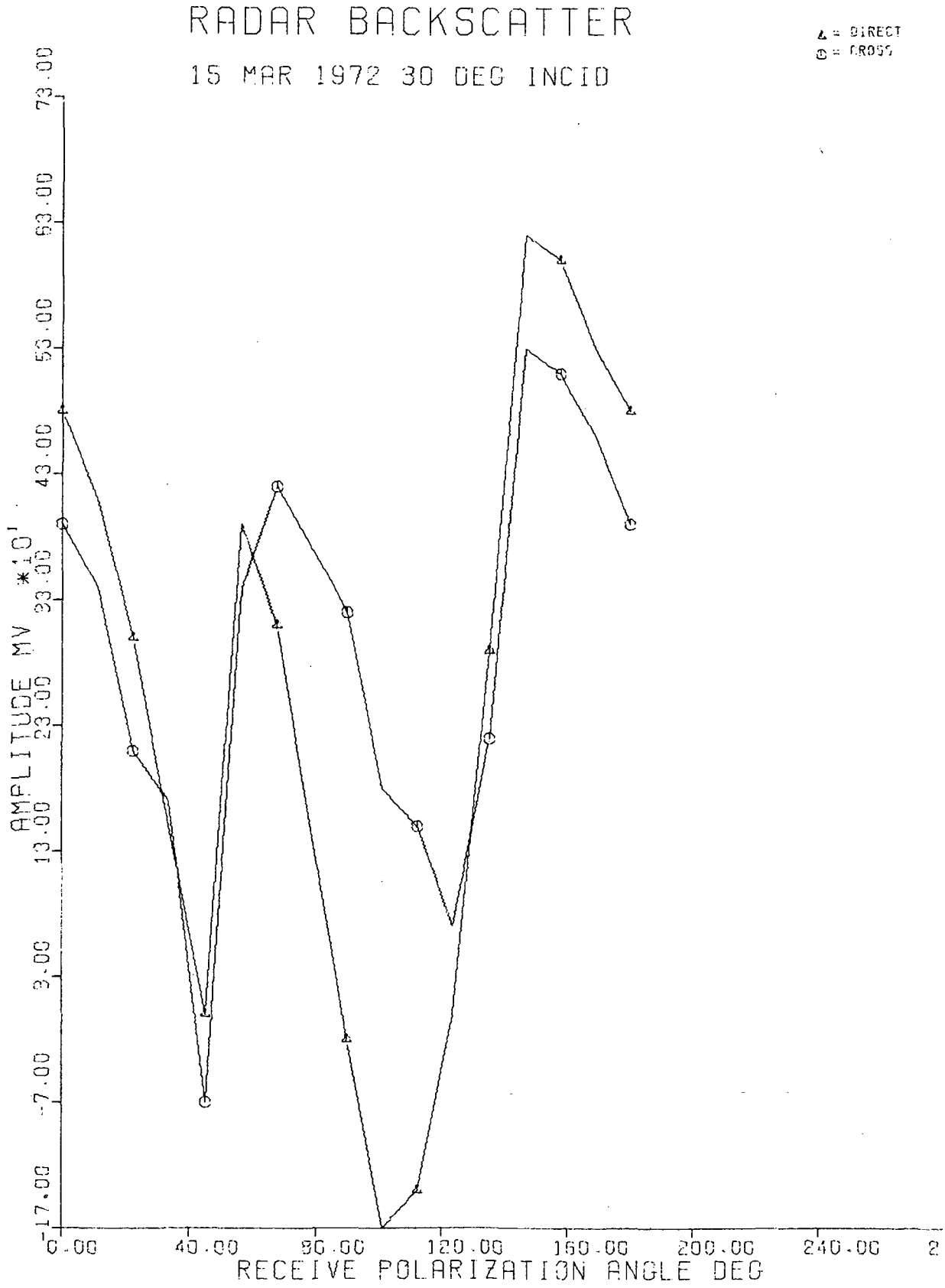
RADAR BACKSCATTER
15 MAR 1972 30 DEG INCID
Δ = DIRECT
○ = CROSS
AMPLITUDE MV *10¹
73.00
53.00
43.00
33.00
23.00
13.00
3.00
-7.00
-17.00
0.00
40.00
80.00
120.00
160.00
200.00
240.00
RECEIVE POLARIZATION ANGLE DEG

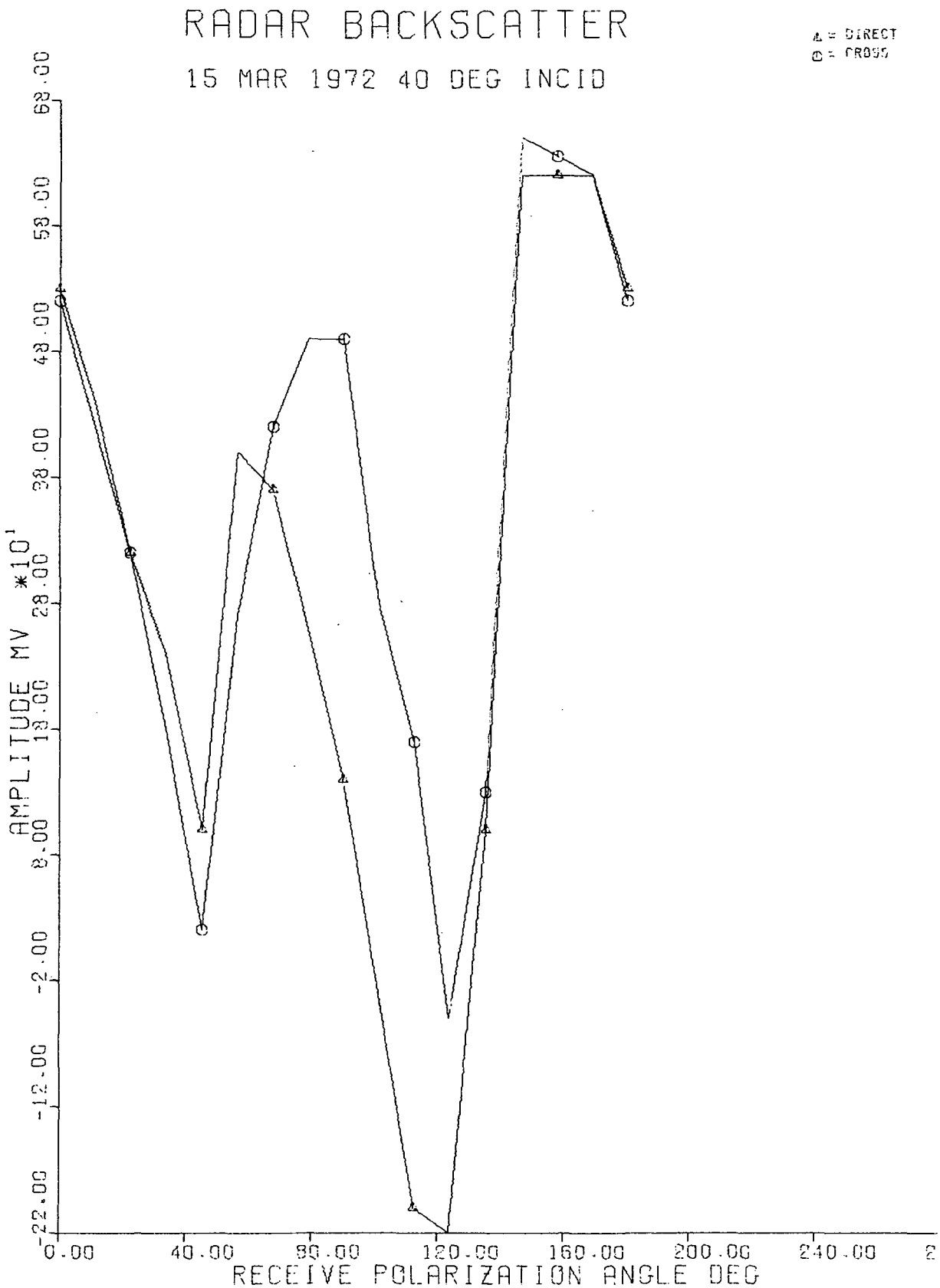
RADAR BACKSCATTER
15 MAR 1972 40 DEG INCID
Δ = DIRECT
○ = CROSS
AMPLITUDE MV *10¹
68.00
58.00
48.00
38.00
28.00
18.00
8.00
-2.00
-12.00
-22.00
0.00
40.00
80.00
120.00
160.00
200.00
240.00
RECEIVE POLARIZATION ANGLE DEG

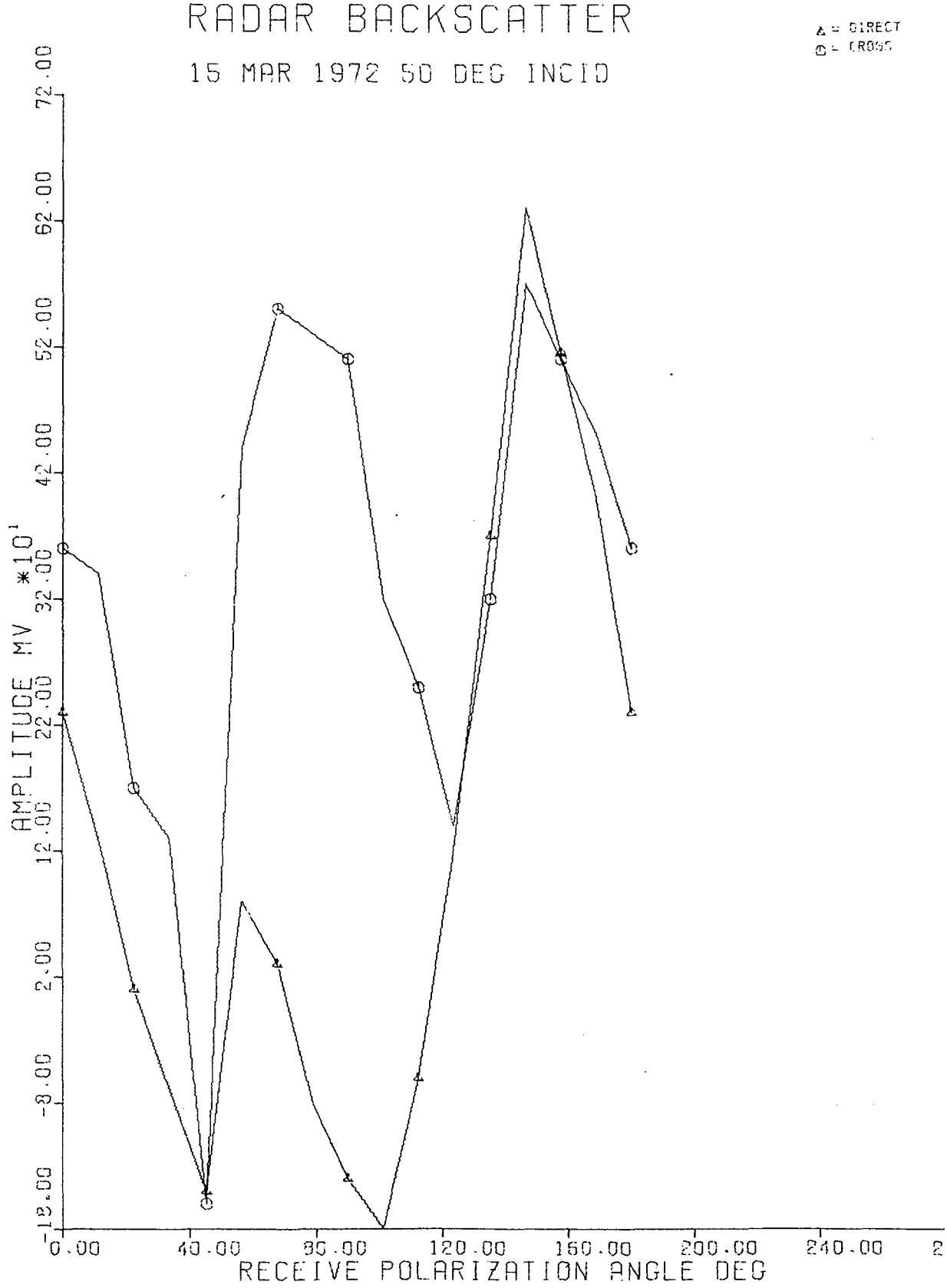
RADAR BACKSCATTER
15 MAR 1972 50 DEG INCID
△ = DIRECT
○ = CROSS
AMPLITUDE MV *10¹
72.00
62.00
52.00
42.00
32.00
22.00
12.00
2.00
-8.00
-18.00
0.00
40.00
80.00
120.00
160.00
200.00
240.00
RECEIVE POLARIZATION ANGLE DEG

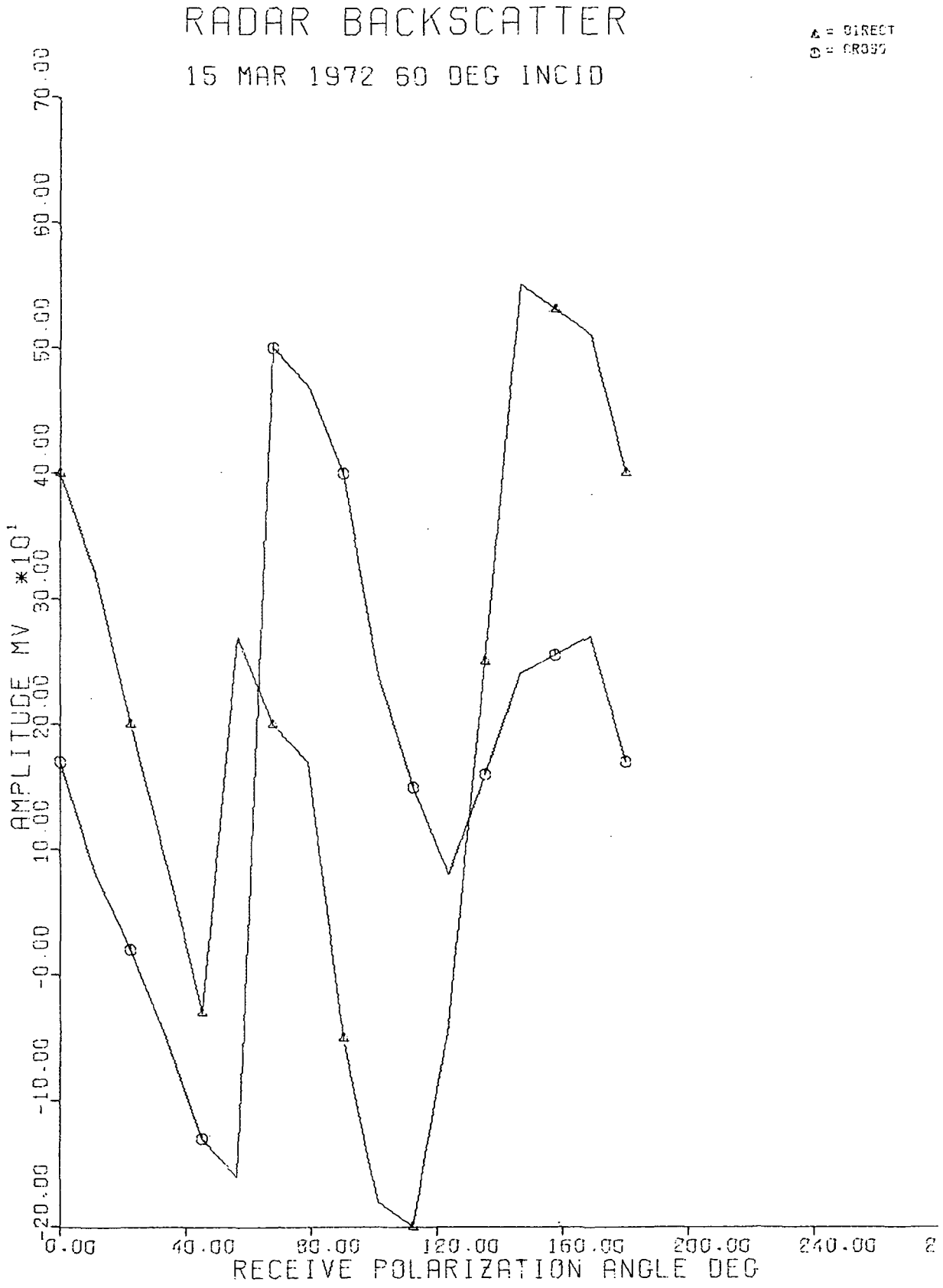
RADAR BACKSCATTER
15 MAR 1972 60 DEG INCID
△ = DIRECT
○ = CROSS
AMPLITUDE MV *10¹
70.00
60.00
50.00
40.00
30.00
20.00
10.00
-0.00
-10.00
-20.00
0.00
40.00
80.00
120.00
160.00
200.00
240.00
RECEIVE POLARIZATION ANGLE DEG

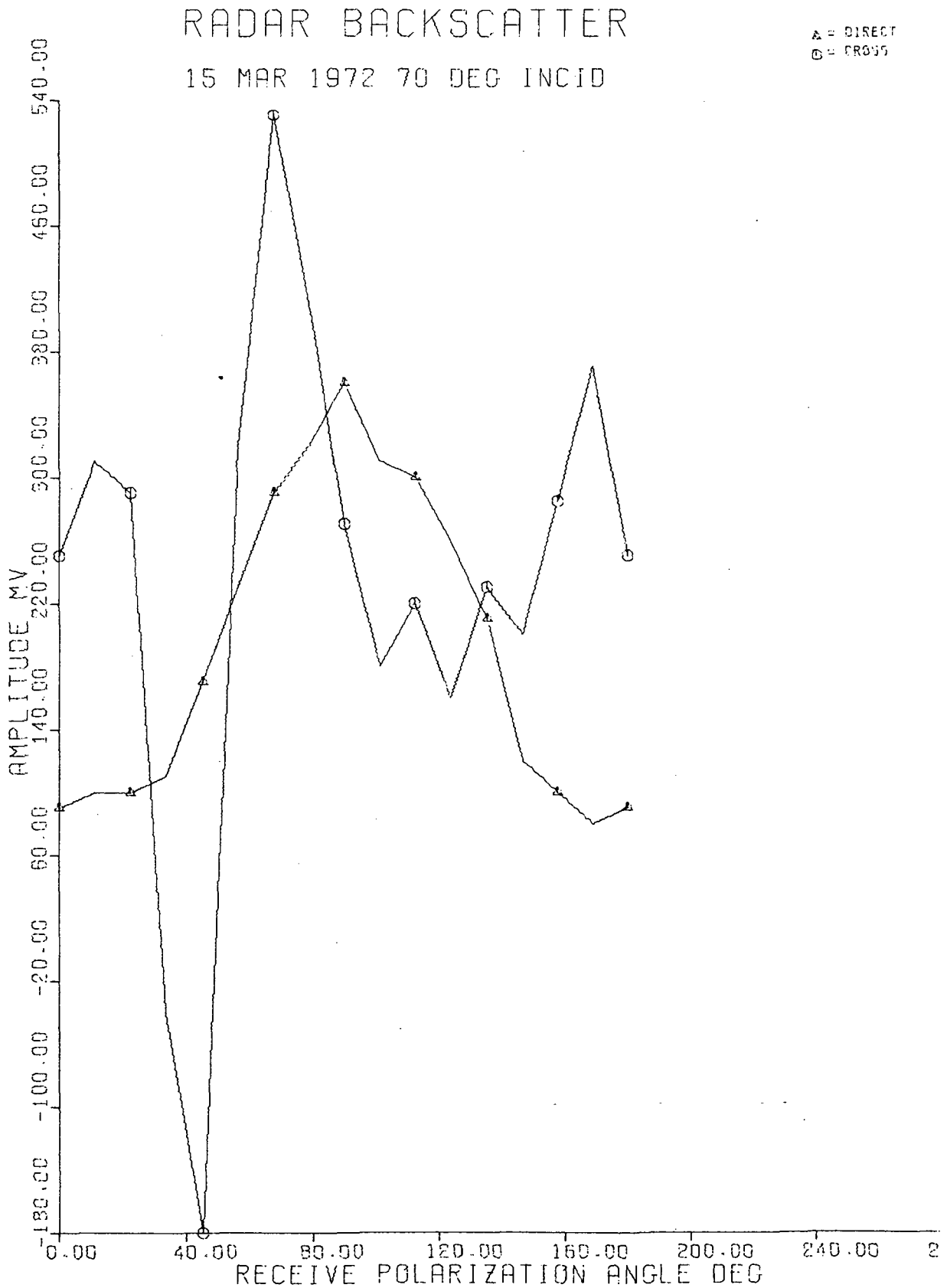
RADAR BACKSCATTER
15 MAR 1972 70 DEG INCID
Δ = DIRECT
◎ = CROSS
AMPLITUDE MV
540.00
460.00
380.00
300.00
220.00
140.00
60.00
-20.00
-100.00
-180.00
0.00
40.00
80.00
120.00
160.00
200.00
240.00
RECEIVE POLARIZATION ANGLE DEG

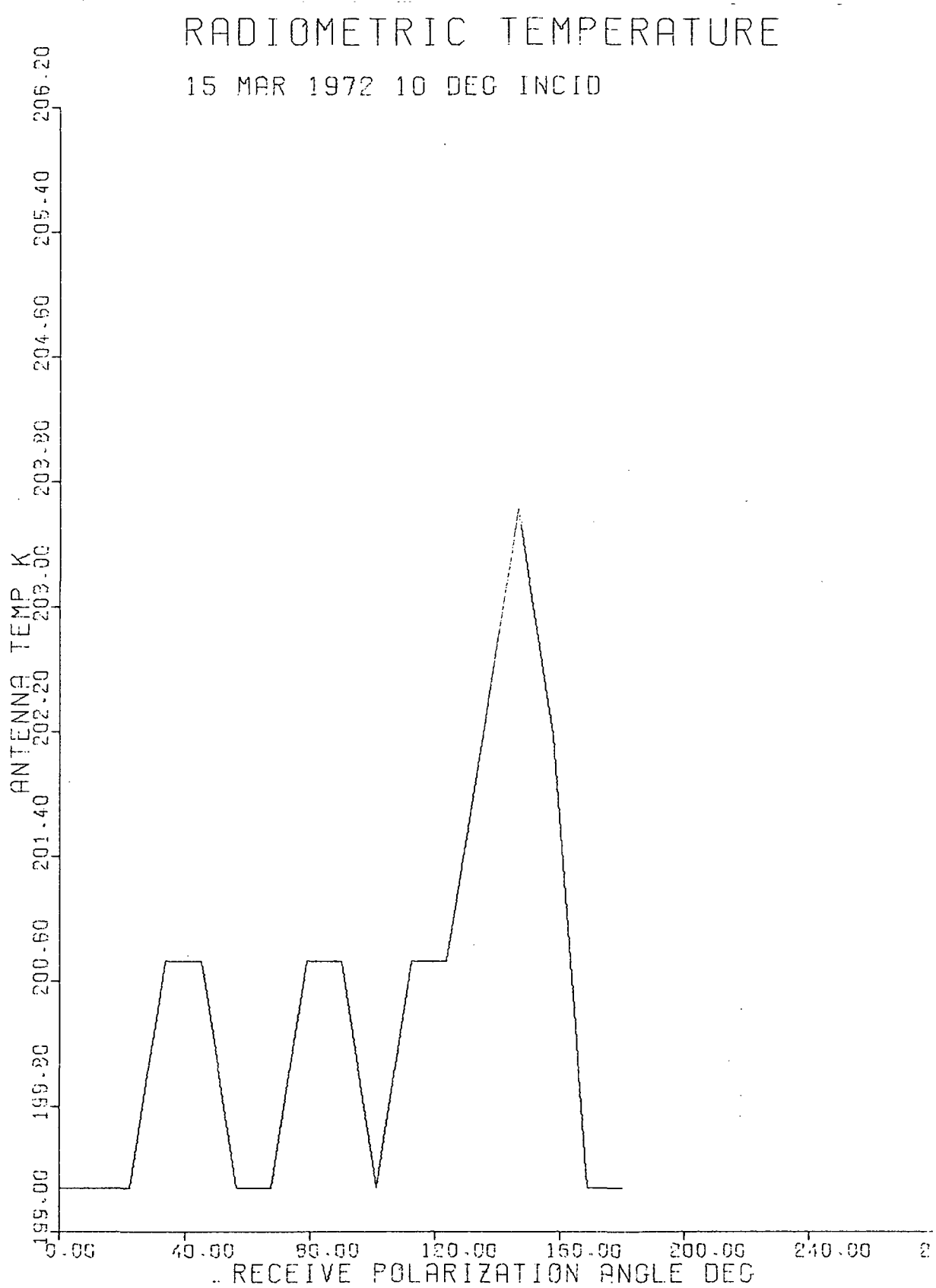
RADIOMETRIC TEMPERATURE
15 MAR 1972 10 DEG INCID
ANTENNA TEMP K
199.00
199.80
200.60
201.40
202.20
203.00
203.80
204.60
205.40
206.20
0.00
40.00
80.00
120.00
160.00
200.00
240.00
RECEIVE POLARIZATION ANGLE DEG

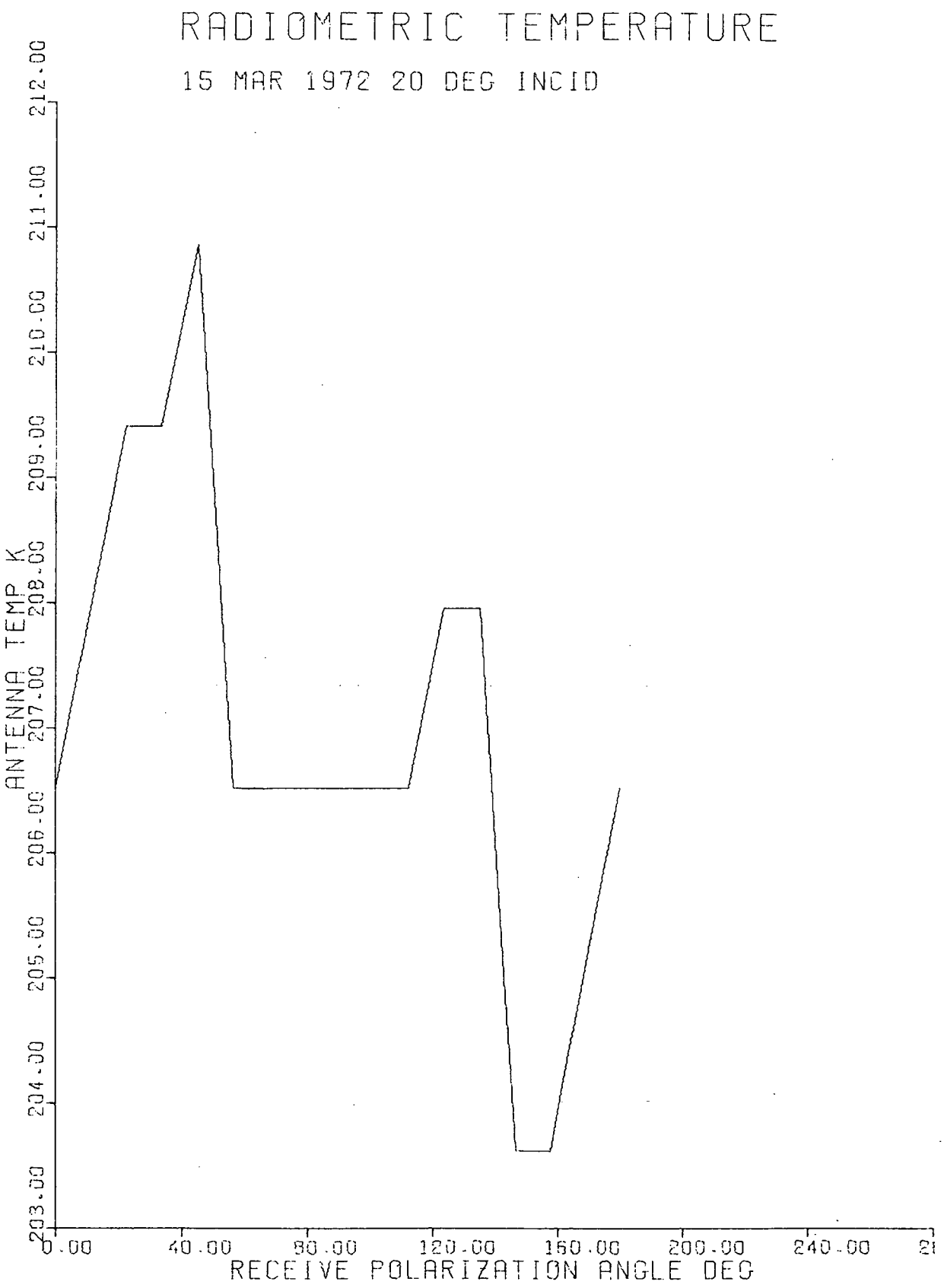
RADIOMETRIC TEMPERATURE
15 MAR 1972 20 DEG INCID
ANTENNA TEMP K
203.00
204.00
205.00
206.00
207.00
208.00
209.00
210.00
211.00
212.00
0.00
40.00
80.00
120.00
160.00
200.00
240.00
RECEIVE POLARIZATION ANGLE DEG

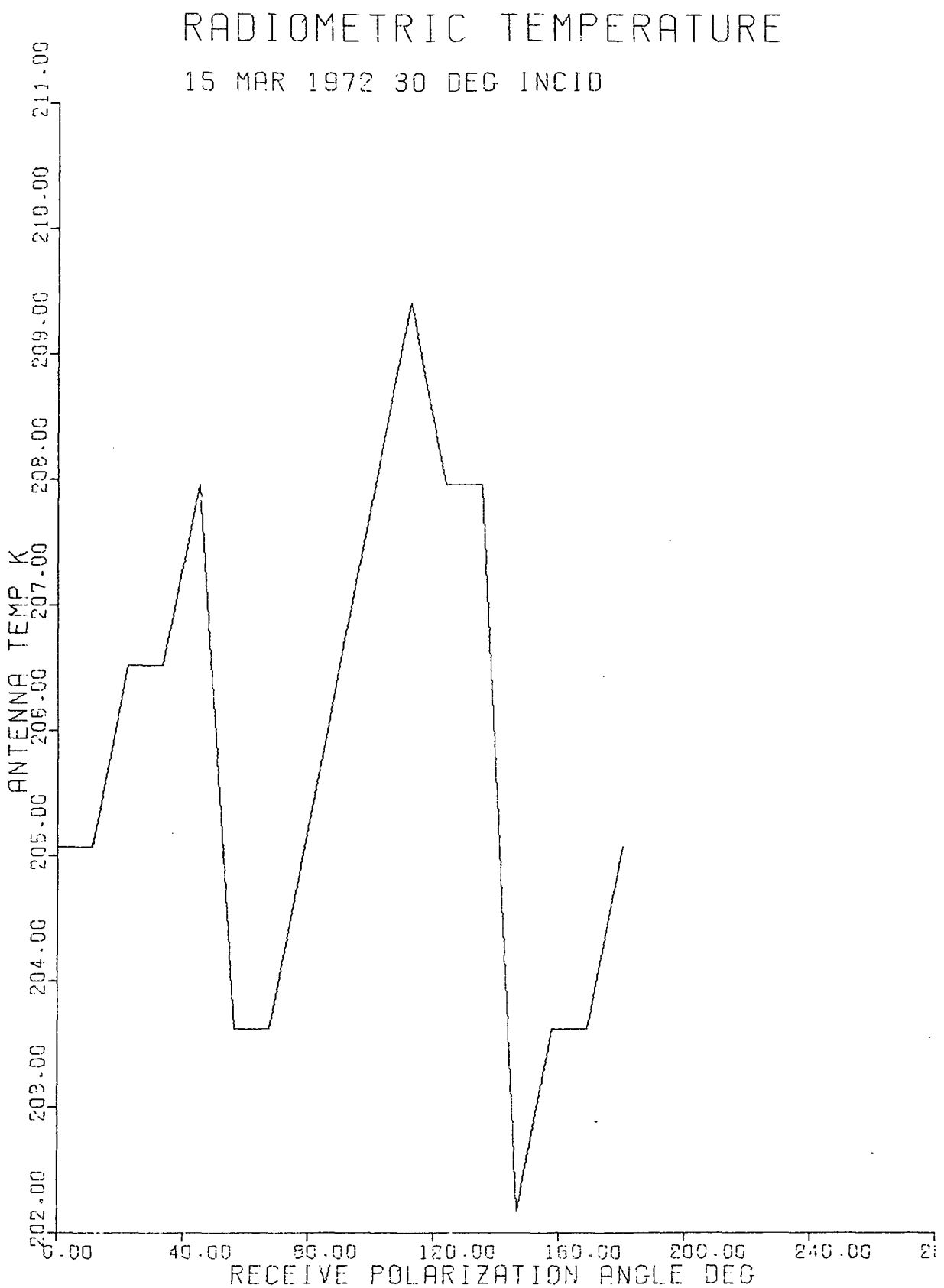
RADIOMETRIC TEMPERATURE
15 MAR 1972 30 DEG INCID
ANTENNA TEMP K
202.00
203.00
204.00
205.00
206.00
207.00
208.00
209.00
210.00
211.00
0.00
40.00
80.00
120.00
160.00
200.00
240.00
RECEIVE POLARIZATION ANGLE DEG

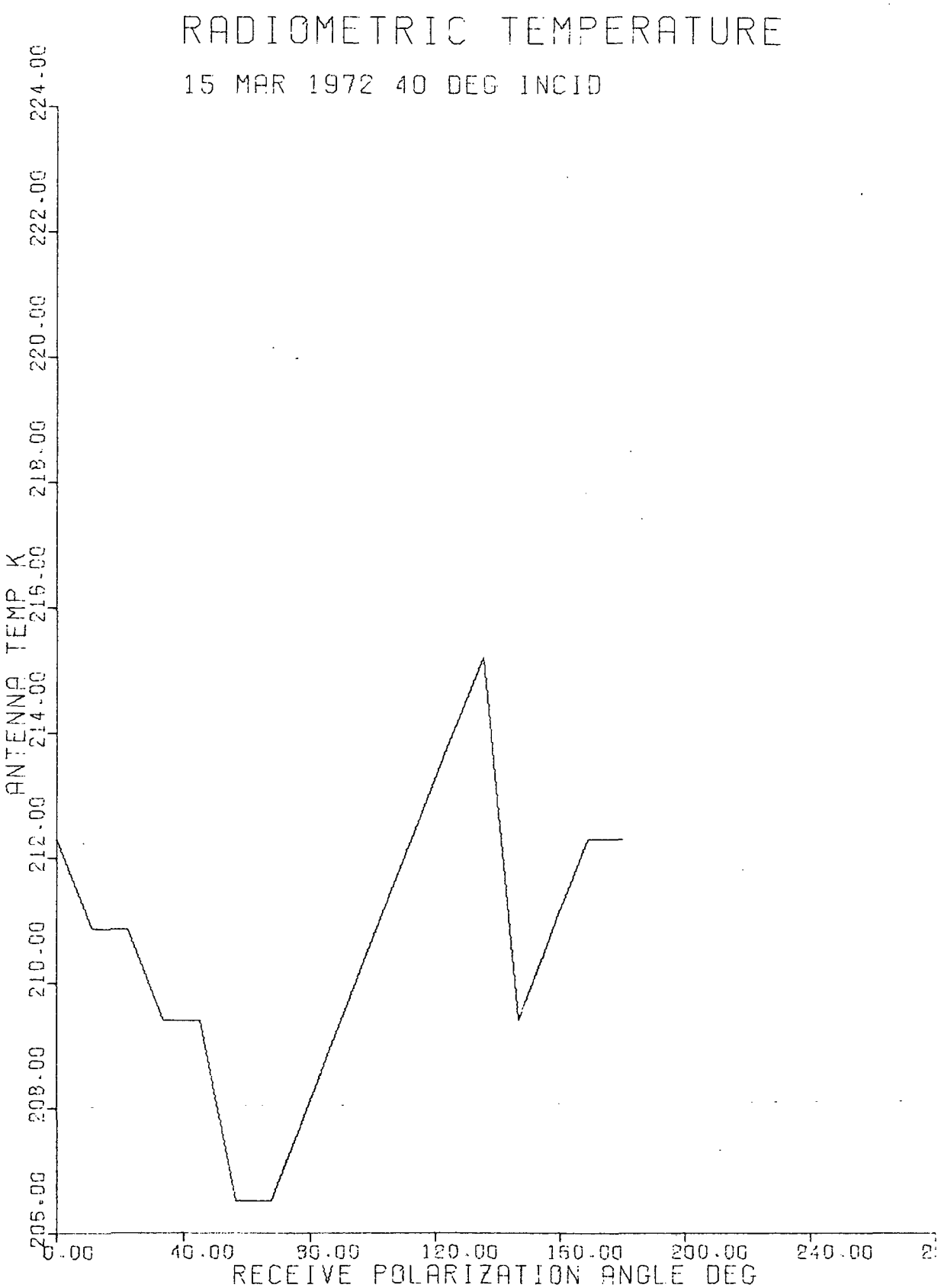
RADIOMETRIC TEMPERATURE
15 MAR 1972 40 DEG INCID
ANTENNA TEMP K
205.00
208.00
210.00
212.00
214.00
216.00
218.00
220.00
222.00
224.00
0.00
40.00
80.00
120.00
160.00
200.00
240.00
RECEIVE POLARIZATION ANGLE DEG

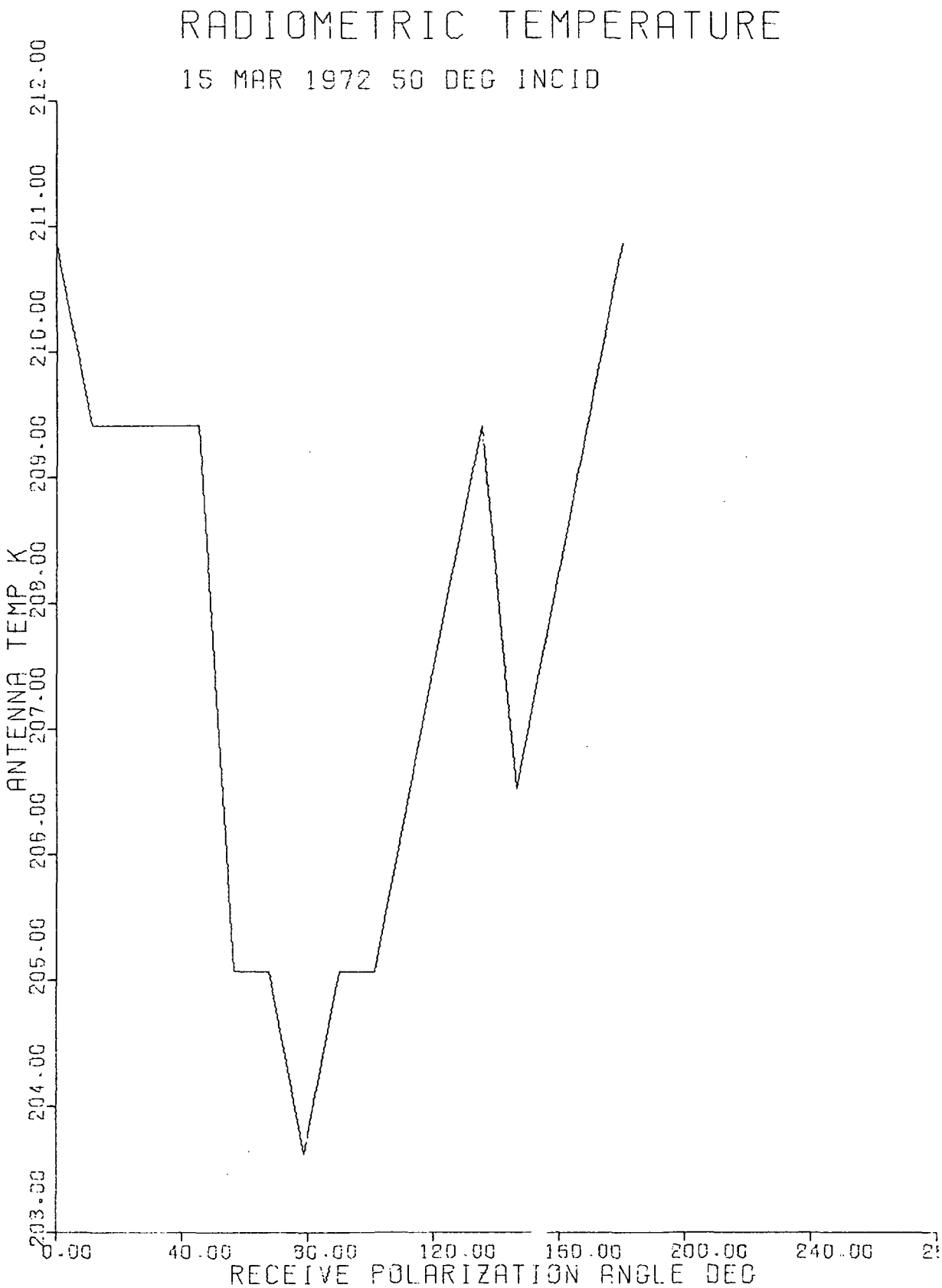
RADIOMETRIC TEMPERATURE
15 MAR 1972 50 DEG INCID
ANTENNA TEMP K
212.00
211.00
210.00
209.00
208.00
207.00
206.00
205.00
204.00
203.00
0.00
40.00
80.00
120.00
160.00
200.00
240.00
RECEIVE POLARIZATION ANGLE DEG

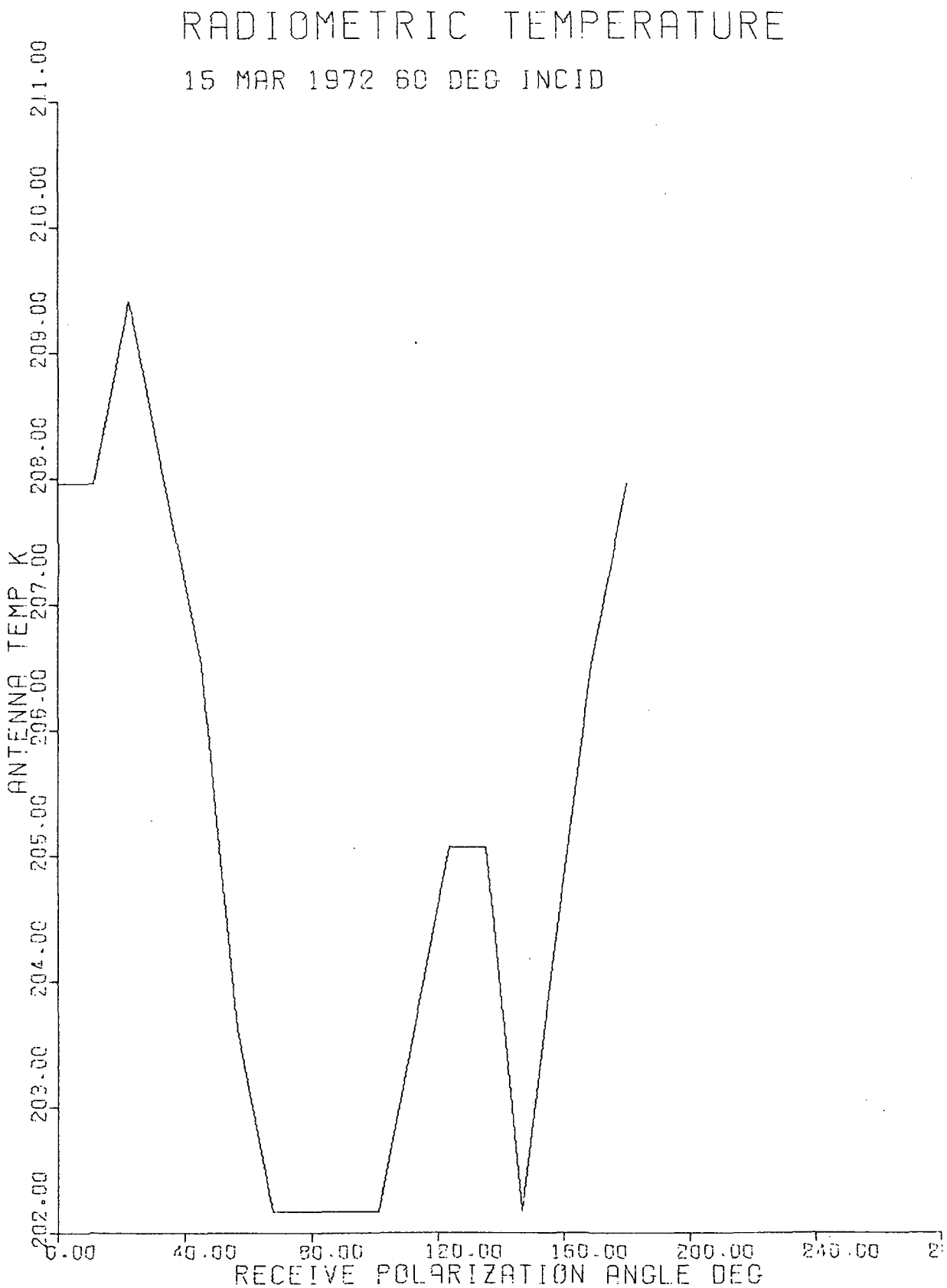
RADIOMETRIC TEMPERATURE
15 MAR 1972 60 DEG INCID
ANTENNA TEMP K
202.00
203.00
204.00
205.00
206.00
207.00
208.00
209.00
210.00
211.00
0.00
40.00
80.00
120.00
160.00
200.00
240.00
RECEIVE POLARIZATION ANGLE DEG

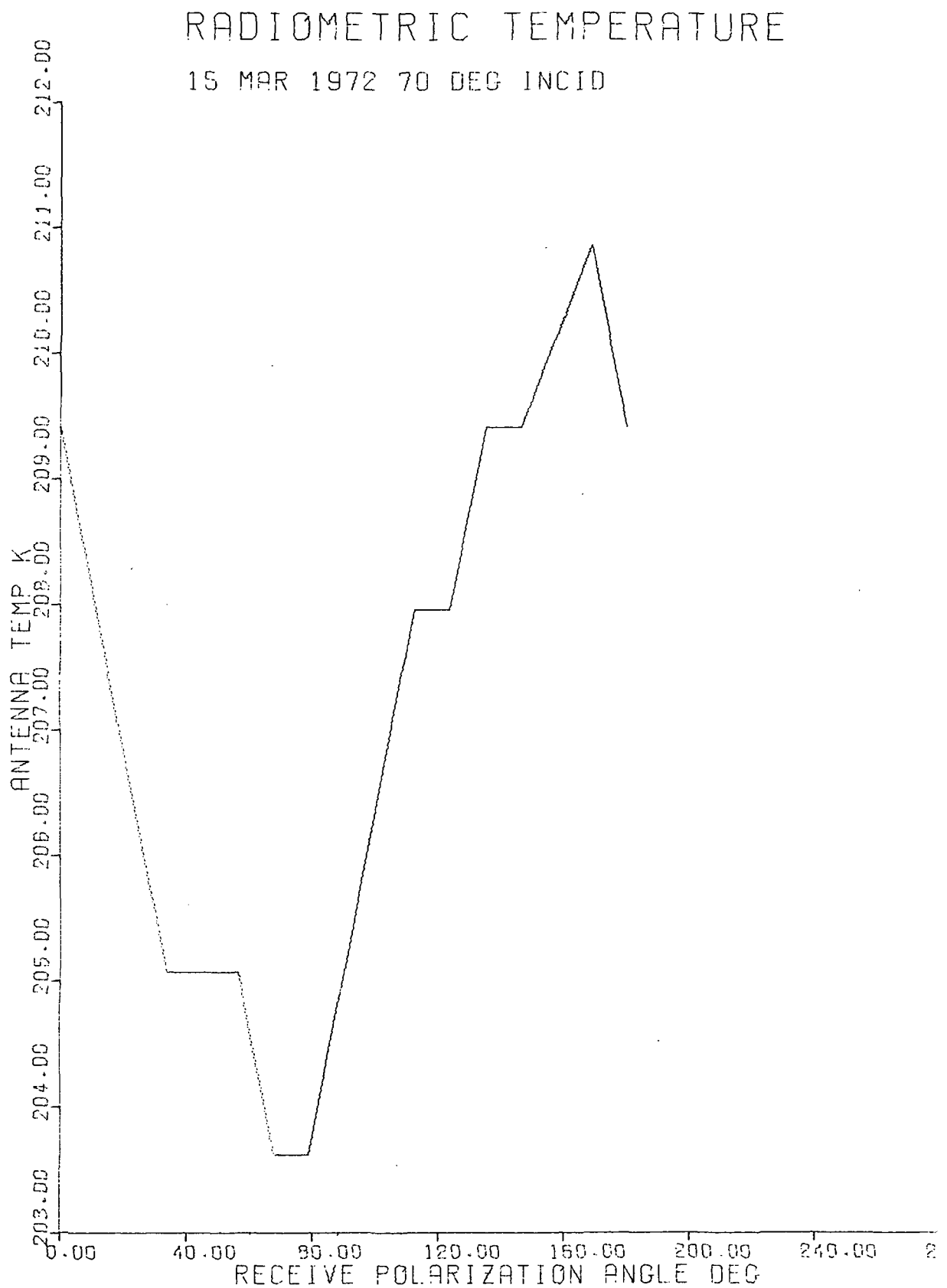
RADIOMETRIC TEMPERATURE
15 MAR 1972 70 DEG INCID
ANTENNA TEMP K
203.00
204.00
205.00
206.00
207.00
208.00
209.00
210.00
211.00
212.00
0.00
40.00
80.00
120.00
160.00
200.00
240.00
RECEIVE POLARIZATION ANGLE DEG

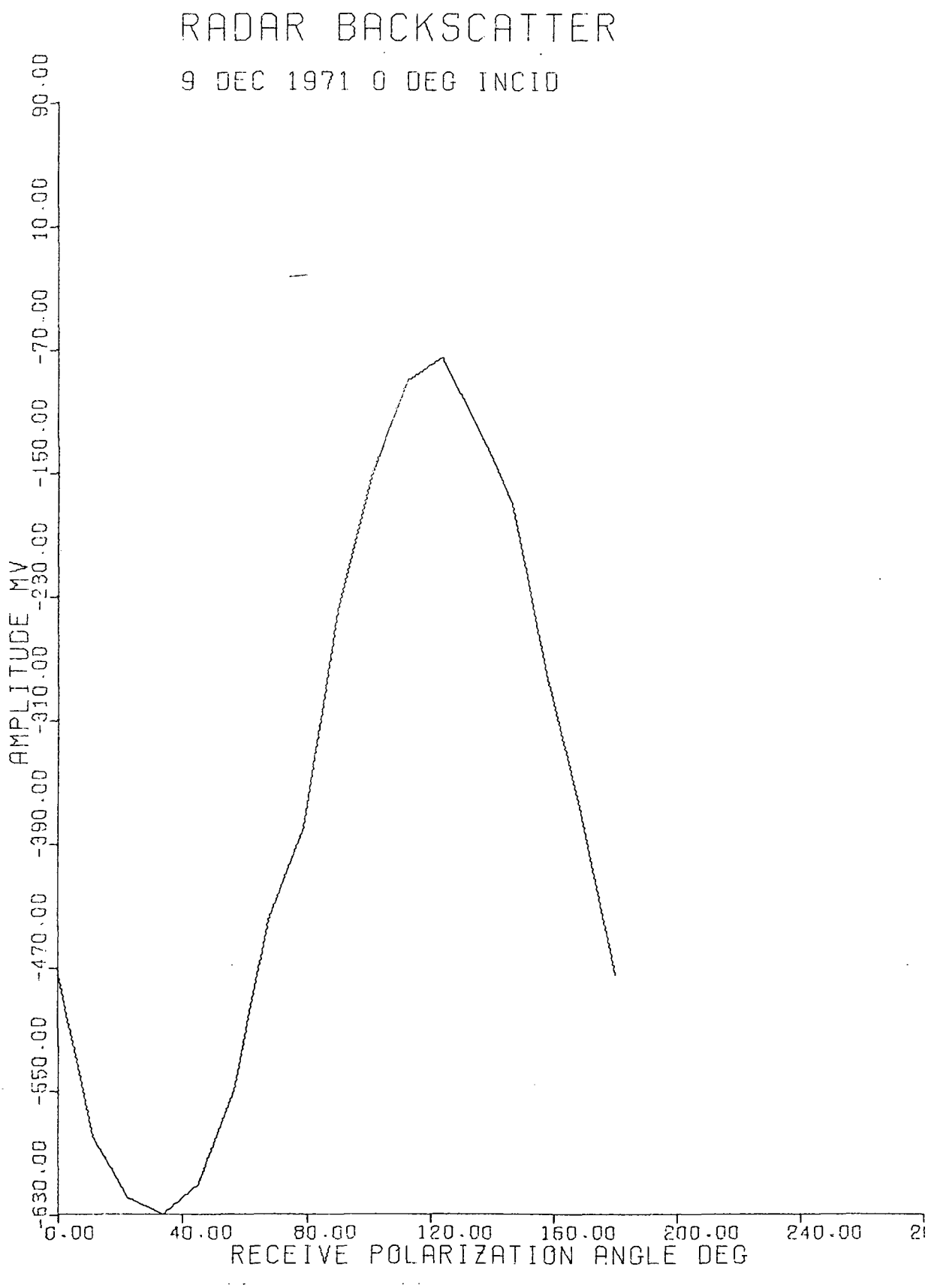
RADAR BACKSCATTER
9 DEC 1971 0 DEG INCID
AMPLITUDE MV
90.00
10.00
-70.00
-150.00
-230.00
-310.00
-390.00
-470.00
-550.00
-630.00
0.00
40.00
80.00
120.00
160.00
200.00
240.00
RECEIVE POLARIZATION ANGLE DEG

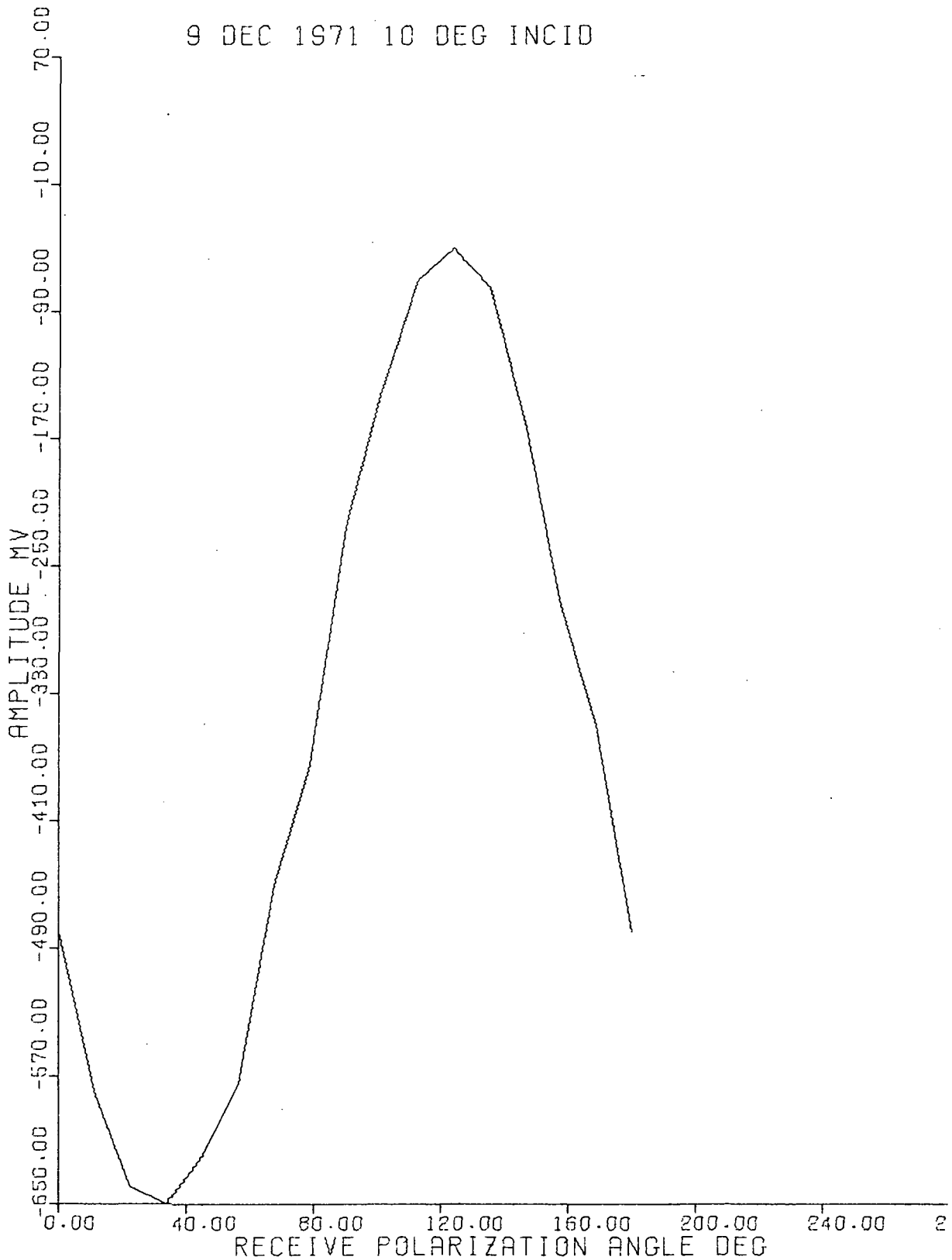
RADAR BACKSCATTER
9 DEC 1971 10 DEG INCID
AMPLITUDE MV
-10.00
-90.00
-170.00
-250.00
-330.00
-410.00
-490.00
-570.00
-650.00
0.00
40.00
80.00
120.00
160.00
200.00
240.00
RECEIVE POLARIZATION ANGLE DEG

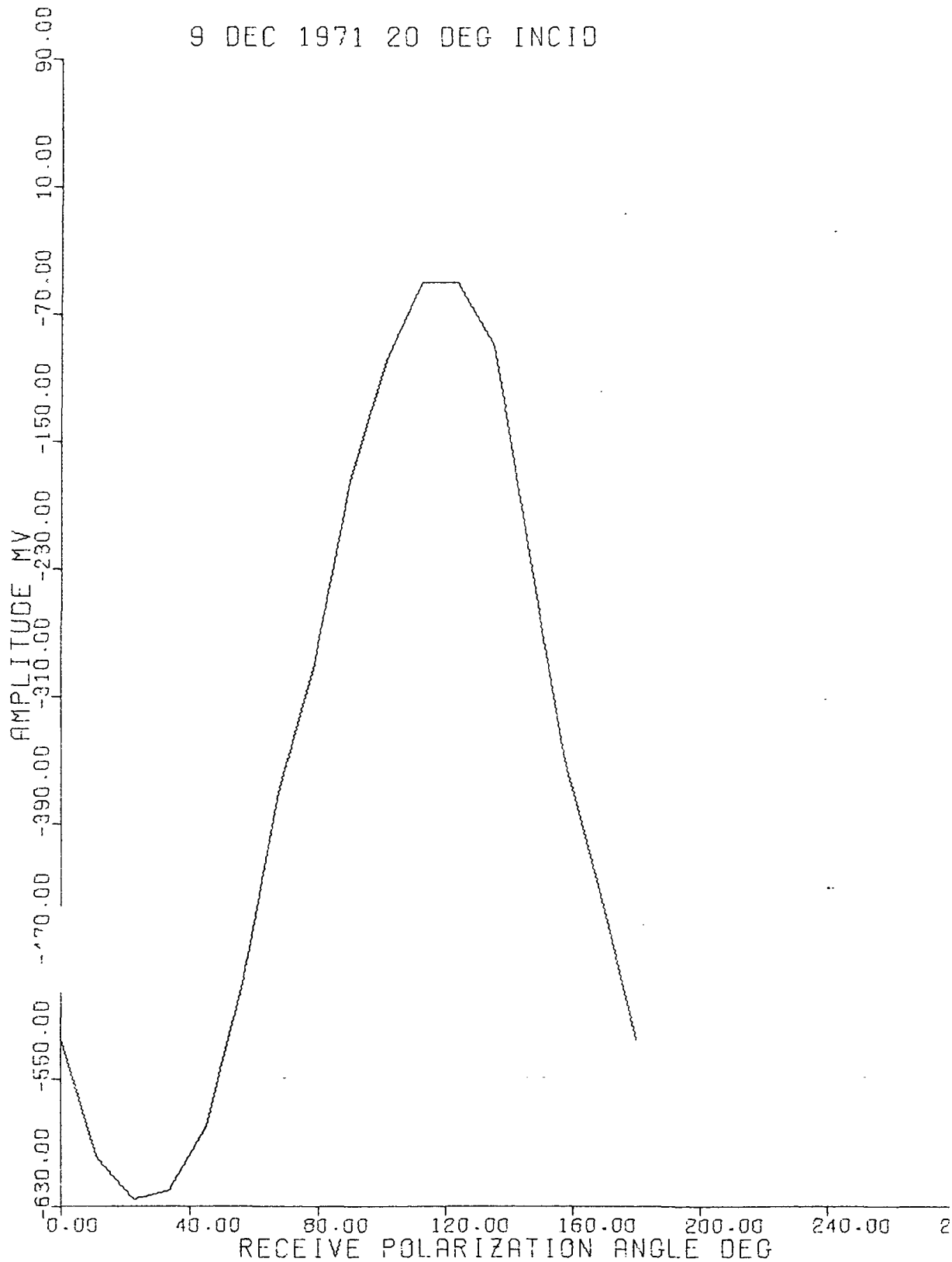
RADAR BACKSCATTER
9 DEC 1971 20 DEG INCID
AMPLITUDE MV
90.00
10.00
-70.00
-150.00
-230.00
-310.00
-390.00
-470.00
-550.00
-630.00
0.00
40.00
80.00
120.00
160.00
200.00
240.00
RECEIVE POLARIZATION ANGLE DEG

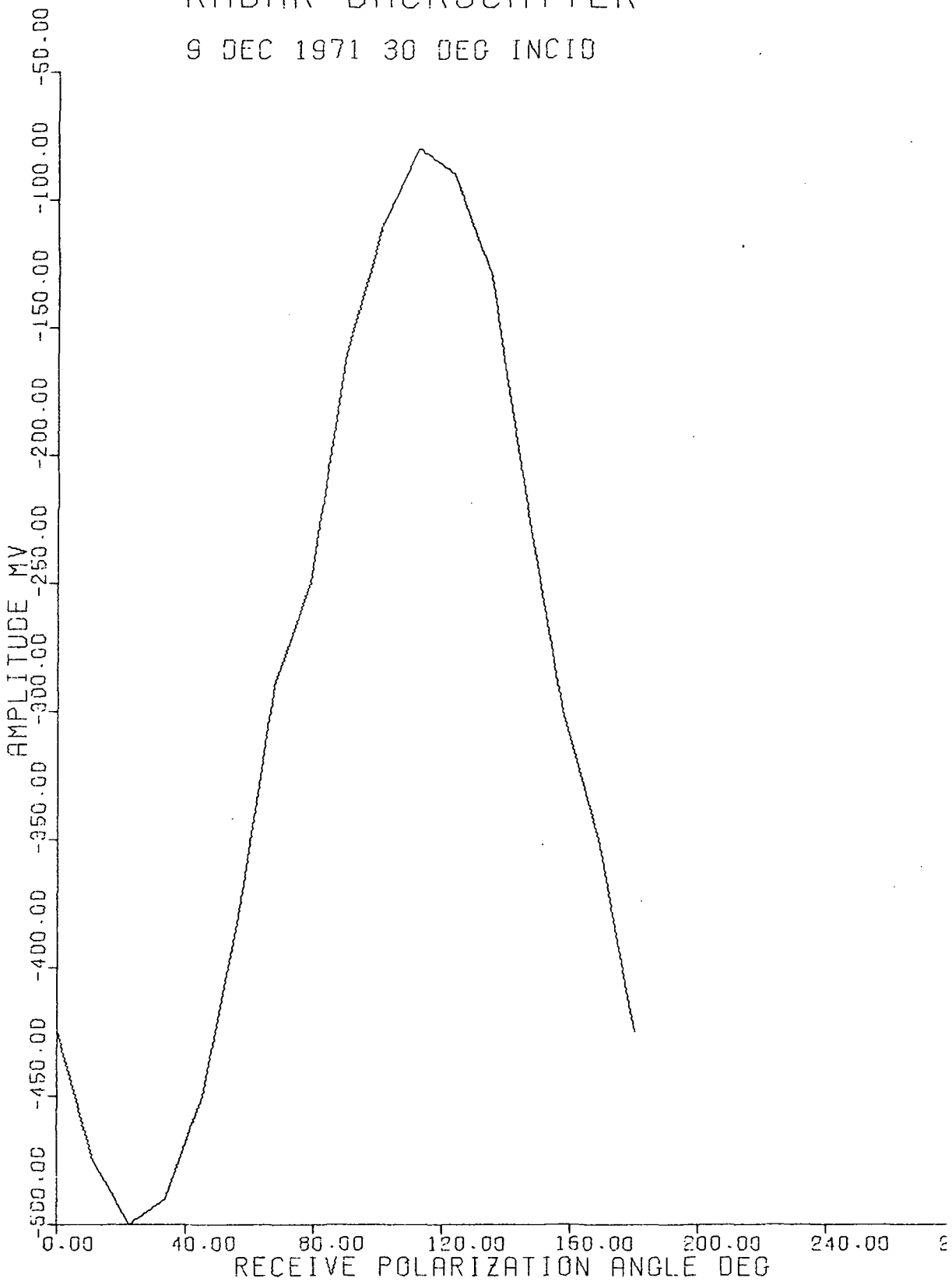
RADAR BACKSCATTER
9 DEC 1971 30 DEG INCID
AMPLITUDE MV
-50.00
-100.00
-150.00
-200.00
-250.00
-300.00
-350.00
-400.00
-450.00
-500.00
0.00
40.00
80.00
120.00
160.00
200.00
240.00
RECEIVE POLARIZATION ANGLE DEG

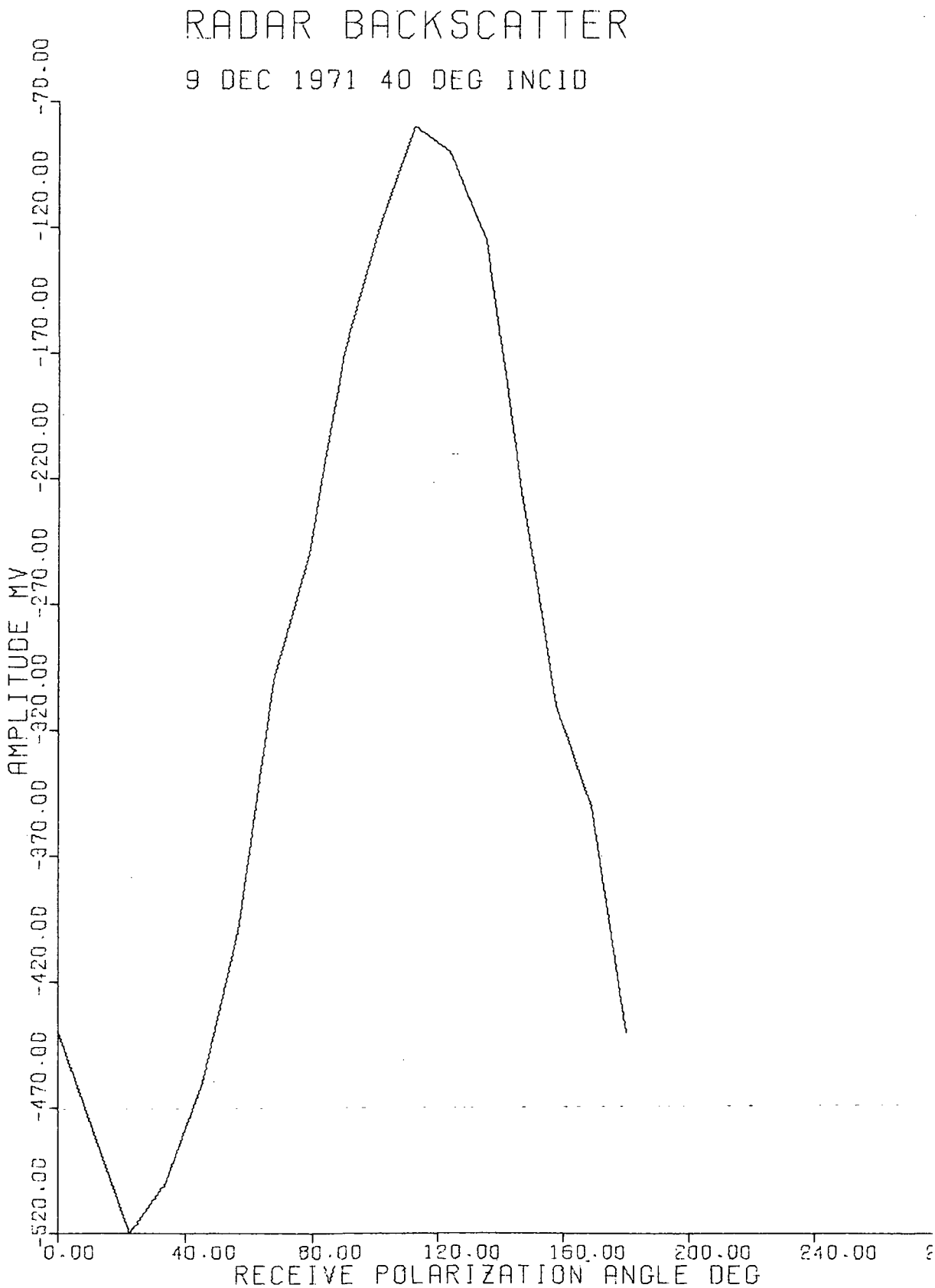
RADAR BACKSCATTER
9 DEC 1971 40 DEG INCID
AMPLITUDE MV
-70.00
-120.00
-170.00
-220.00
-270.00
-320.00
-370.00
-420.00
-470.00
-520.00
0.00
40.00
80.00
120.00
160.00
200.00
240.00
RECEIVE POLARIZATION ANGLE DEG

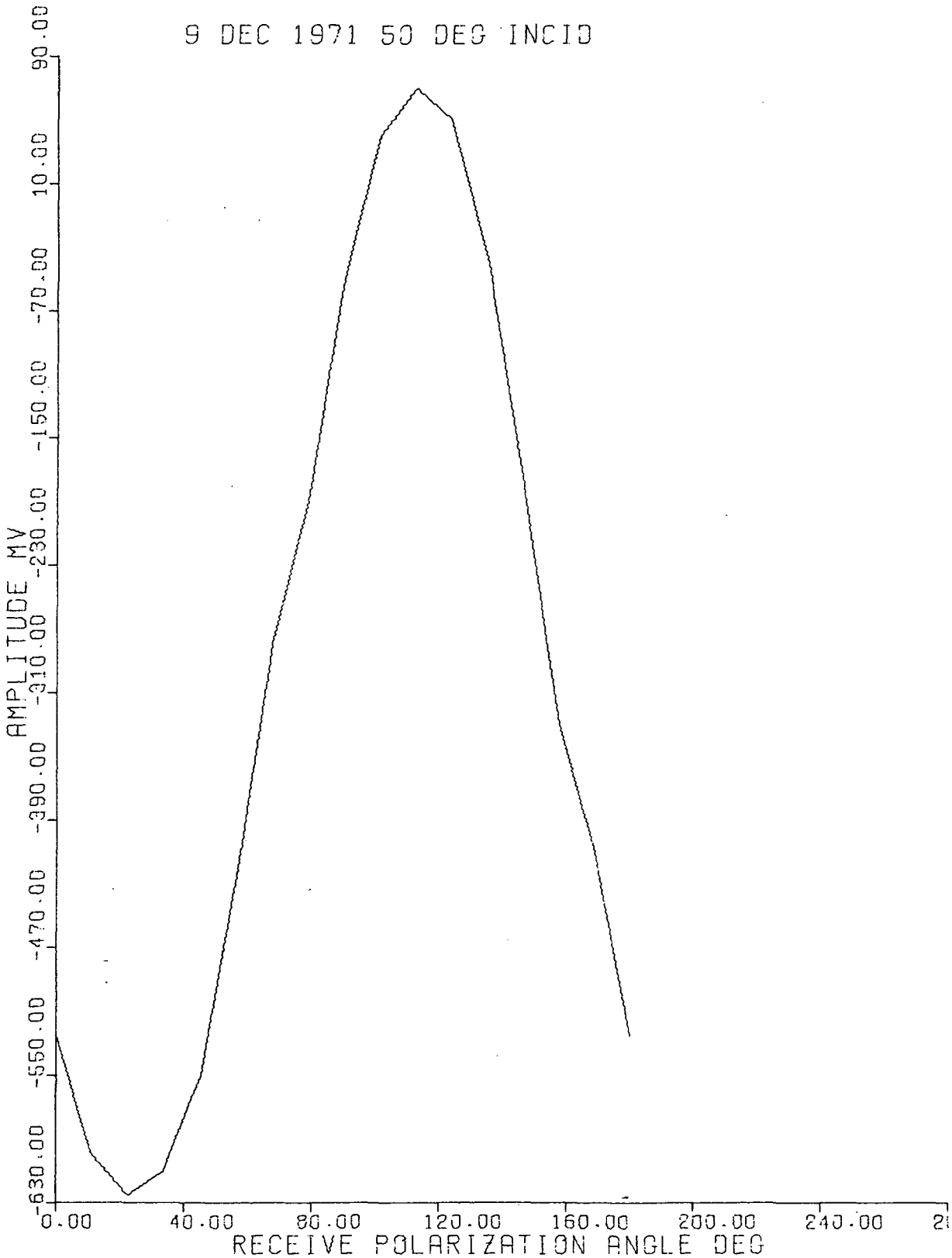
RADAR BACKSCATTER
9 DEC 1971 50 DEG INCID
AMPLITUDE MV
90.00
10.00
-70.00
-150.00
-230.00
-310.00
-390.00
-470.00
-550.00
-630.00
0.00
40.00
80.00
120.00
160.00
200.00
240.00
RECEIVE POLARIZATION ANGLE DEG

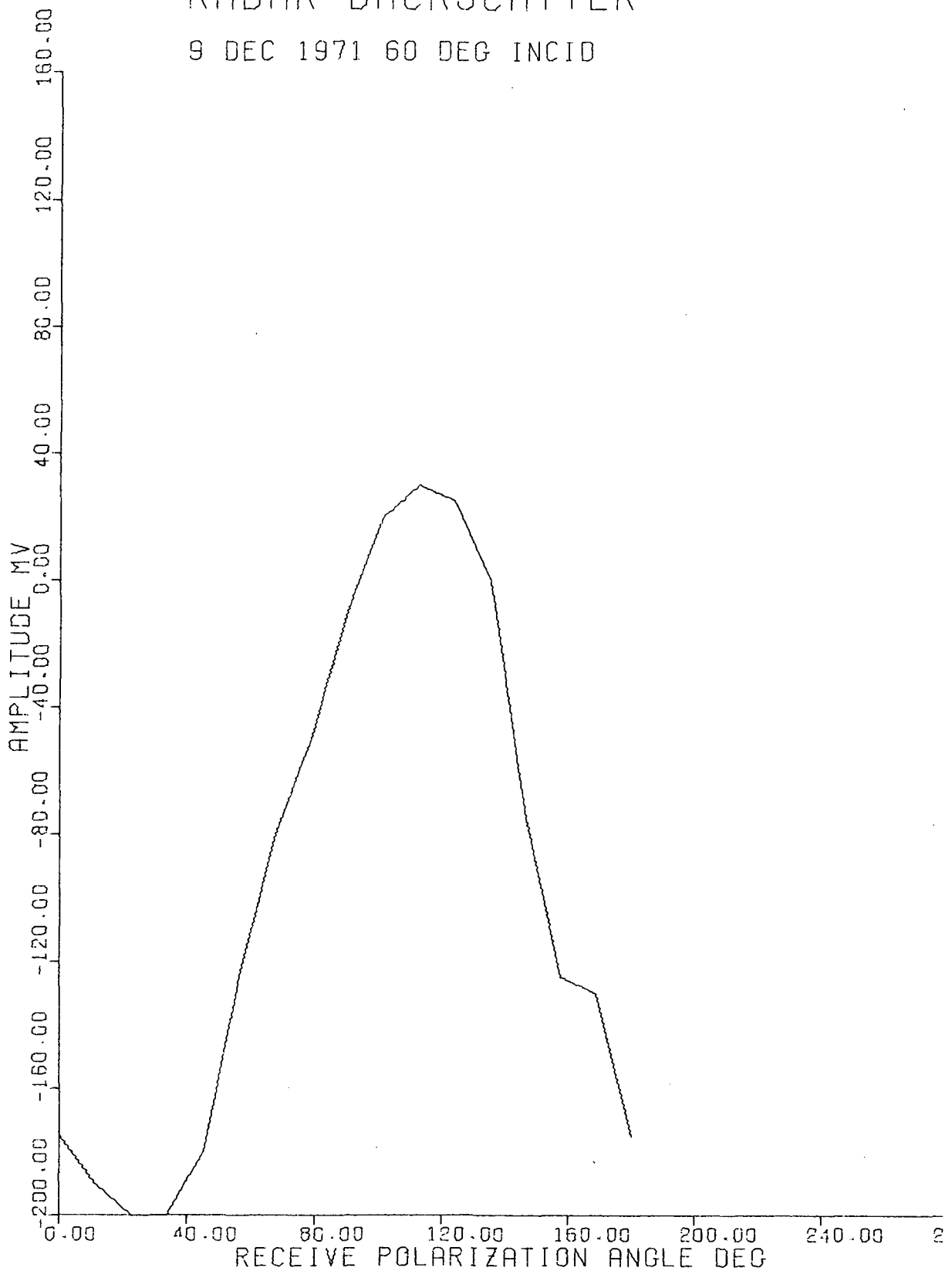
RADAR BACKSCATTER
9 DEC 1971 60 DEG INCID
AMPLITUDE MV
160.00
120.00
80.00
40.00
0.00
-40.00
-80.00
-120.00
-160.00
-200.00
0.00
40.00
80.00
120.00
160.00
200.00
240.00
RECEIVE POLARIZATION ANGLE DEG

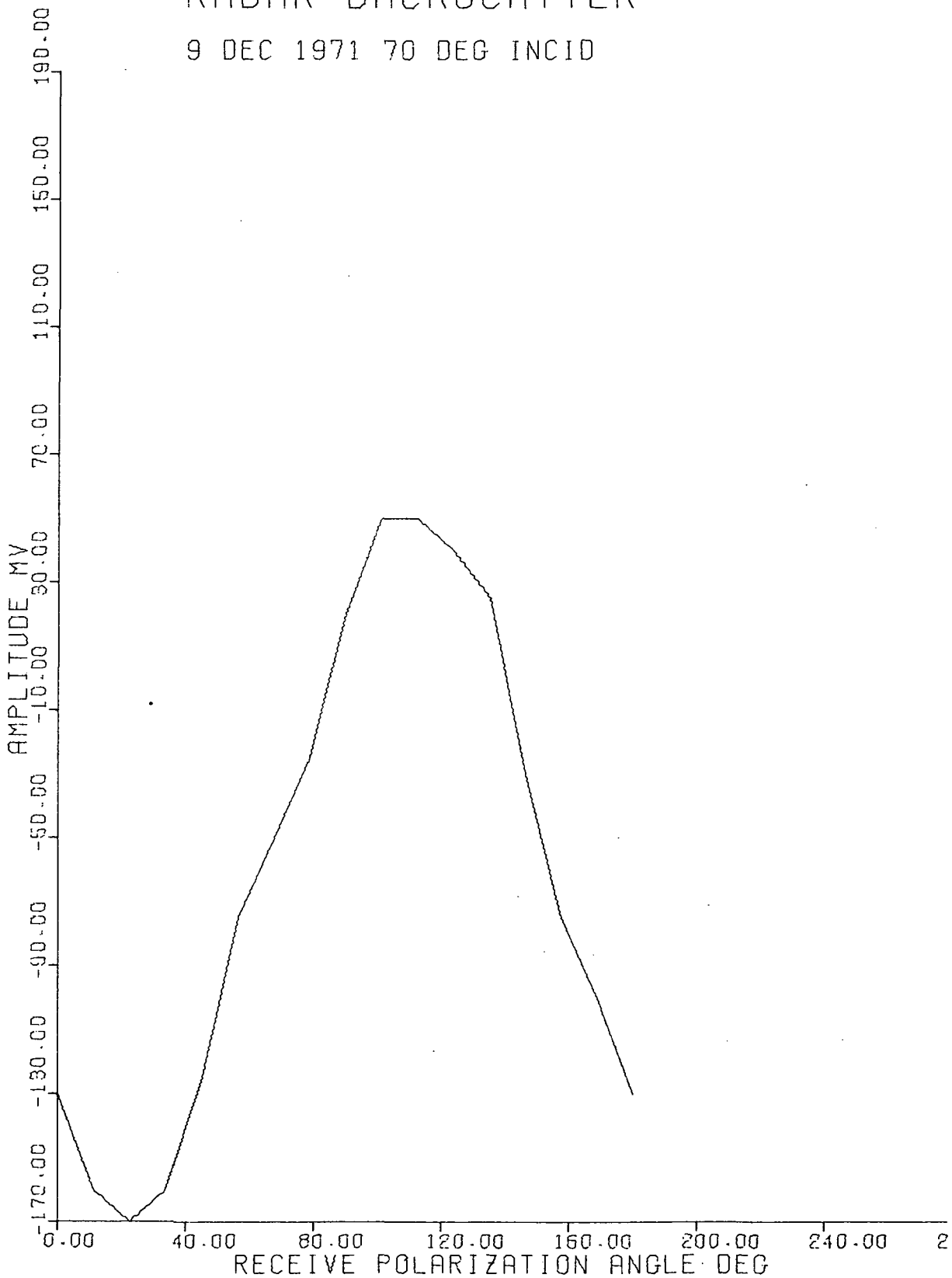
RADAR BACKSCATTER
9 DEC 1971 70 DEG INCID
AMPLITUDE MV
190.00
150.00
110.00
70.00
30.00
-10.00
-50.00
-90.00
-130.00
-170.00
0.00
40.00
80.00
120.00
160.00
200.00
240.00
RECEIVE POLARIZATION ANGLE DEG

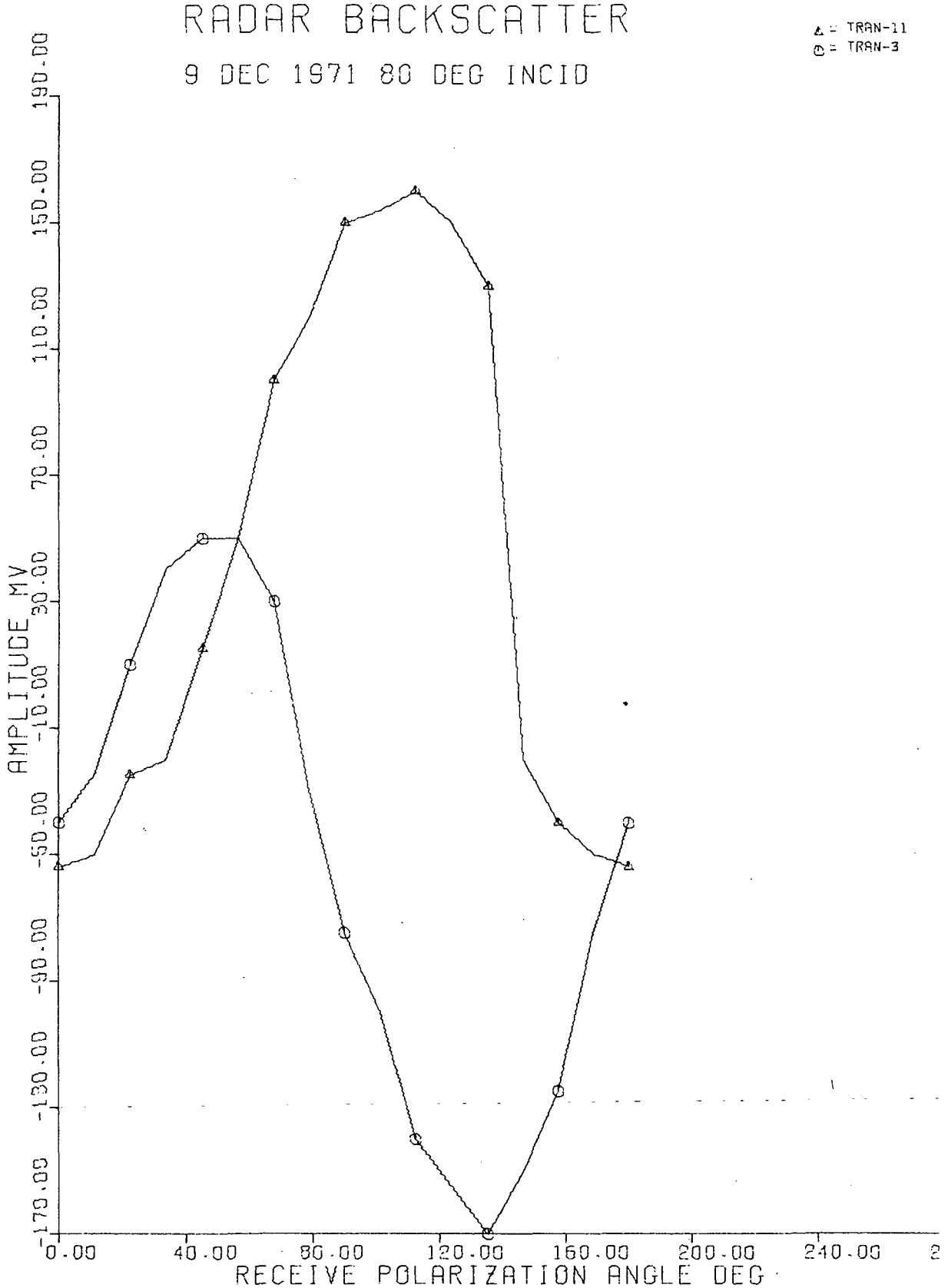
RADAR BACKSCATTER
9 DEC 1971 80 DEG INCID
△ = TRAN-11
◷ = TRAN-3
AMPLITUDE MV
190.00
150.00
110.00
70.00
30.00
-10.00
-50.00
-90.00
-130.00
-170.00
0.00
40.00
80.00
120.00
160.00
200.00
240.00
RECEIVE POLARIZATION ANGLE DEG

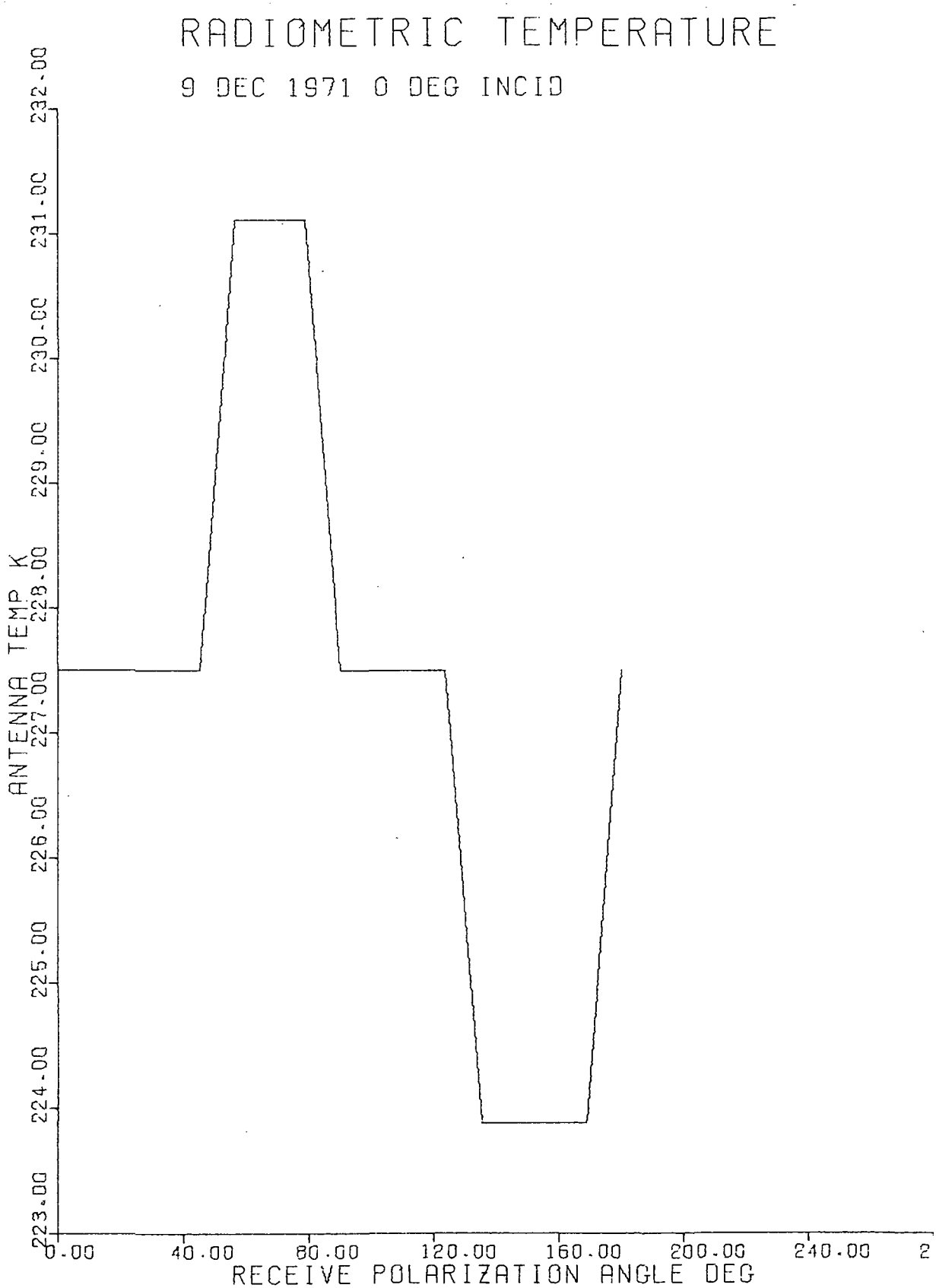
RADIOMETRIC TEMPERATURE
9 DEC 1971 0 DEG INCID
ANTENNA TEMP K
232.00
231.00
230.00
229.00
228.00
227.00
226.00
225.00
224.00
223.00
0.00
40.00
80.00
120.00
160.00
200.00
240.00
RECEIVE POLARIZATION ANGLE DEG

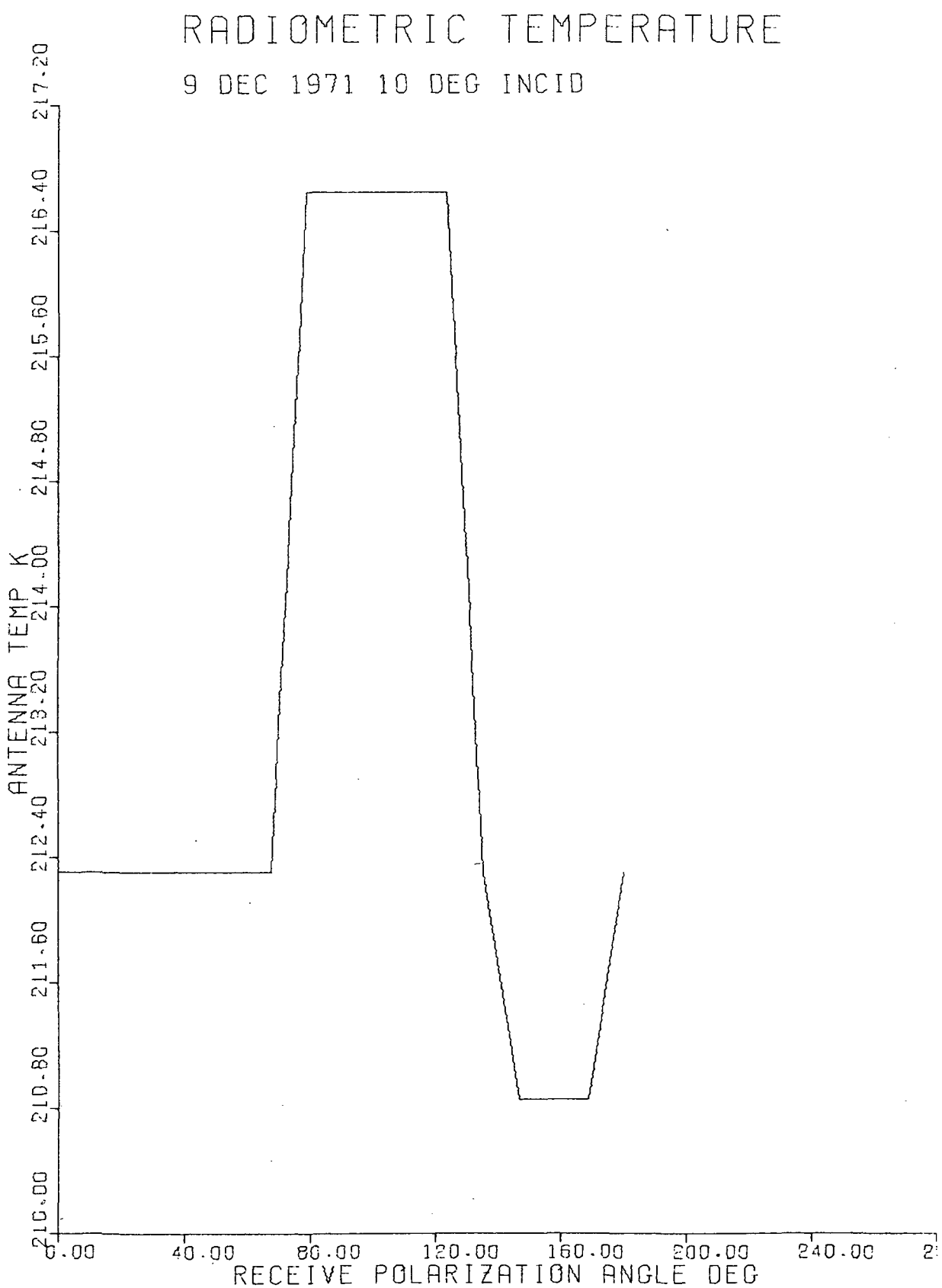
RADIOMETRIC TEMPERATURE
9 DEC 1971 10 DEG INCID
ANTENNA TEMP K
210.00
210.80
211.60
212.40
213.20
214.00
214.80
215.60
216.40
217.20
0.00
40.00
80.00
120.00
160.00
200.00
240.00
RECEIVE POLARIZATION ANGLE DEG

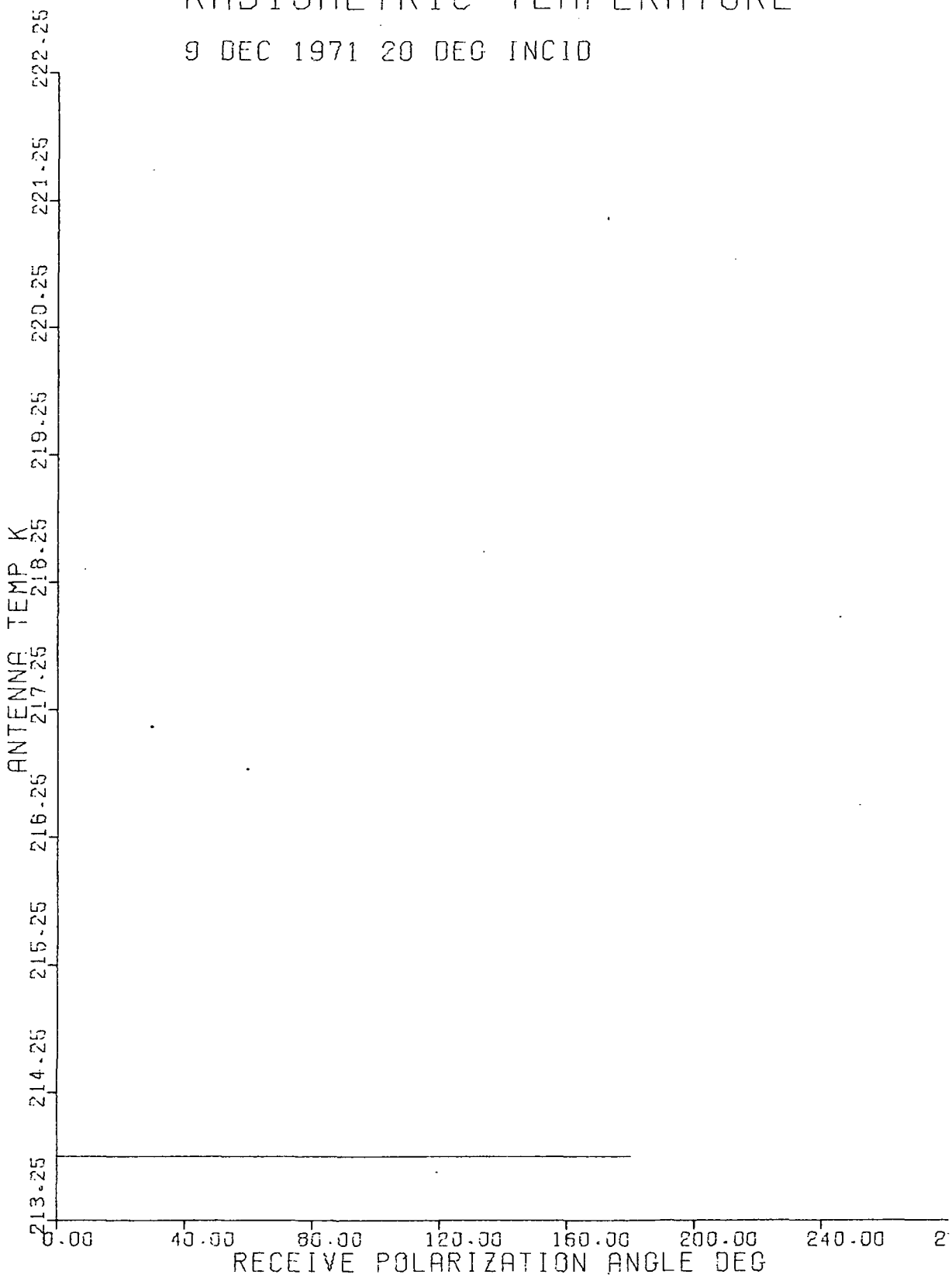
RADIOMETRIC TEMPERATURE
9 DEC 1971 20 DEG INCID
ANTENNA TEMP K
213.25
214.25
215.25
216.25
217.25
218.25
219.25
220.25
221.25
222.25
0.00
40.00
80.00
120.00
160.00
200.00
240.00
RECEIVE POLARIZATION ANGLE DEG

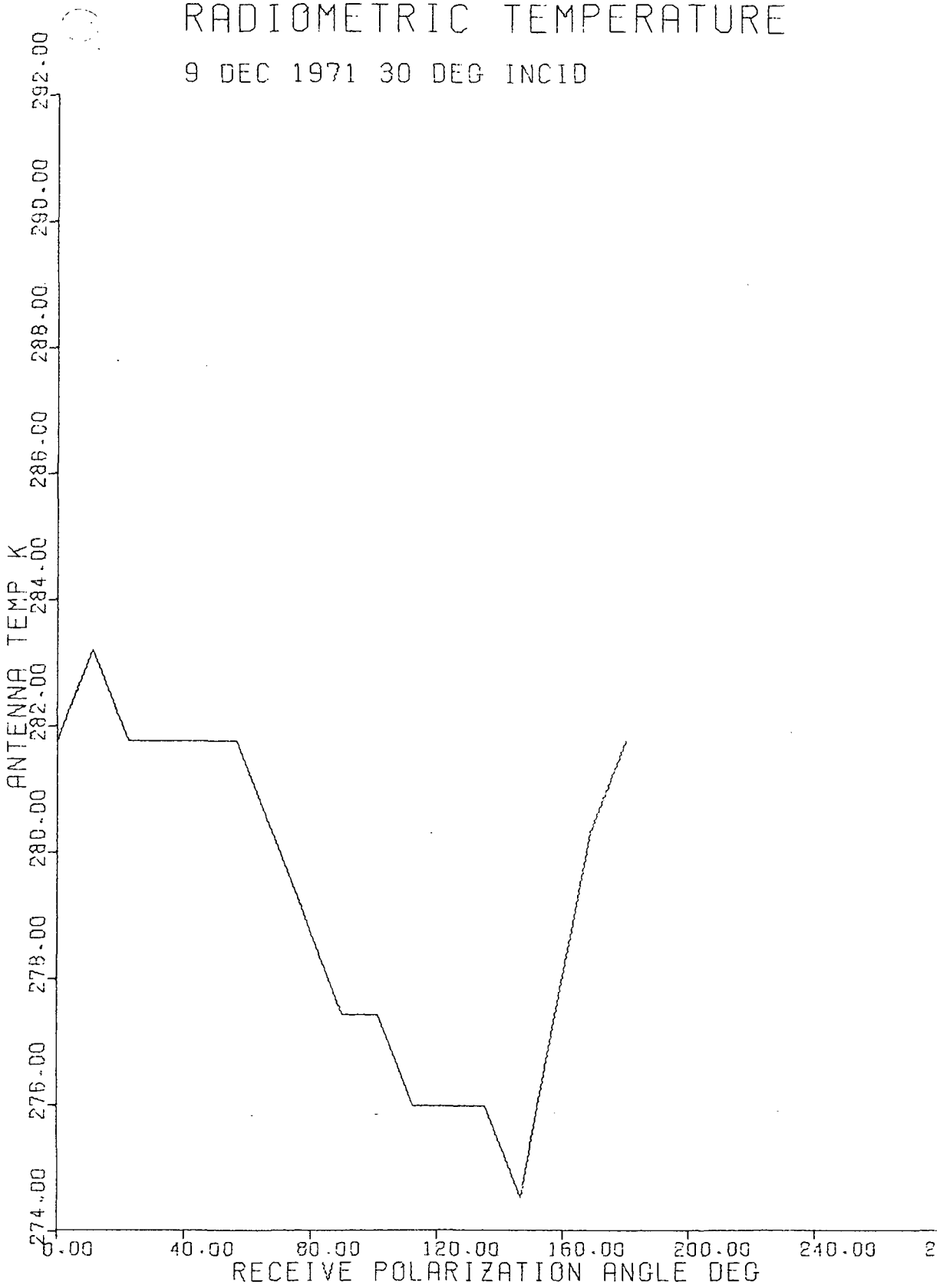
RADIOMETRIC TEMPERATURE
9 DEC 1971 30 DEG INCID
ANTENNA TEMP K
292.00
290.00
288.00
286.00
284.00
282.00
280.00
278.00
276.00
274.00
0.00
40.00
80.00
120.00
160.00
200.00
240.00
RECEIVE POLARIZATION ANGLE DEG

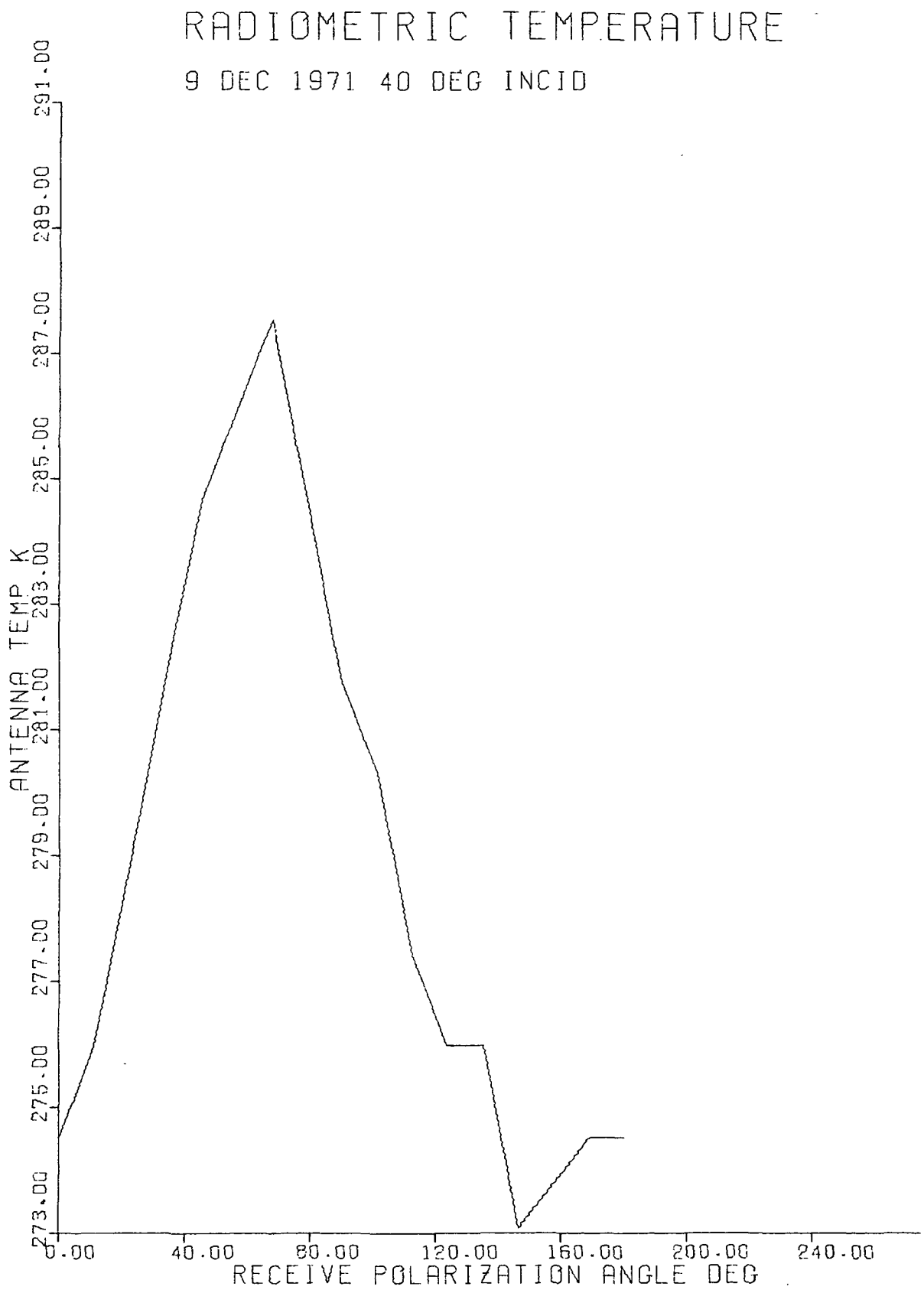
RADIOMETRIC TEMPERATURE
9 DEC 1971 40 DEG INCID
ANTENNA TEMP K
273.00
275.00
277.00
279.00
281.00
283.00
285.00
287.00
289.00
291.00
0.00
40.00
80.00
120.00
160.00
200.00
240.00
RECEIVE POLARIZATION ANGLE DEG

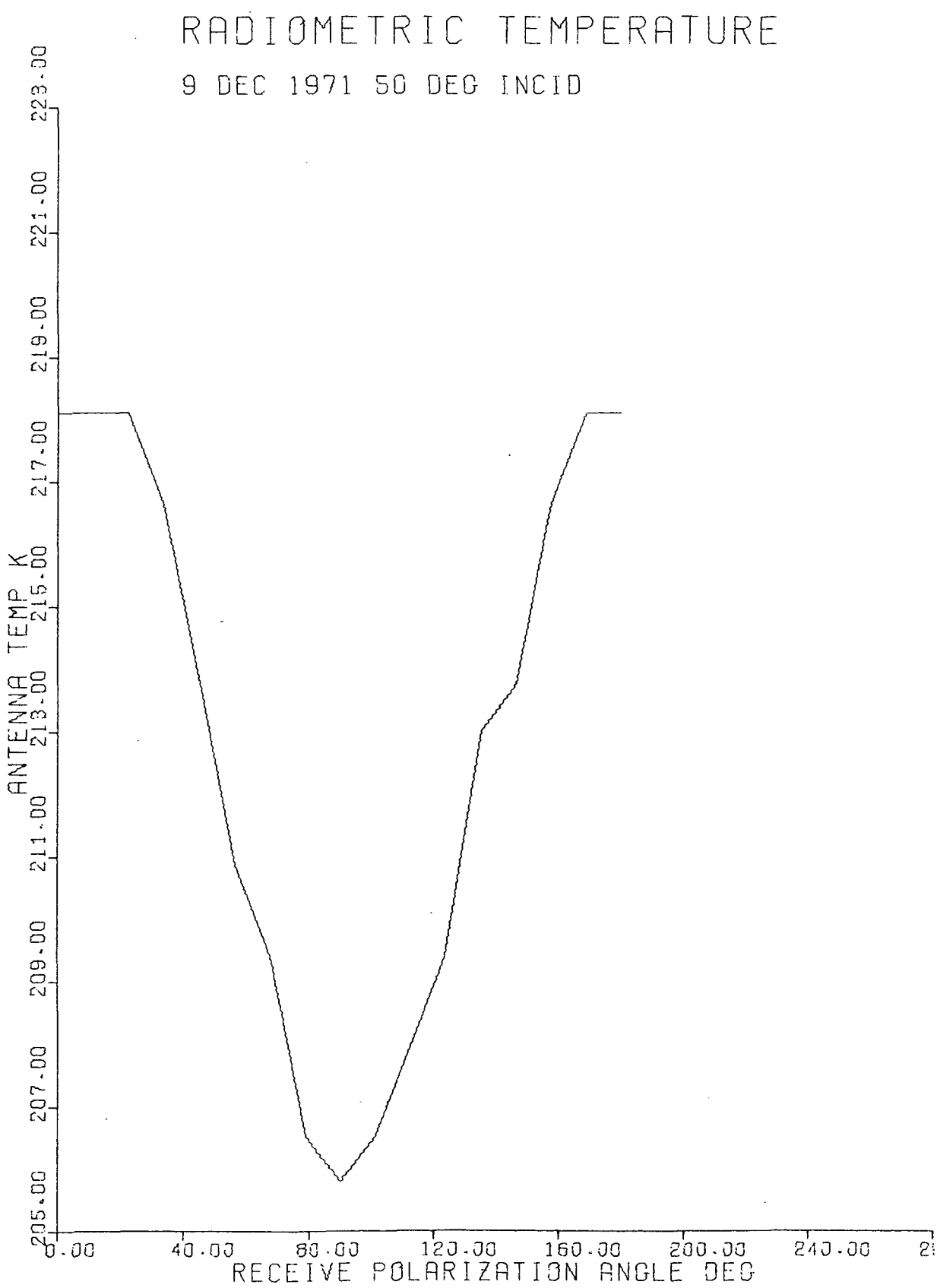
RADIOMETRIC TEMPERATURE
9 DEC 1971 50 DEG INCID
ANTENNA TEMP K
205.00
207.00
209.00
211.00
213.00
215.00
217.00
219.00
221.00
223.00
0.00
40.00
80.00
120.00
160.00
200.00
240.00
RECEIVE POLARIZATION ANGLE DEG

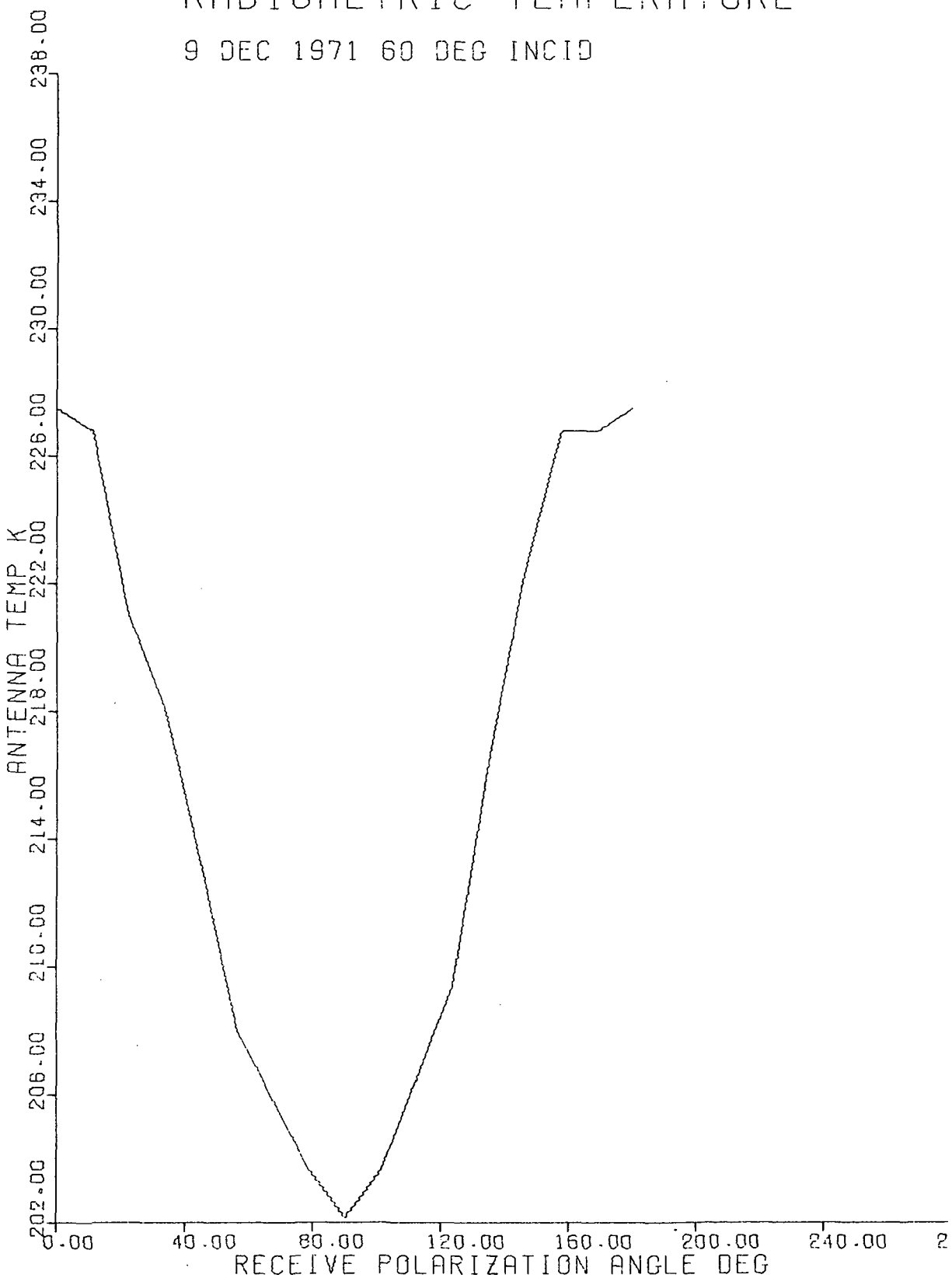
RADIOMETRIC TEMPERATURE
9 DEC 1971 60 DEG INCID
ANTENNA TEMP K
238.00
234.00
230.00
226.00
222.00
218.00
214.00
210.00
206.00
202.00
0.00
40.00
80.00
120.00
160.00
200.00
240.00
RECEIVE POLARIZATION ANGLE DEG

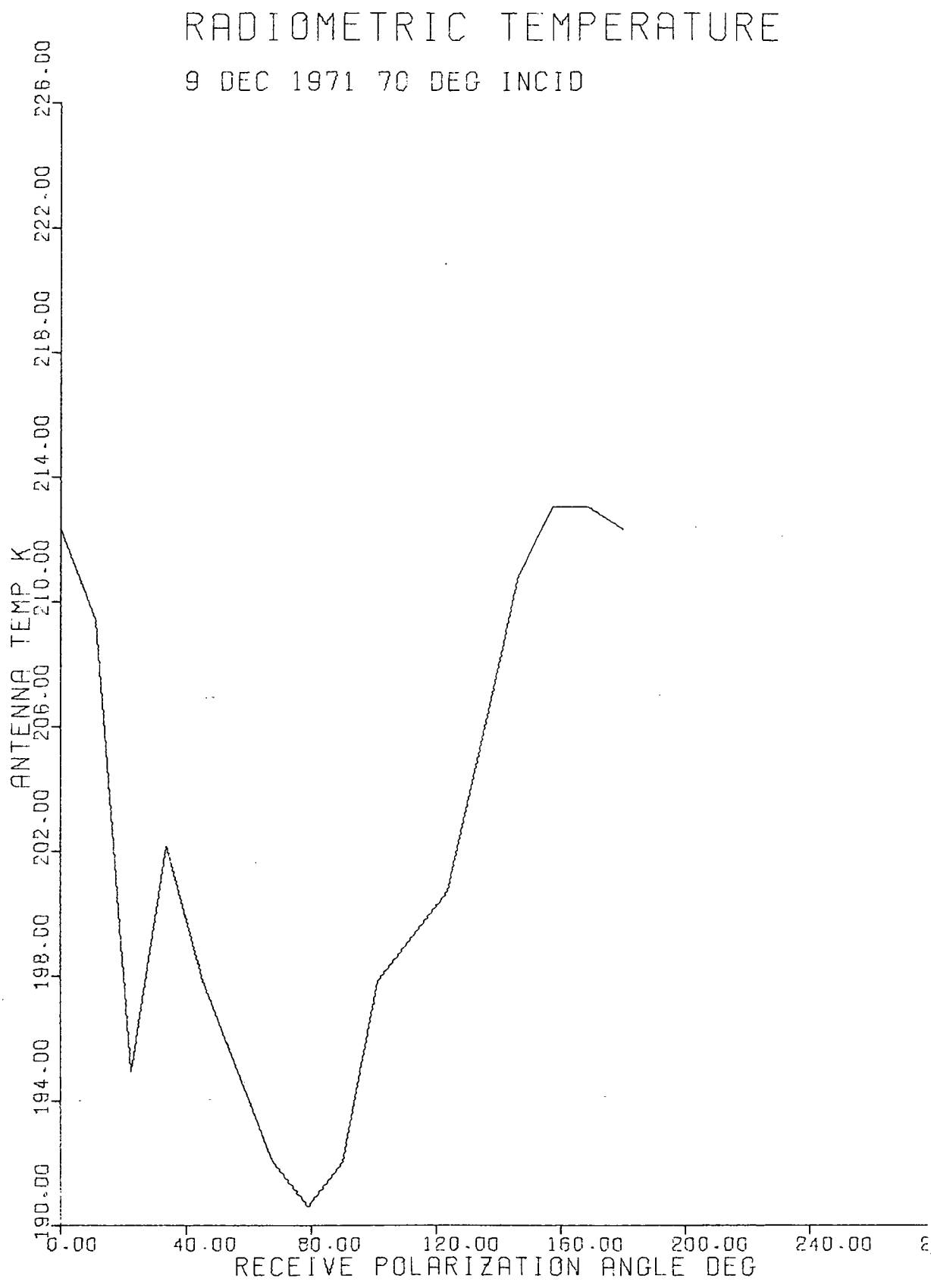
RADIOMETRIC TEMPERATURE
9 DEC 1971 70 DEG INCID
ANTENNA TEMP K
190.00
194.00
198.00
202.00
206.00
210.00
214.00
218.00
222.00
226.00
0.00
40.00
80.00
120.00
160.00
200.00
240.00
RECEIVE POLARIZATION ANGLE DEG

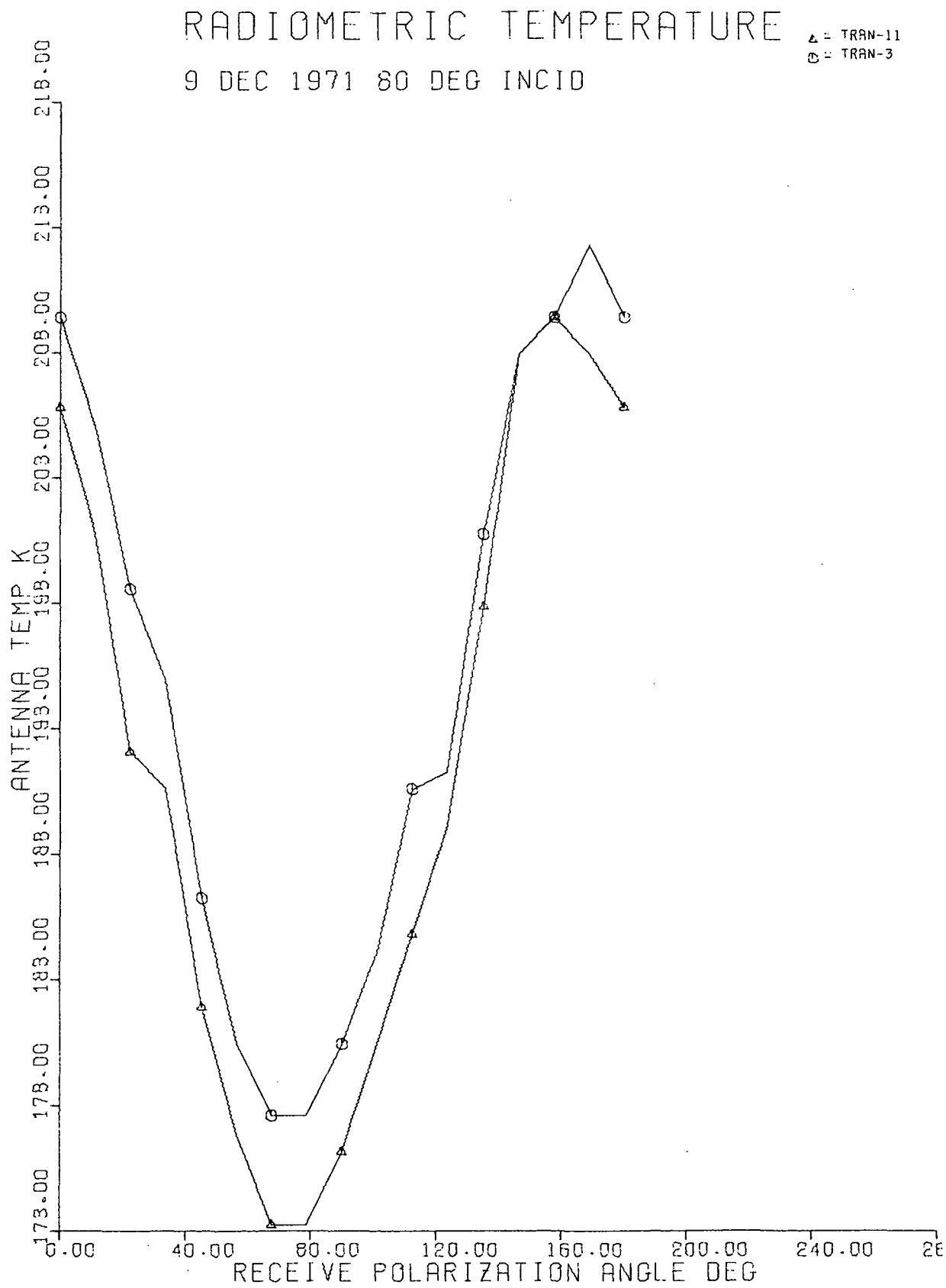
RADIOMETRIC TEMPERATURE
9 DEC 1971 80 DEG INCID
△ = TRAN-11
○ = TRAN-3
ANTENNA TEMP K
173.00
178.00
183.00
188.00
193.00
198.00
203.00
208.00
213.00
218.00
0.00
40.00
80.00
120.00
160.00
200.00
240.00
RECEIVE POLARIZATION ANGLE DEG